ESD-TR-66-455

Technical Note	1966-53
	L. P. Whitehill
Survey on Earth Albedo	
	11 October 1966

Lincoln Laboratory

MASSACHUSETTS INSTITUTE OF TECHNOLOGY

Lexington, Massachusetts

AD 643649

The work reported in this document was performed at Lincoln Laboratory, a center for research operated by Massachusetts Institute of Technology, with the support of the U.S. Air Force under Contract AF 19(628)-5167.

This report may be reproduced to satisfy needs of U.S. Government agencies.

Distribution of this document is unlimited.

MASSACHUSETTS INSTITUTE OF TECHNOLOGY

LINCOLN LABORATORY

SURVEY ON EARTH ALBEDO

L. P. WHITEHILL

Group 63

TECHNICAL NOTE 1966-53

11 OCTOBER 1966

LEXINGTON   MASSACHUSETTS

ABSTRACT

This paper is a study of the conditions that can be expected for the intensity of light reflected and scattered from the earth. The albedo of the earth is defined and the albedo of various surfaces, and regions of the earth are discussed. An attempt is made to survey typical results of measurements of Tiros data. The albedo of the earth covered by a Rayleigh atmosphere is presented in graphical form and the intensity distribution over the earth is plotted for various orientations of observer viewed spot and sun. A calculation of expected minimum response is made for a specific photodiode for a certain geometry and a method is presented to enable interested persons to easily perform similar calculations for different geometries.

SURVEY ON EARTH ALBEDO

Before beginning the discussion, the oft-used term "albedo" must be clearly understood. The albedo of an object is simply the ratio of the emergent flux of light scattered and reflected in a given spectral region to the incident flux of light in the same spectral region. It is mathematically computable if the emergent spectral intensity [in units of (power)(unit projected area)$^{-1}$ (steradian)$^{-1}$ (unit wavelength interval)$^{-1}$] is known. Then

$$a_1 = a_1 (\lambda_1, \lambda_2) = \text{albedo} = \frac{\int_{\lambda_1}^{\lambda_2} \int_0^{2\pi} \int_0^{\pi/2} I_\lambda (\theta, \varphi) \cos \theta \sin \theta \, d\theta \, d\varphi}{\int_{\lambda_1}^{\lambda_2} \pi \, F_\lambda \, \cos Z \, d\lambda}$$

where

I_λ is the emergent spectral intensity

F_λ is the incident spectral intensity = incident spectral flux [(power)(unit area)$^{-1}$ (unit wavelength interval)$^{-1}$] divided by π for a source like the sun.

Z is the solar zenith angle shown in Fig. 1.
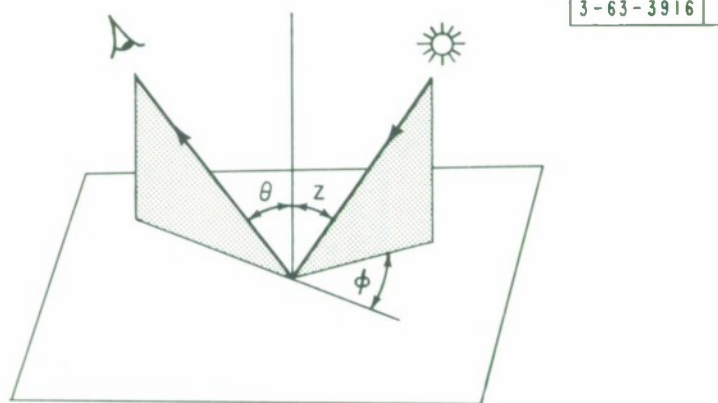

3-63-3916

Fig. 1

1

The albedo just defined is, strictly speaking, the albedo of a point. The albedo of the entire object would have to be obtained by averaging "a" over the object.

To measure the albedo of a point on the earth's surface from an orbiting satellite requires quite a different definition:

$$a_2 = \frac{F}{\cos Z \int S_\lambda \, \phi(\lambda) \, d\lambda}$$

where

> F is the flux measured by the sensor
>
> S_λ is the incident spectral flux
>
> $\phi(\lambda)$ is the effective spectral response of the sensor

The value F is not directly measureable because, to accurately measure F, sensors would have to be placed at all points in a hemisphere centered on the viewed area and the intensities would have to be averaged over the hemisphere. Since this is clearly not a practical idea, an assumption has to be made as to the scattering function of the area. The assumption that is invariably made is that the surface scatters isotropically, i.e., according to Lambert's law. It is then a simple matter to produce a number $F = \pi I$ since the intensity in all directions is assumed constant.

The albedo of an area measured in this way is dependent (especially for a portion of the earth where scattering from the atmosphere is the major contributor) on the exact shape of the spectral response curve of the sensor. To see this assume two sensors with their 3 db points at the same wavelength but having differently shaped spectral response curves as in Fig. 2 below. If the relative intensity of the scattered sunlight as function of wavelength is as shown below (Fig. 3), sensor (b) will record a much higher albedo than sensor (a).
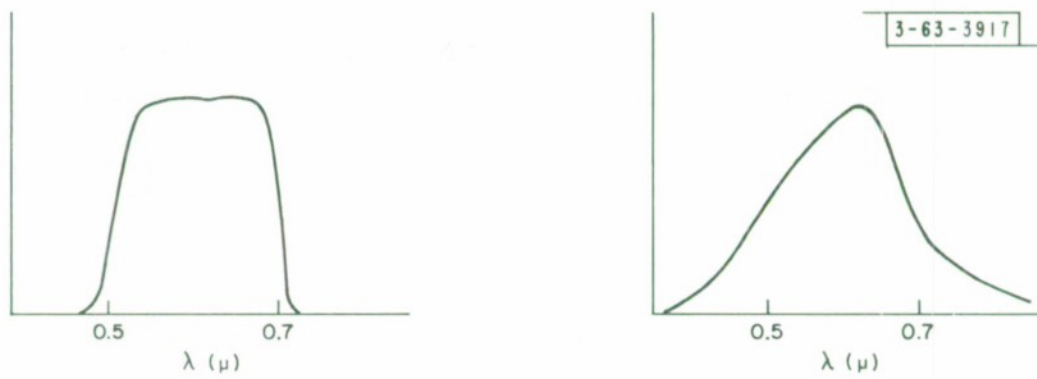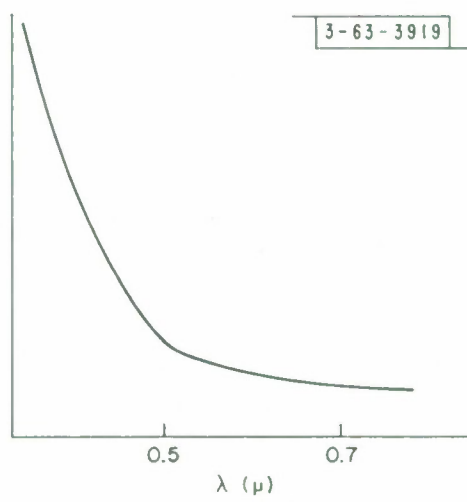
Fig. 2

Fig. 3

The realization that the measured albedo depends on the exact shape of the spectral response curve as well as the bandwidth has never been encountered in the literature.

Two alternative definitions of albedo are proposed below, although they are not definitions of albedo in the generally accepted sense and would more properly be called (for want of a better name) backscatter coefficients.

$$b_1(\lambda) = \frac{I_\lambda(\theta, \varphi, Z)}{H_\lambda} = \text{spectral backscatter coefficient}$$

where

I_λ is the spectral intensity of the scattered sunlight at a given wavelength

H_λ is the spectral intensity of sunlight at the same wavelength

Since only the ratio of these two factors is important, H_λ may be set to 1 for theoretical calculations. The spectral flux seen through a solid "$d\omega$" from a point above the surface is just $b_1 H_\lambda d\omega$.

$$b_2 = \frac{\int_\lambda I_\lambda(\theta, \varphi, Z) \phi(\lambda) d\lambda}{\int_\lambda H_\lambda \phi(\lambda) d\lambda} = \text{sensor backscatter coefficient}$$

where ϕ is the effective spectral response of the sensor.

The effective flux flowing into "$d\omega$" is just

$$b_2 \int_\lambda H_\lambda \phi(\lambda) d\omega = dS(\theta, \varphi, Z)$$

These backscatter coefficients are explicit functions of 3 variables θ, φ, and Z, and implicit functions of the type of area viewed, i.e., forests, deserts, oceans, etc., and the sensor itself. Hence, they would be very difficult to tabulate. All that is undertaken in the latter half of this paper is to obtain values for b_1 and b_2 for very specific minimum intensity cases for a specific sensor.*

---

* The Fairchild Planar Photodiode 1N3734

4

The following is a survey of some of the information available on albedo of the earth as it was defined in this paper.

The albedo of the entire earth is generally computed by observing earth-light reflected from a new moon or by satellite measurements. In the visible region 30% - 40% are respectable limits for the albedo of the earth at any time with a time average value of 36-39% depending on the investigator. For a cloudless earth the albedo is 16%, for a cloud-covered earth it is 56%. The albedo is about 50% in the UV region and 28% in the IR region.

The albedo of various cloud types for the entire spectrum is shown in Table I below.[1]

TABLE I

Albedo of Various Cloud Types.

Cloud Type	Albedo
Very dense clouds of extensive area and great depth	78
Dense clouds, quite opaque	55-62
Dense clouds, nearly opaque	44
Thin clouds	36-40
Stratocumulus, overcast	56-81
Altostratus, occasional breaks	17-36
Altostratus, overcast	39-59
Cirrostratus and altostratus	49-64
Cirrostratus, overcast	44-50
Stratus, 680-1000 ft. thick	78

Data for several types of terrain are given below in Table II.

TABLE II

Albedo of Various Surfaces.

Surface	Albedo (per cent)
Desert	24-28
Fields, various types	3-25
Forest, green	3-10
Grass, various conditions	14-37
Ground, bare	7-20
Sand, dry	18
Sand, wet	9
Snow or ice	46-86

Water (direct sun only) Z (degrees)	
0	2.0
20	2.1
40	2.5
50	3.4
60	6.0
70	13.4
80	34.8
85	58.4
90	100.0

where Z is the zenith angle of the sun.

The albedo of water according to one author is closely approximated by the above numbers, calculated from Fresnel's law of reflection, even when the wind is 10 mph. Angstrom states that in ordinary geophysical problems the data in Table II are applicable.[1]

A good source of values for earth albedo is the results of radiation measurements from the Tiros meteorological satellite series. The results gotten by Nordberg and Bandeen[2] are given below as an example of what information can be culled from Tiros data.

The Tiros satellites are generally equipped with two types of radiometers. The first is a non-scanning radiometer with a broad response in both the visible and infrared regions and a rather low spatial resolution. Its aperture is approximately 55 degrees. The second is a scanning radiometer which scans as the satellite spins. It is of medium spatial resolution, has a 5 degree aperture, and responds to radiation in five different spectral regions separated by filters. Three of these regions are in the infared between 5.0 and 6.7 microns, between 7.5 and 13.5 microns, and between 7.0 and 32.0 microns. The other two regions lie mainly in the visible portion of the spectrum, that is, between 0.2 and 7.0 microns and between 0.50 and 0.75 microns. It is the latter, channel 5, which is of interest here. Note: The satellite is flying in a nearly circular orbit with an approximate altitude of 780 km.

Shown in Fig. 4 through Fig. 6 are albedo maps made with the channel 5 sensor. These values of albedo, as all other albedo values derived from Tiros data, assumes an isotropic reflecting surface.

The data of interest for minimum intensity considerations is to the left of the sub-satellite path where specular reflection from the water does not occur. Minimum albedo for this area, with the sun near zenith, is 4%.

Figure 4.   Tiros Albedo Percentages

Albedo percentages measured by channel 5 (approximately
0.5 - 0.75μ) of the medium resolution radiometer between
1439 and 1445 GMT, Orbit 117, 20 July 1961.   The skies
are mostly clear, except for some minor scattered clouds.
Averages of these data are given for the areas enclosed by
dashed lines.   The heavy dashed line is the sub-satellite
path with points each minute.

8

The next albedo map is for the eastern United States under mostly cloudy skies.

3-63-3920
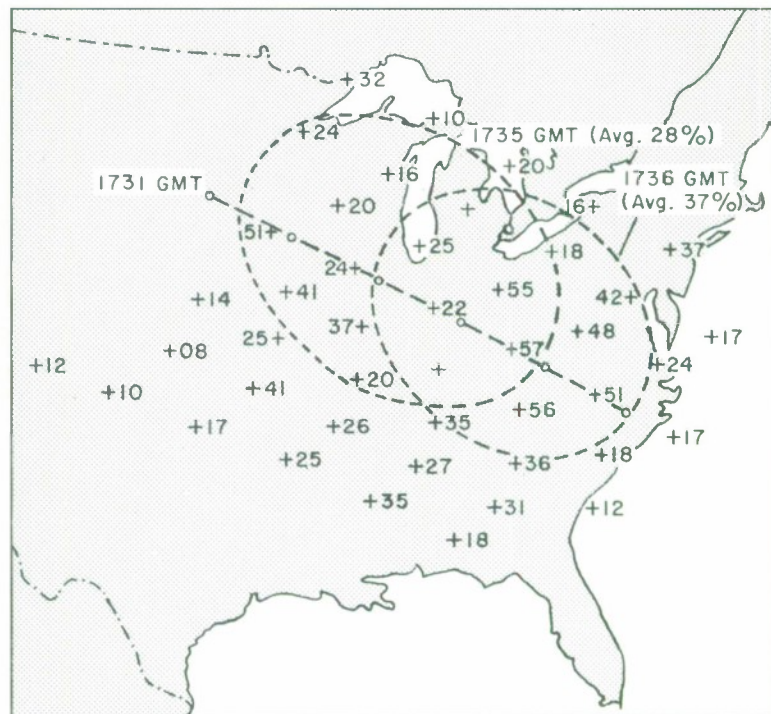
Figure 5.   Albedo Percentages Measured by Channel 5.

Notice the low value of 8% in the absence of clouds.

The last albedo map shows the North African Desert under clear skies.
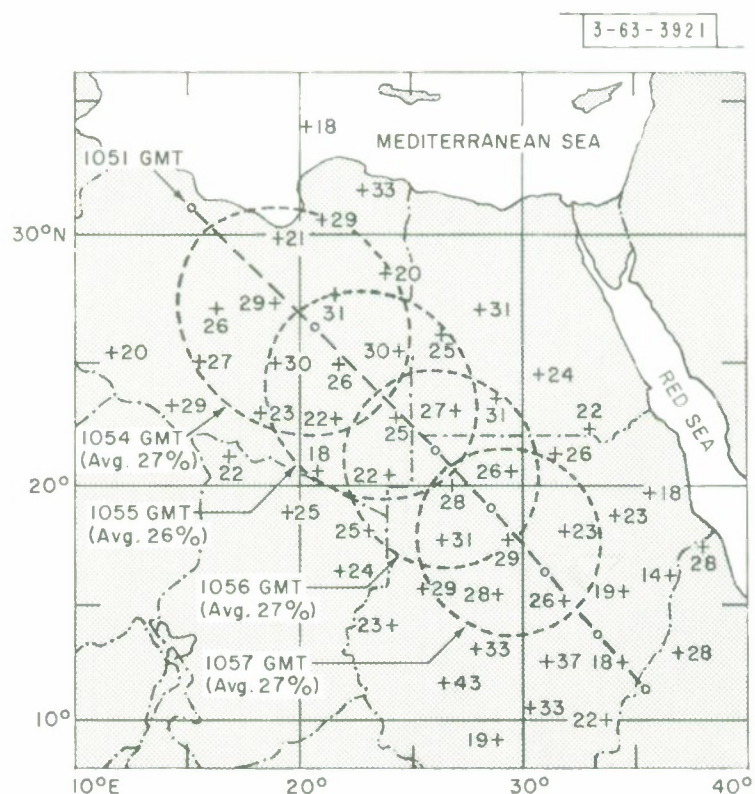
Figure 6.   Albedo Percentages Measured by Channel 5.

The albedo values presented in the above maps do not take into account the
fact that the earth does not scatter isotropically.   To get a quantitative idea
as to the extent to which anisotropy occurs, the following computation with
Tiros III data was performed.[3]

10

A selected area of the earth, Fig. 7, is viewed by the radiometer twice during the orbit with the scans 3 to 4 minutes apart. The satellites have moved far enough in the time for the scattering angle of the scattered and reflected radiation to have changed quite significantly. The two maps above show the same area. Notice the difference in the appearance of the two maps, a difference which is not acknowledged in the previous albedo maps. It should be noted that the smaller scattering angles[*] in this study are associated with the larger nadir angles.[**] There is a large difference in nadir angle between the two sets of data along X. However, when this difference is reduced, as along Y, the fluxes for the smaller scattering angles remain considerably higher. Since the solar zenith angle varies in an identical manner along both lines, the difference in flux can be least qualitatively be attributed to the difference in scattering angle. The variation of channel 5 flux along X and Y for the two different viewing geometry is shown in Fig. 8.

The data of both solar channels suggest that the scattering angle effect is largest in areas of least cloudiness. This suggests the possibility that specular reflection from the ocean surface could have been responsible for the larger flux differences in the areas of relatively low flux. Along Y, this effect could have entered since this line lies nearly in the plane of the sun. Since both X and Y show the same relationship between flux difference maximas and regions of relatively low flux, specular reflection alone could not have been the cause. Increased atmospheric scattering for the smaller scattering angles, regardless of the viewed surface, is probably the important factor.

In the report just considered, the data sample included significant differences in the radiometric nadir angle associated with the separate scans of the overlapping data. Therefore, the increase in forward scatter could have been effected by the variation in the viewed volume. However, even as in a subsequent publication, when the nadir angle difference of the two scans is reduced to zero, the measured albedo remain higher for smaller scattering angles (Fig. 9).[4]

Notice in the figure that in general, effective blackbody temperature measured with the channel 2 sensor (approximately 8.0-12.0 microns) decreases

---

[*]scattering angle $\equiv 180^O$ -(angle between sun, viewed spot and satellite sensor)
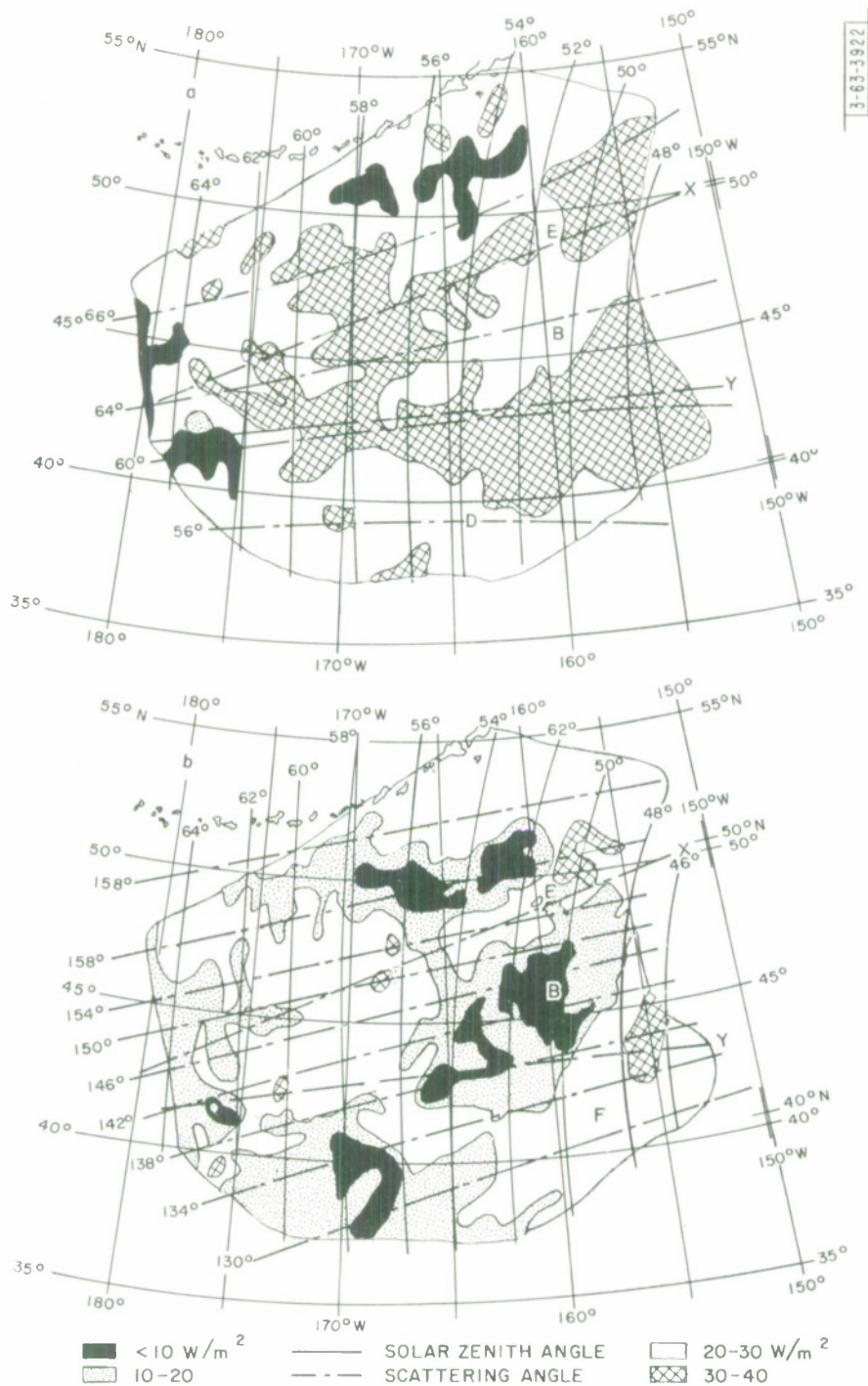[**]nadir angle $\equiv$ angle between local vertical at the sensor and the direction of the viewed spot.

Figure 7. Relative Patterns of Channel 5 Flux for Area with Overlapping
Scanlines from Orbit 5, Tiros III
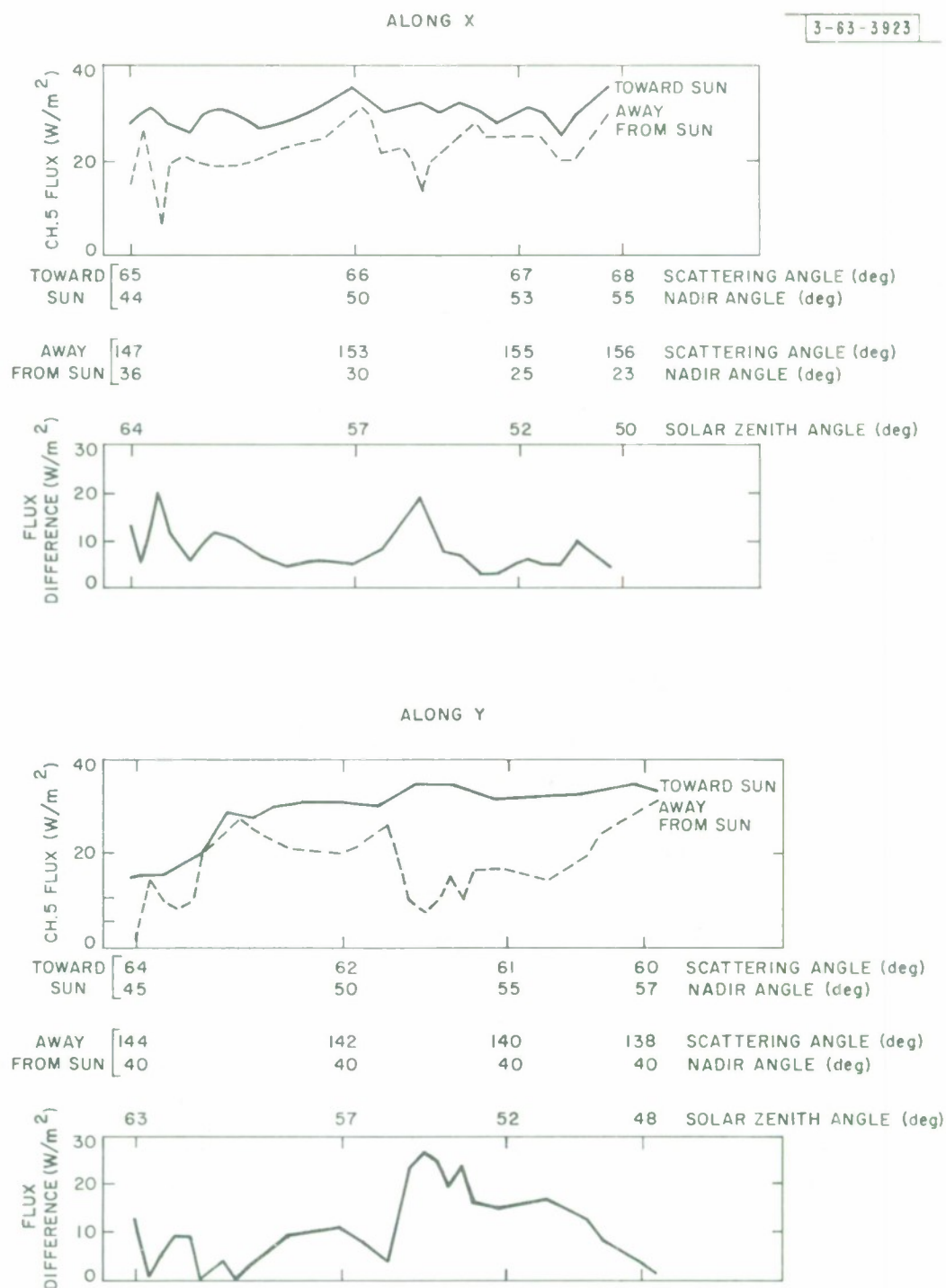(a) Initial Alternating Open Mode Data
(b) Complemental Single Open Mode Data

Figure 8. Variation of Channel 5 Flux for Radiometer Scans Towards and Away from the Sun and the Variation of Their Difference Along X and Y.
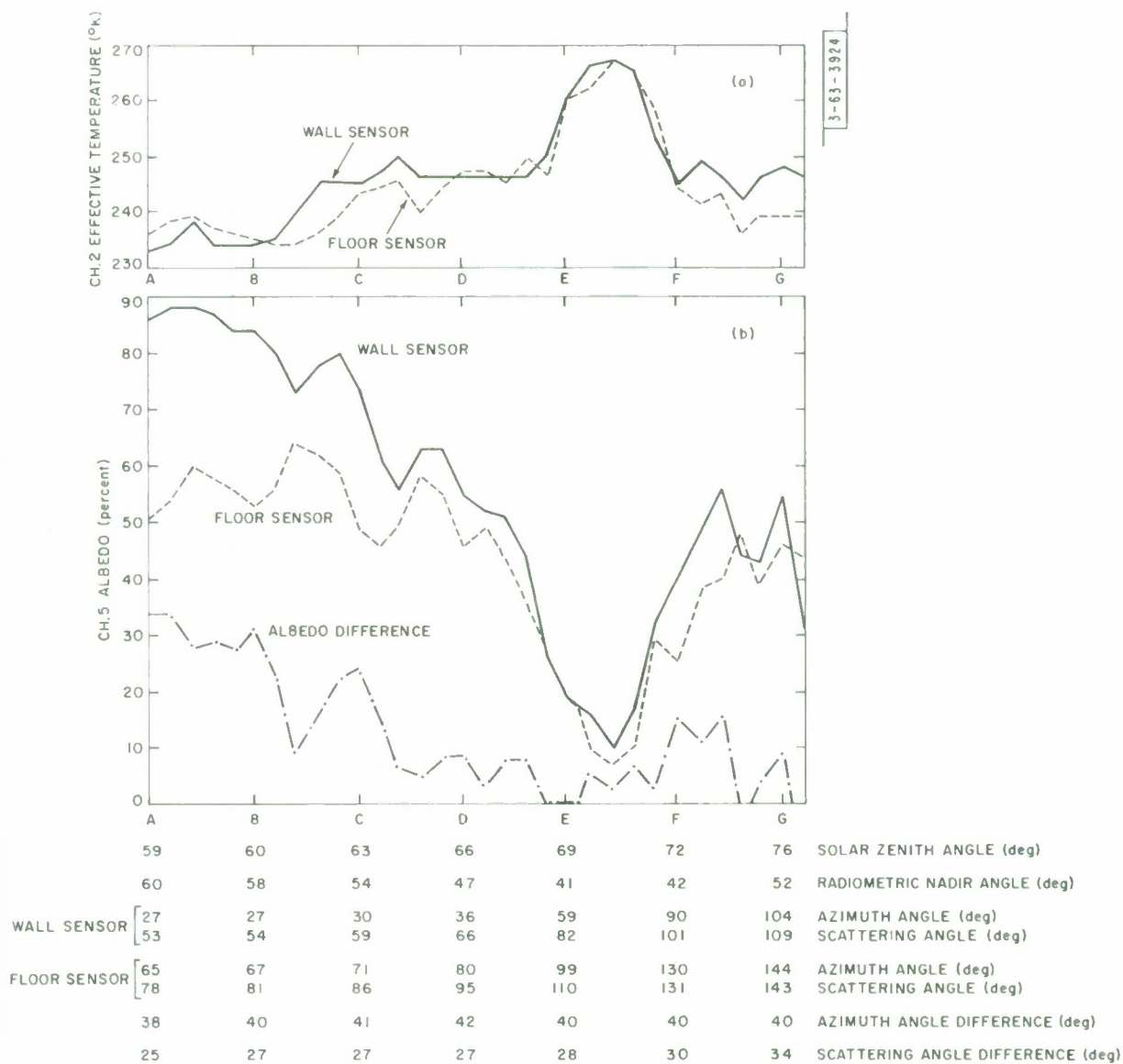
13

Figure 9. Comparison of Data from the Wall and Floor Sensors Along the
Isopleth of Zero Nadir Angle Difference
(a) Channel 2 Effective Temperatures
(b) Channel 5 Albedos and Albedo Differences

14

as the albedo increases. This is due to the fact that the tops of clouds are much colder than the less reflective underlying surface.

It would seem that a careful study of raw Tiros data could yield information on the minimum light intensities and reflected and scattered from the earth. This path of investigation was not chosen, however, because of two considerations. The spectral regions of the Tiros sensors and the sensor under consideration are different enough to make the Tiros data almost inapplicable for this study; also it has been noticed that many authors tend to disregard Tiros-derived albedos whenever they fall below the albedo that can be expected from scattering by a Rayleigh atmosphere. As an example one author found the albedo of a point over ocean to be 6%. For the same geometry and for approximately the same spectral regions the albedo of a standard atmosphere with Rayleigh scattering and zero surface reflectivity deduced by computations by K. L. Coulson is 8%. It is stated that the difference is dependent on the degradation of the instrumental response, although a proper evaluation should include the effects on the Rayleigh albedo of molecular absorption and the scattering and absorption by aerosols.

RAYLEIGH SCATTERING

The problem of atmospheric scattering is not an easy one and has been tackled only recently by Chandrasekhar in his book on Radiative Transfer.[5] The equations which he introduces have been tabulated by K. L. Coulson in his various publications on scattering by a Rayleigh atmosphere. Some of his results and the results of others working along similar lines are discussed in the succeeding pages.

The values that follow have been computed for parallel unpolarized radiation of net flux π per unit area incident on the top of an idealized plane parallel atmosphere. The atmosphere is assumed to be uniform and infinite in the horizontal, non-absorbing, composed of scattering centers which are small compared with the wavelength of the light, and of finite optical thichness.

For the sun at a given zenith angle θ_0 the total outward flux from the top of the atmosphere in a unit frequency interval and unit time is given by

$$D_\nu = \int_0^{2\pi} \int_0^{\pi/2} I_\nu (\theta, \varphi) \sin \theta \cos \theta \, d\theta \, d\varphi$$

θ, φ, and θ_0 are defined by Fig. 1 with Z replaced by θ_0. $I_\nu (\theta, \varphi)$ is a tabulated function.

The spectral albedo or the monochromatic reflectance is

$$R_\nu = \frac{D_\nu}{\pi \mu_0}$$

where

$$\mu_0 = \cos \theta_0$$

Below, R_ν is tabulated for various wavelengths and zenith angles.

Table III is represented graphically in Fig. 10. The values indicate the reflectance increases for decreasing wavelength at all sun elevations due to the inverse fourth power dependence of Rayleigh scattering.[5]

TABLE III

Reflectance of the Atmospheric Model at Various Wavelengths for Representative Values of Sun Elevation and Surface Reflectivity. (Lambertian reflector)[*6]

A	μ_o	λ3150A	4000	5000	6000	7000	8000
0	0.02	0.754	0.638	0.565	0.503	0.430	0.325
0	0.10	0.705	0.552	0.396	0.247	0.154	0.094
0	0.40	0.550	0.304	0.152	0.079	0.044	0.024
0	0.80	0.400	0.181	0.085	0.039	0.022	0.013
0	1.00	0.345	0.148	0.068	0.033	0.017	0.009
0.25	0.02	0.791	0.712	0.665	0.625	0.574	0.494
0.25	0.10	0.752	0.643	0.536	0.427	0.362	0.319
0.25	0.40	0.623	0.445	0.345	0.298	0.276	0.285
0.25	0.80	0.492	0.347	0.293	0.271	0.260	0.257
0.25	1.00	0.450	0.322	0.280	0.264	0.256	0.255
0.80	0.02	0.922	0.910	0.904	0.896	0.885	0.865
0.80	0.10	0.918	0.892	0.866	0.842	0.826	0.815
0.80	0.40	0.860	0.830	0.812	0.805	0.803	0.800
0.80	0.80	0.811	0.798	0.798	0.798	0.798	0.799
0.80	1.00	0.794	0.792	0.794	0.796	0.798	0.799

* Note a more complete table by Coulson is given in Appendix I.
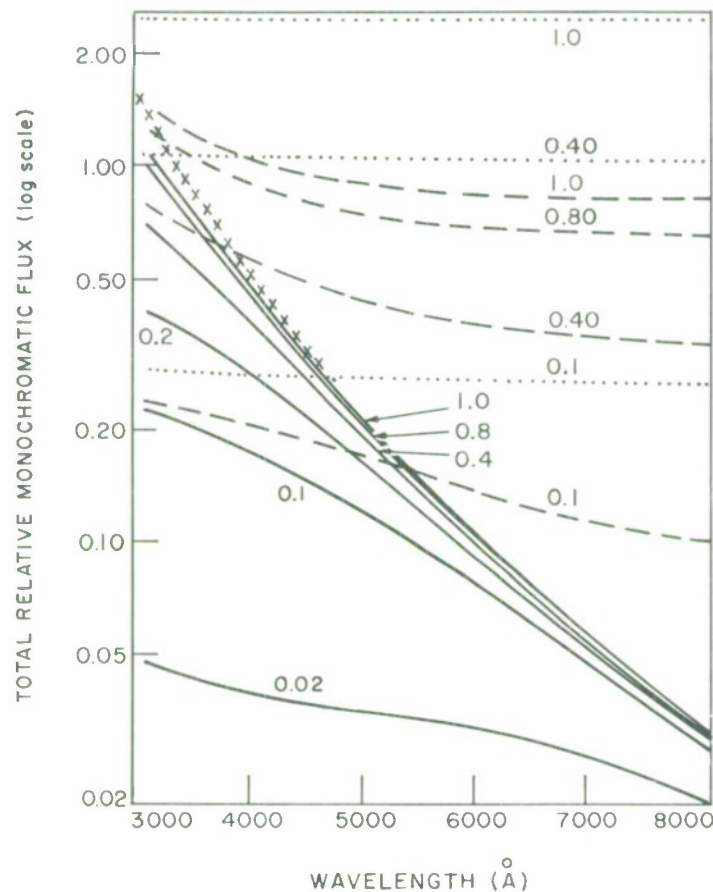
Figure 10. Total relative monochromatic flux emerging from the top of the atmosphere as a function of wavelength, for various sun elevations and three values of surface reflectivity: A = 0 (solid curves), A = 0.25 (dashed curves) and A = 0.80 (dotted curves). Curves are labeled with values of μ_o. A curve (X) for primary Rayleigh, scattering and no attenuation is included for comparison.

18

This graph, however, is only relative and assumes all the incident flux to be the same at all wavelengths. If we assume a source with the same variation with wavelength as the sun the graph of Fig. 11 is obtained.[6]
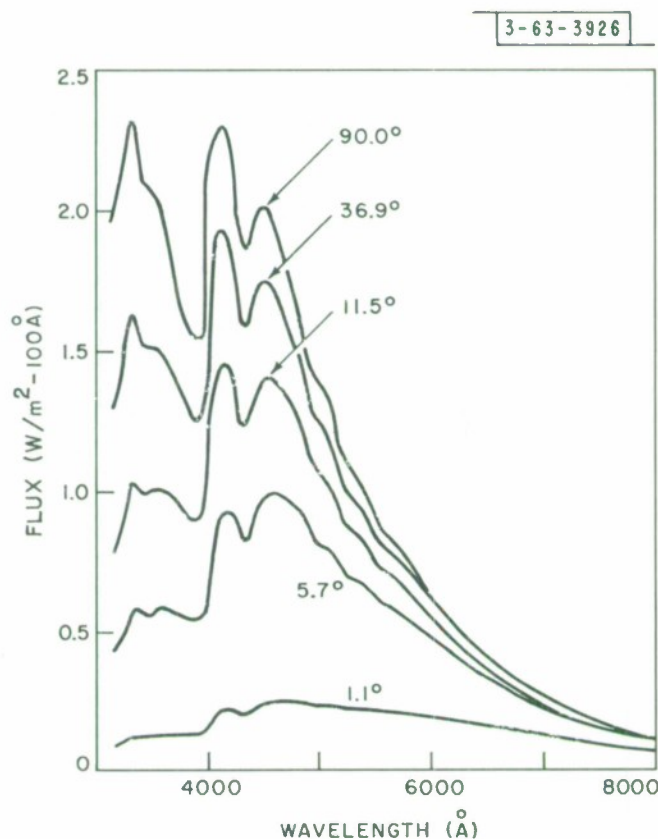
Figure 11. Absolute monochromatic flux from the top of the model atmosphere as a function of wavelength, for zero surface reflectivity and five different sun elevations (μ_o = 1.0, 0.40, 0.20, 0.10, 0.02; A = 0)

Using the graphs of Fig. 11 the albedo for a plane parallel earth as a function of sun elevation for the spectral region 3200 A $\leq \lambda \leq$ 8000 A can be obtained. The results obtained by Coulson[6] are plotted in Fig. 12 and tabulated in Table IV.

TABLE IV

Values and Comparisons of the Total Absolute Flux for $3200 \overset{o}{A} \leq \lambda \leq 8000 \overset{o}{A}$ at Six Different Sun Elevations. (Units of flux: W/m^2)

Sun elevation	1.1^o	5.7^o	11.5^o	23.6^o	53.1^o	90.0^o
F_o	15.4	77.0	154.0	307.9	615.8	769.9
$(J)_o$	8.0	25.0	34.3	44.0	48.9	51.8
$(J)_{25}$	9.7	37.1	62.4	103.6	179.9	214.8
$(J)_{80}$	13.7	65.9	128.3	249.6	488.6	609.6
$(\alpha)_0$	0.519	0.325	0.223	0.143	0.079	0.067
$(\alpha)_{25}$	0.630	0.482	0.405	0.336	0.292	0.279
$(\alpha)_{80}$	0.890	0.856	0.833	0.811	0.793	0.792
$(F_{0g})_0$	7.4	52.0	119.7	263.9	566.9	718.1
$(F_{0g})_{25}$	7.6	53.2	122.1	272.4	581.2	740.1
$(F_{0g})_{80}$	8.5	55.5	128.5	291.5	636.0	801.5

* F_o : Incident flux on horizontal surface at top of atmosphere.

$(J)_A$: Emergent flux through horizontal surface at top of atmosphere. (Subscript A represents value of surface reflectivity: 0.025 or 0.80).

$(\alpha)_A$: $\dfrac{(J)_A}{F_0}$ = Albedo: ratio of emergent to incident flux.

$(F_{0g})_A$: Flux incident on horizontal surface at ground.
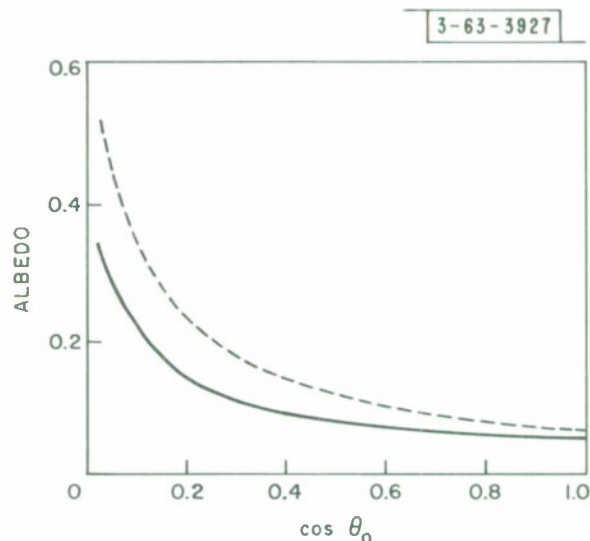
Figure 12. Approximated albedo for the entire solar spectrum (solid curve) and computed albedo for the spectral range 3200 Å $\geq \lambda \geq$ 8000 Å (dashed curve) as a function of sun elevation (A = 0).

Coulson also did a calculation of the planetary albedo of the spherical earth due to atmospheric scattering. The disk of the earth was divided into concentric plane parallel rings and the sun elevation for each ring was considered constant. A value of 7.6% was obtained for the entire spectrum. This value is reduced by ozone absorption in the region near and below 3000 Å. The corrected albedo for this more realistic case is given as 6.9%.

Some additional graphs computed by Coulson in a later publication[7] for a plane parallel atmosphere with a Lambertian surface at the bottom are presented in Figs. 13 - 17. Figures 13 - 15 are a graphical representation of the values tabulated in Appendix I. It can be easily seen that the atmosphere itself scatters back a large portion of the short-wavelength radiation especially for the larger solar zenith angles, and that at longer wavelengths and smaller solar zenith angles the effect of the reflectance of the underlying surface becomes predominant. Figures 16 - 17 show the strong dependence of system reflectance for large solar zenith angles particularly pronounced for small values of A (for the entire solar spectrum (Fig. 16) and for 3 spectral regions (Fig. 17)).
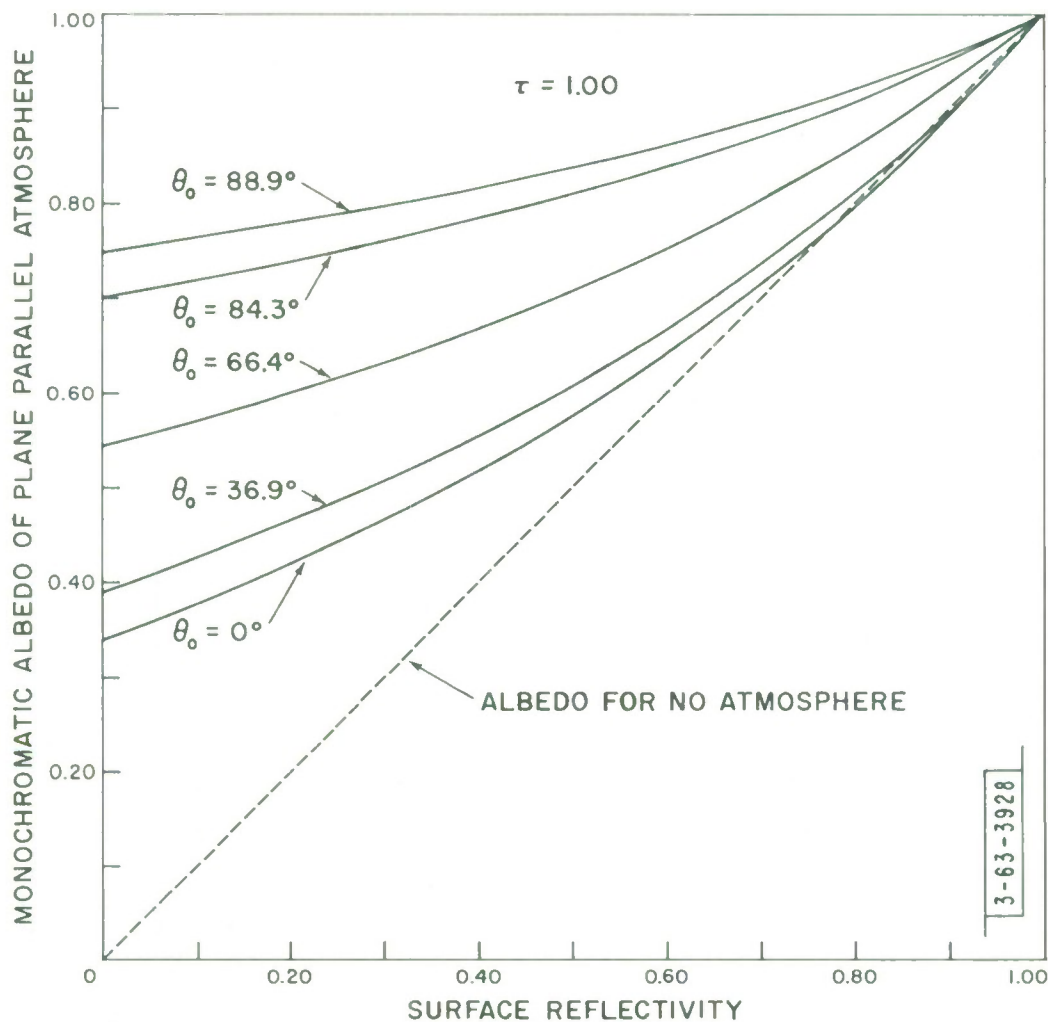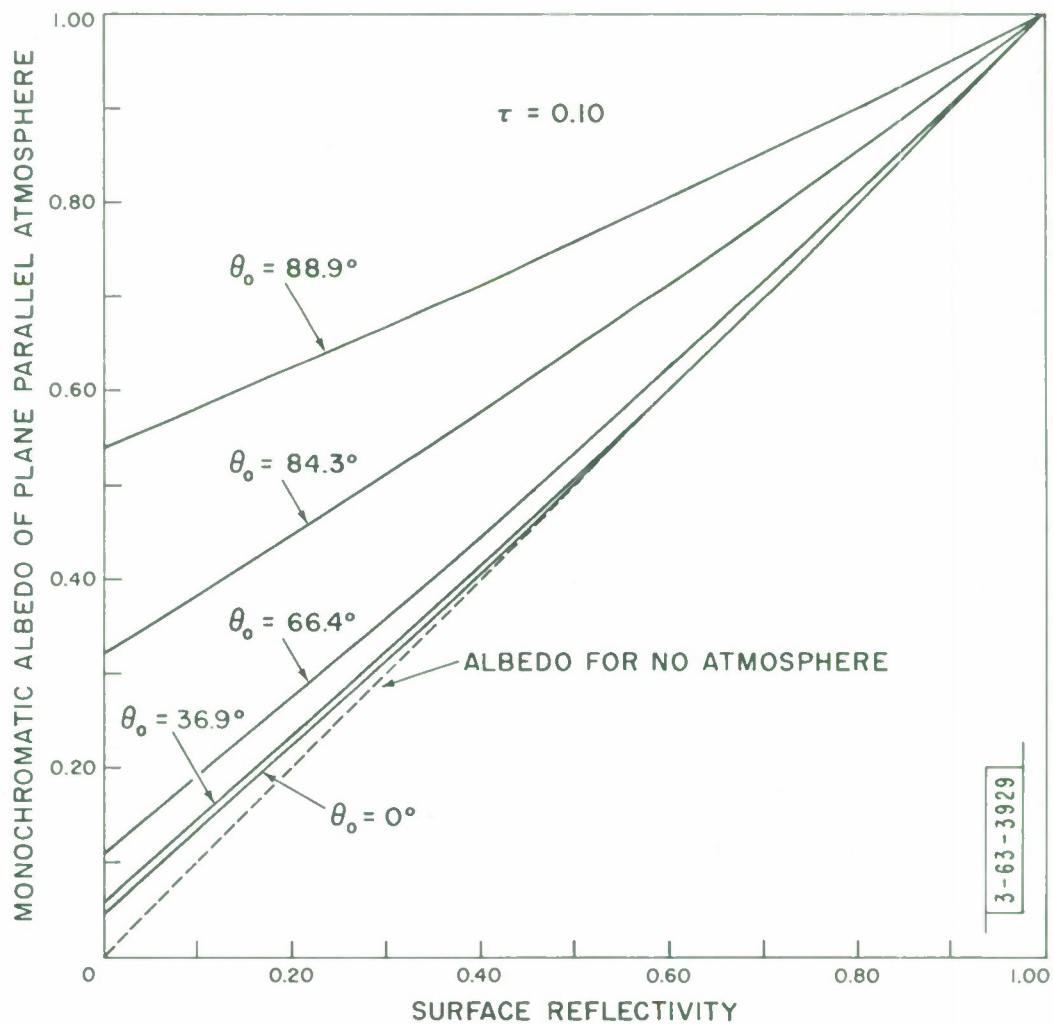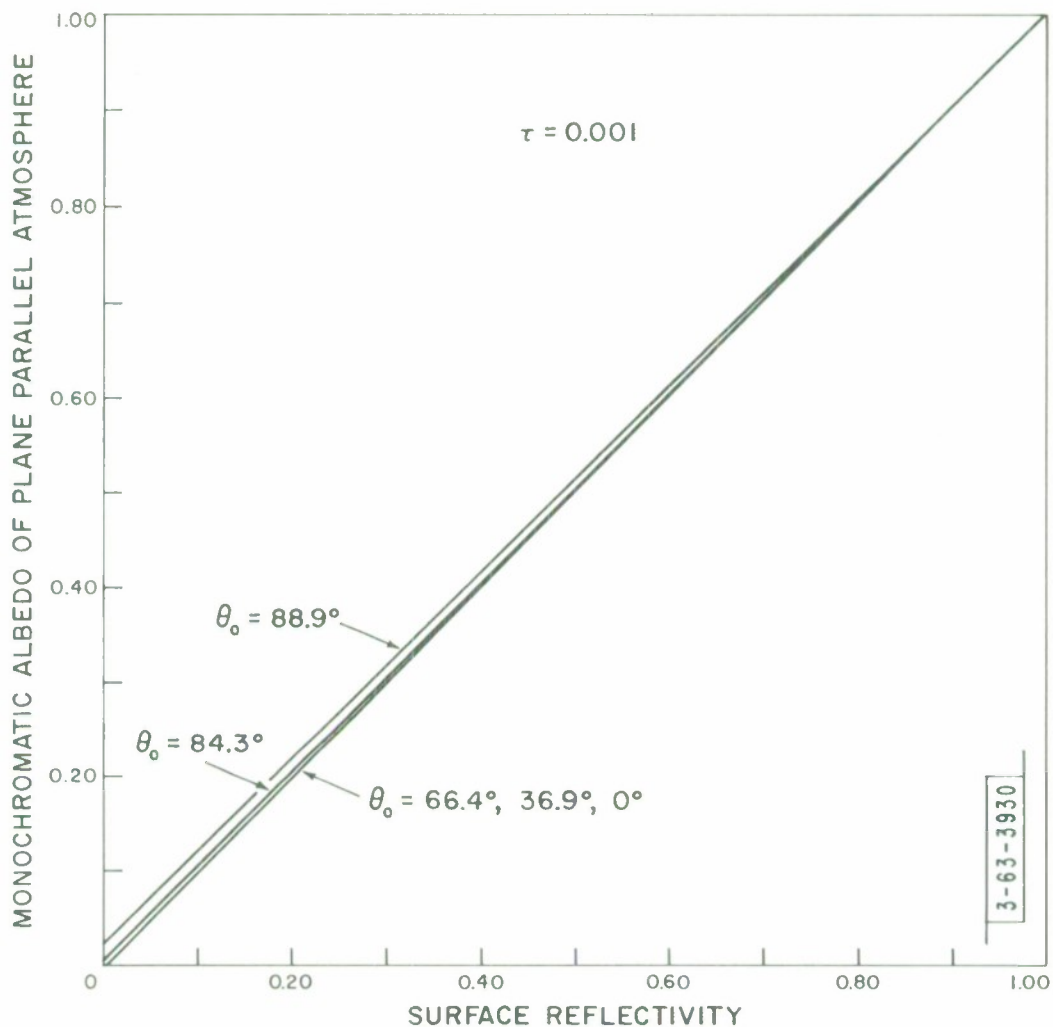
Fig. 13 Monochromatic reflectance of model atmosphere-plus-surface system as a function of surface reflectivity for optical thickness $\tau = 1.00$ for five different solar zenith angles $\tau = 1.00$, corresponding to wavelength $\lambda = 3120$ Å at sea level.
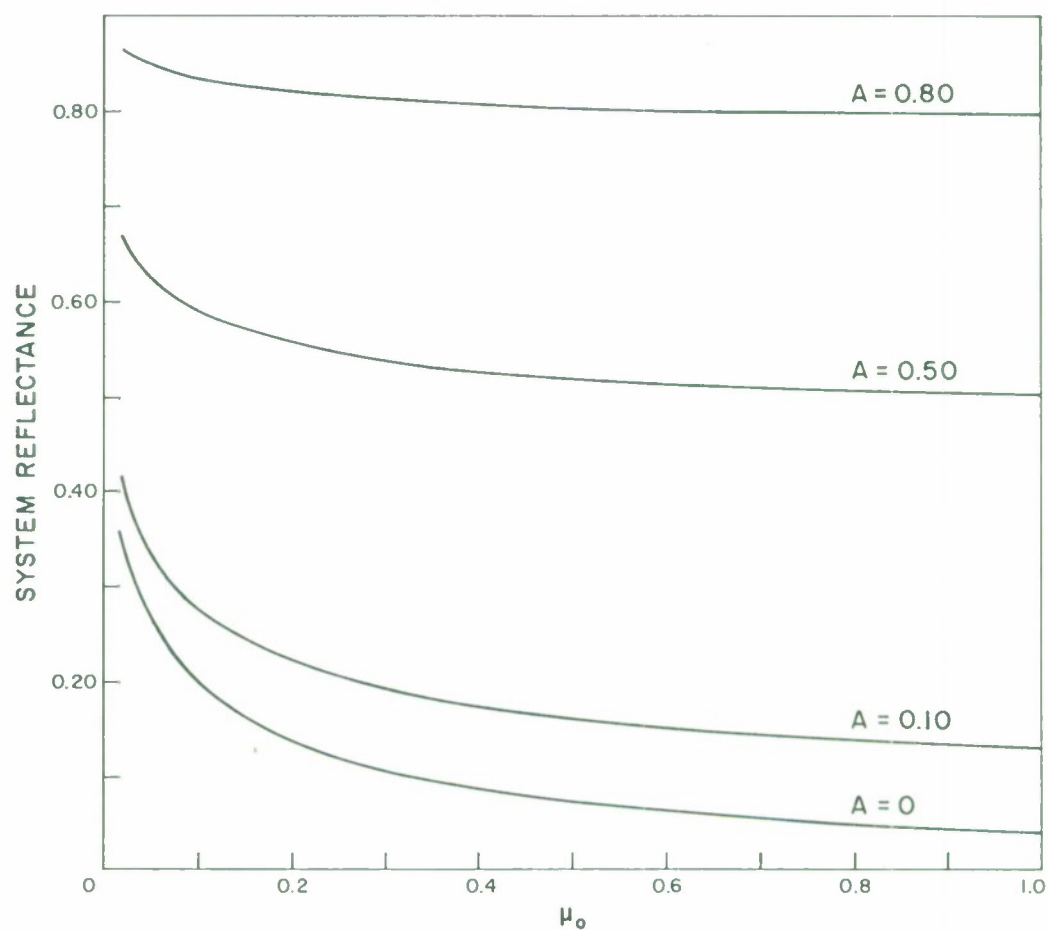
Fig. 14 Monochromatic reflectance of model atmosphere-plus-surface system as a function of surface reflectivity for optical thickness $\tau = 0.10$ for five different solar zenith angles $\tau = 0.10$, corresponding to wavelength $\lambda = 5460$ Å.

Fig. 15 Monochromatic reflectance of model atmosphere-plus-surface system as a function of surface reflectivity for optical thickness $\tau = 0.001$ for five different solar zenith angles $\tau = 0.001$, corresponding to wavelength $\tau = 17,000$Å.

Fig. 16 Reflectance of model atmosphere-plus-surface system as a function of cosine of solar zenith angle μ_o for spectral interval 3100 $\overset{o}{A} \leq \lambda \leq 25,000$ $\overset{o}{A}$ for different values of surface reflectivity.
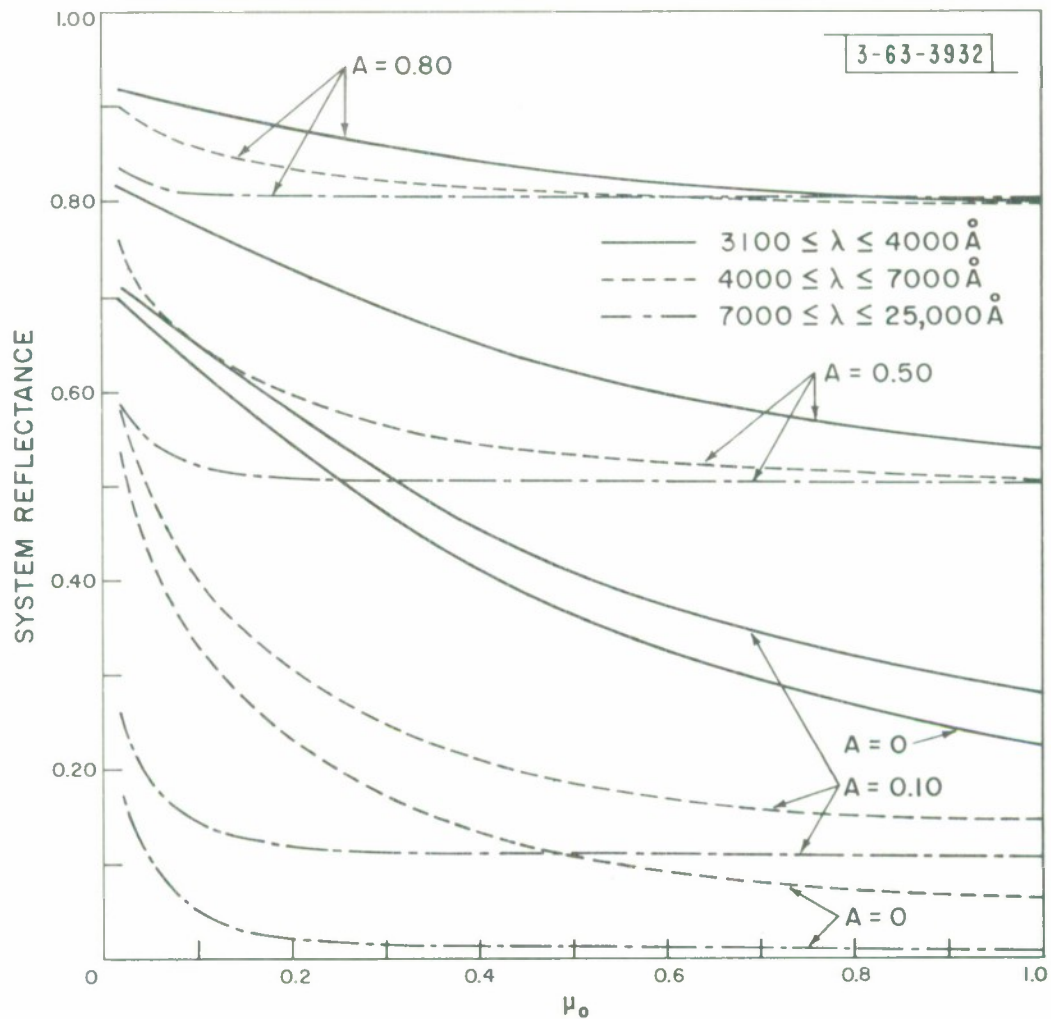
Fig. 17 Reflectance of model atmosphere-plus-surface system as a function of cosing of solar zenith angle μ_o, with spectrum divided into ultraviolet (3100 $\overset{\circ}{A} < \lambda < 4000$ $\overset{\circ}{A}$), visible (4000 $\overset{\circ}{A}$), and infrared (7000 $\overset{\circ}{A} < \lambda < 25,000$ $\overset{\circ}{A}$)

The graphs and tables that have been presented so far, for the most part, have indicated the total amount of light reflected from the plane-parallel atmosphere. Relatively little information has been presented about the expected minimum light conditions at various configurations of observer, viewed spot and source. The material on the succeeding pages will provide information on the expected intensities and "backscatter coefficients" of the reflected and scattered light.

Some of the results are presented in a form which makes it necessary to discuss briefly the concept of optical thickness, τ. τ is defined as

$$\tau = \int_{o}^{z_o} n(z)\, \sigma_\lambda(z)\, dz$$

where

n = number of scattering centers/unit volume

σ_λ = scattering cross-section

z_o is usually taken as the height of the atmosphere

Then the intensity of light on the ground is

$$I = I_o\, e^{-\tau}$$

τ is related to λ by the following Table (Table V) and Fig. 18.

TABLE V

1.00	.50	.25	.15	.10	.05	.02
3120	2715	4365	4950	5460	6440	8090

All graphs in Figs. 19 and 20 take into account the effect of primary and multiple scattering (unless otherwise indicated) and increased path lengths for oblique rays. The relative intensities indicated on the graphs are relative to an incident intensity of 1.0.
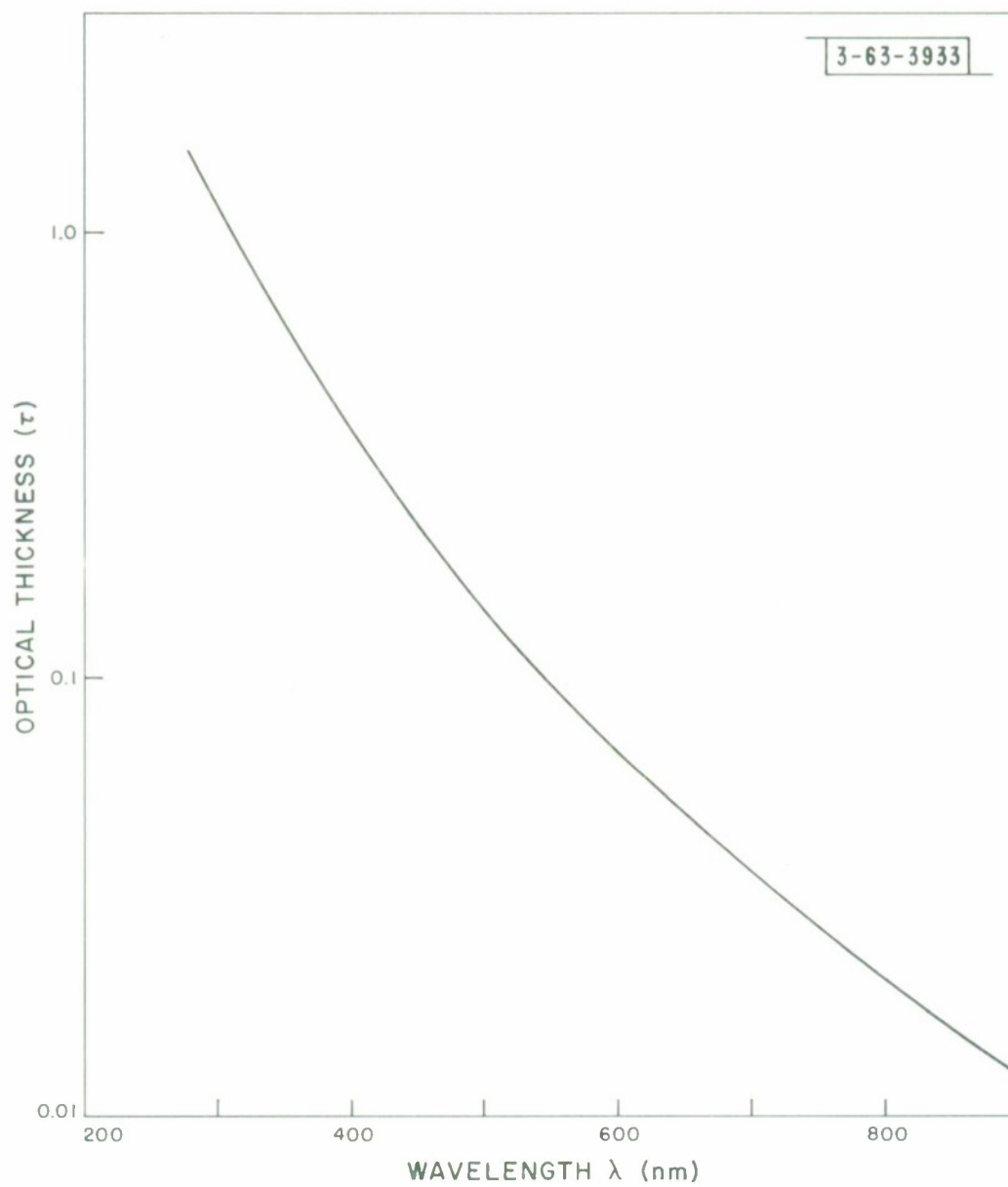
Fig. 18 Optical thickness of the earth's atmosphere as a function of wavelength.
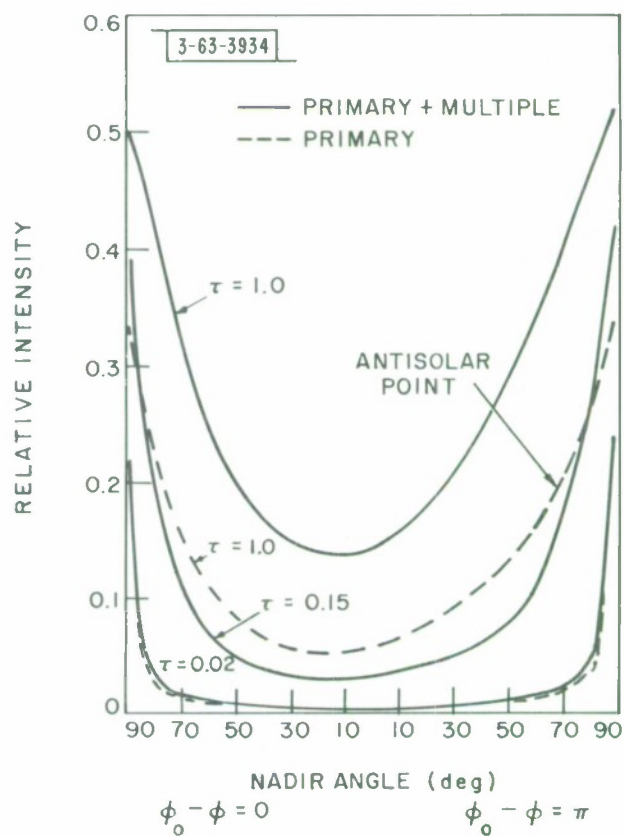
Figure 19. Relative intensity for three different values of optical thickness as a function of direction in the sun's vertical. Dashed curves are primary scattering only; solid curves include higher order scattering ($\theta_o = 66.3^\circ$, $A = 0$).
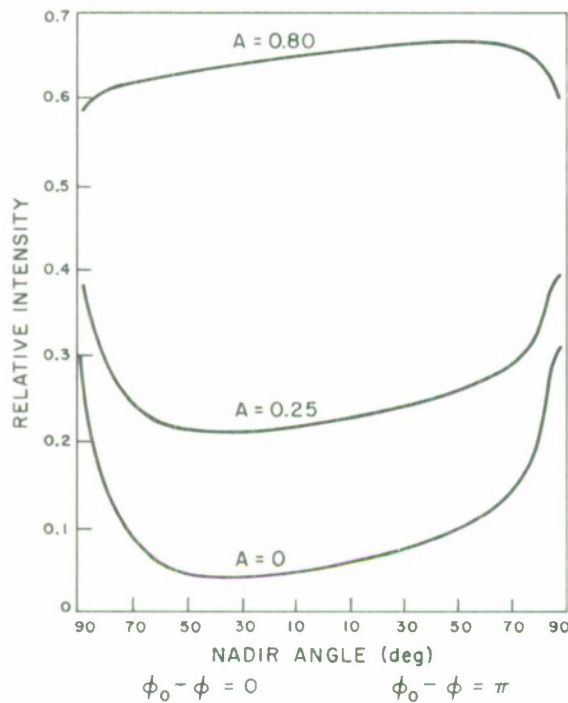
Figure 20. Relative intensity as a function of direction in the sun's vertical, for moderate optical thickness, sun elevation 53° and three values of surface reflectivity ($\tau = 0.15$, $\theta_o = 36.9^O$).

The plot in Fig. 20 shows that for moderate optical thickness the surface reflected light may constitute the major part of the emergent light. For values of A approaching 1 the surface begins to look like a Lambertian surface. For higher optical thickness the reflectivity is relatively less dominant but very important, even for optical thickness near 1.0.

In a recent paper by William Snoddy[8] the case of the plane-parallel atmosphere was extended for a spherical earth. The portion of the earth visible at a particular altitude was divided into 400 plane parallel sections and the

30

intensity computed for each section. The irradiation incident on a differential element at a given altitude was computed and compared to the irradiation expected if the earth were a diffuse surface to obtain an "effective albedo". Note that this definition is different from the other definitions of albedo presented earlier and could have extensive use with an earth sensor of very wide aperture. The geometry of the situation is presented in Figs. 21 - 22.

Towards the limb of the earth, incident light travels through a smaller air mass than if the atmosphere were plane-parallel. The air mass through which an incident beam will travel has been calculated by Bemporad and the air mass is given in Fig. 23 together with the air mass for a plane parallel atmosphere. This graph is used to correct the data obtained for a plane parallel atmosphere for large angles of incidence.

Figures 24 - 56 are plots of intensity over the planetary sphere with isophotes drawn through the points of equal intensity. The sun moves to the right along the horizontal diameter of the circles. The differential element is above the center of the circles.

Figures 24 - 30 illustrate the variation as a function of θ_o with $H = 10^6$ km, $\tau = 1.0$ ($\lambda = 3120$ A) and $A = 0$. Figures 31 - 37 show the same variation with θ_o but have $H = 10^3$ km. Variation of intensity with altitude is illustrated in Figs. 38 - 42. Maps showing the effect of the reflectance of the underlying surface are given for an altitude of a million kilometers (Figs. 43 - 45) and a thousand kilometers (Figs. 46 - 48).

Perhaps the most interesting maps from the point of view of using a light sensor with a broad rather than a line bandwidth are the maps showing variation in intensity with optical thickness and hence wavelength. Examples are shown for $\tau = 1.0$, 0.5, 0.25, 0.1, $\theta_o = 30^o$; $A = 0$ and $H = 10^6$ km (Figs. 49 - 52) and 10^3 km (Figs. 53 - 56).

These relative values of intensity are what has been defined previously as the spectral backscatter coefficient, "b_1". The quantity $b_1 H_\lambda \, d\omega$ was then integrated over the sphere and the relative flux intensities plotted in Figs. 57 - 58. As the reflectance of the underlying surface is increased, the maximum flux intensity shifts away from the ultraviolet towards the maximum of the sun.

The spectral effective albedo of the earth is shown in Fig. 59 for $H = 10^3$ km and three values of A. It should be realized that this graph is valid only for the given altitude. In Figs. 60 - 61 the effective albedo for the spectral region between 3050 and 8050 $\overset{\text{o}}{\text{A}}$ (graphs 1) and for the entire spectrum (graph 2) were calculated as a function of A and H for two values of θ_o.

ELEMENT

γ

NORMAL

NORMAL TO
SECTION

h

SUN

$\cos^{-1}\mu$ $\cos^{-1}\mu_0$

α

ONE OF THE
400 "SECTIONS"

ϕ

δ

CENTER OF
EARTH
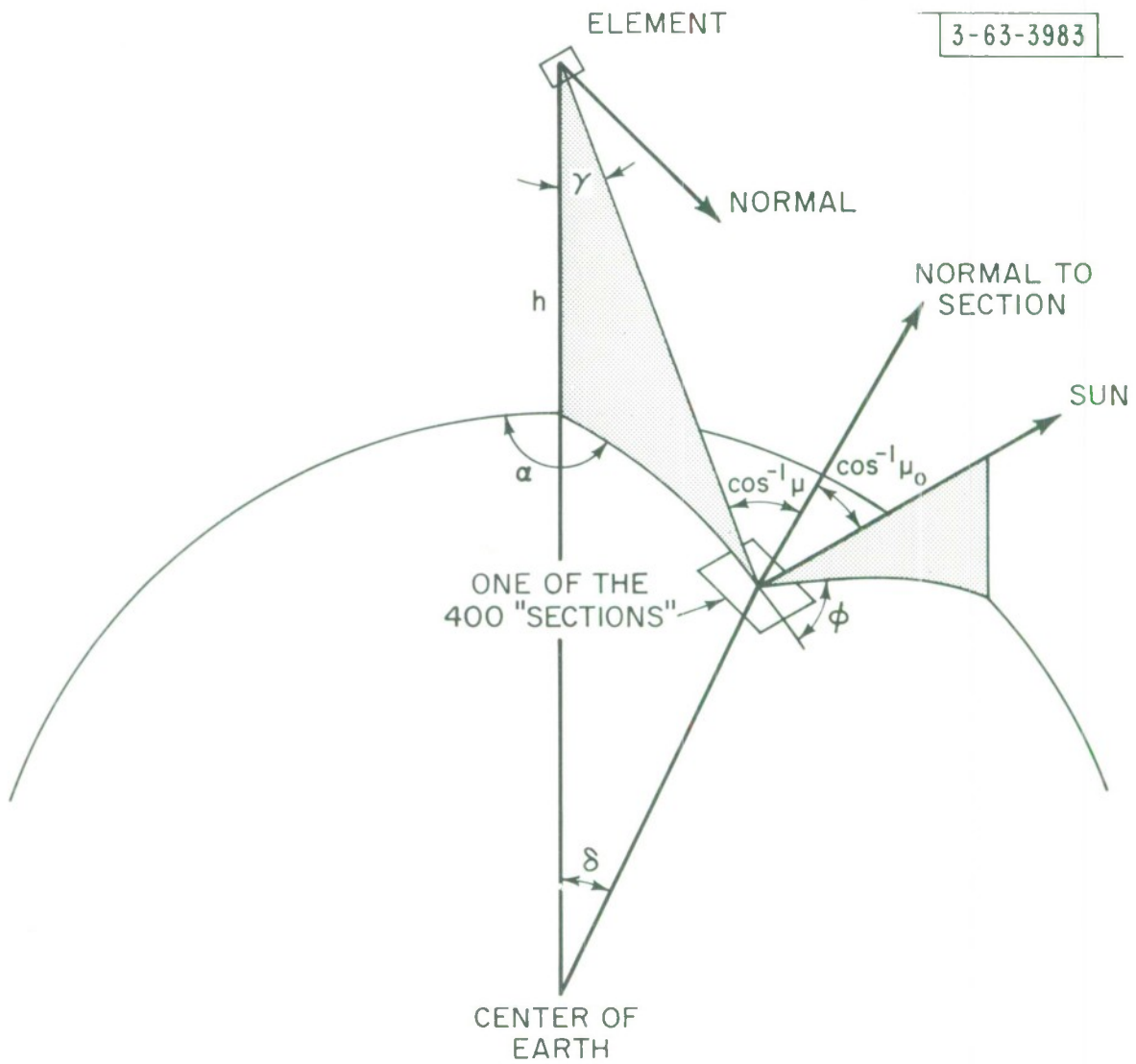
Fig. 21 Section on planet surface
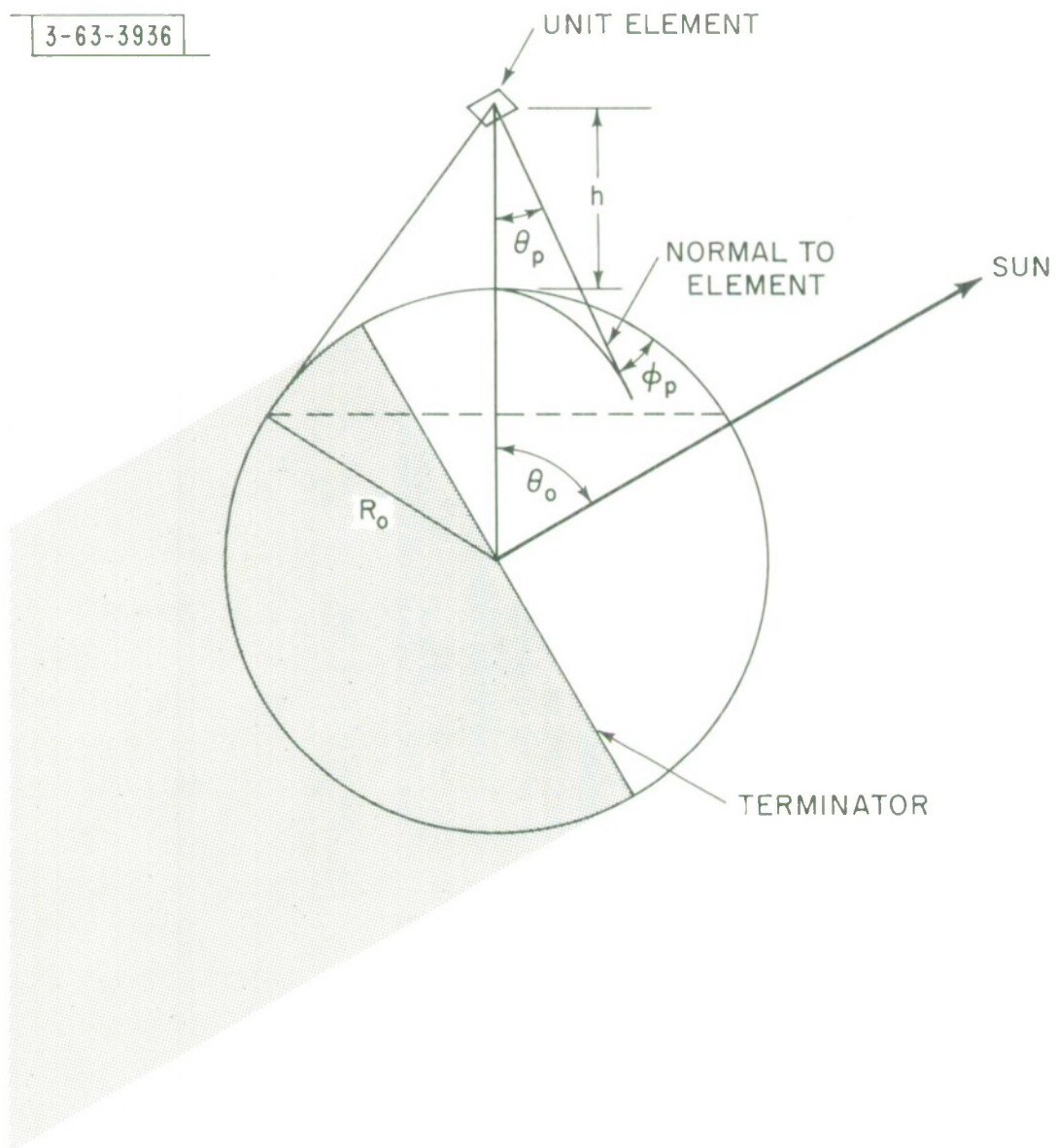
Fig. 22 Element above planet
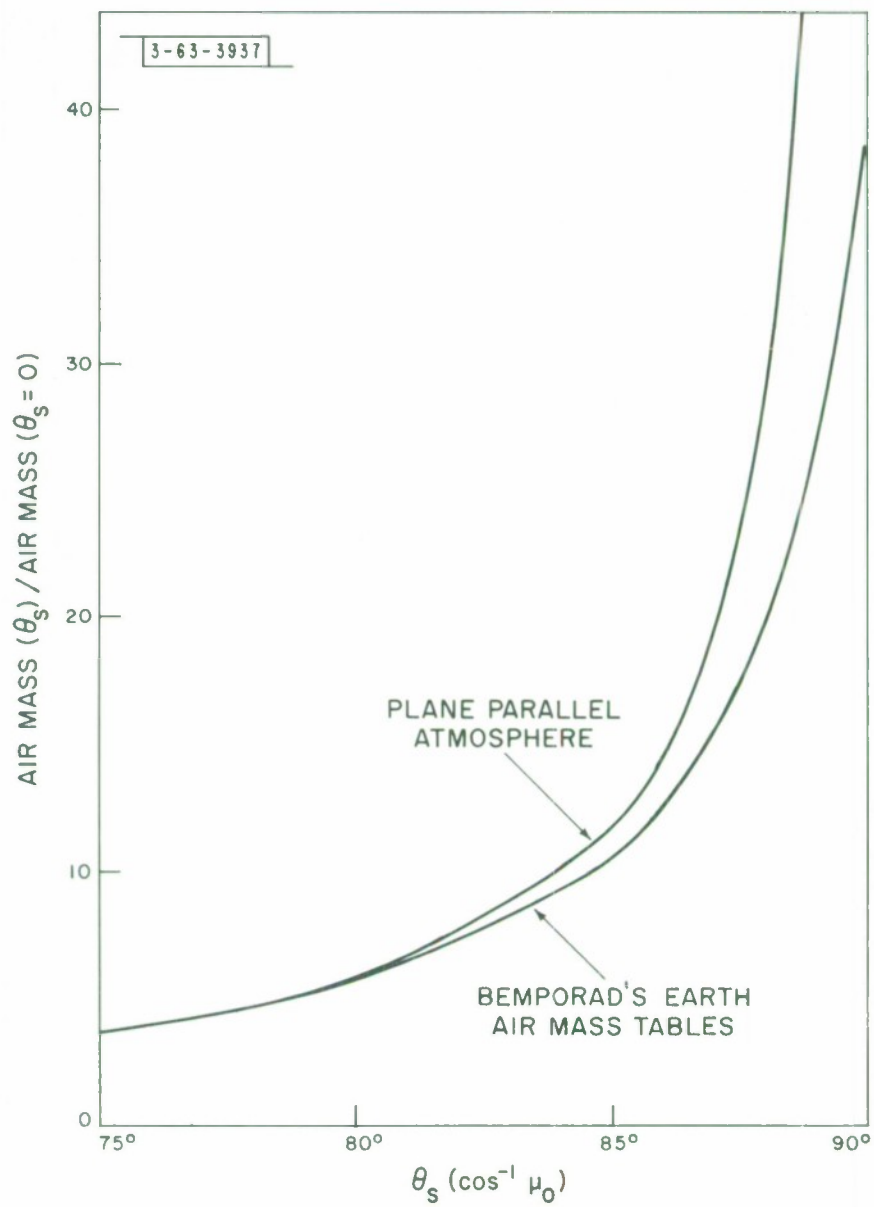
Fig. 23 Air mass as a function of angle of incidence
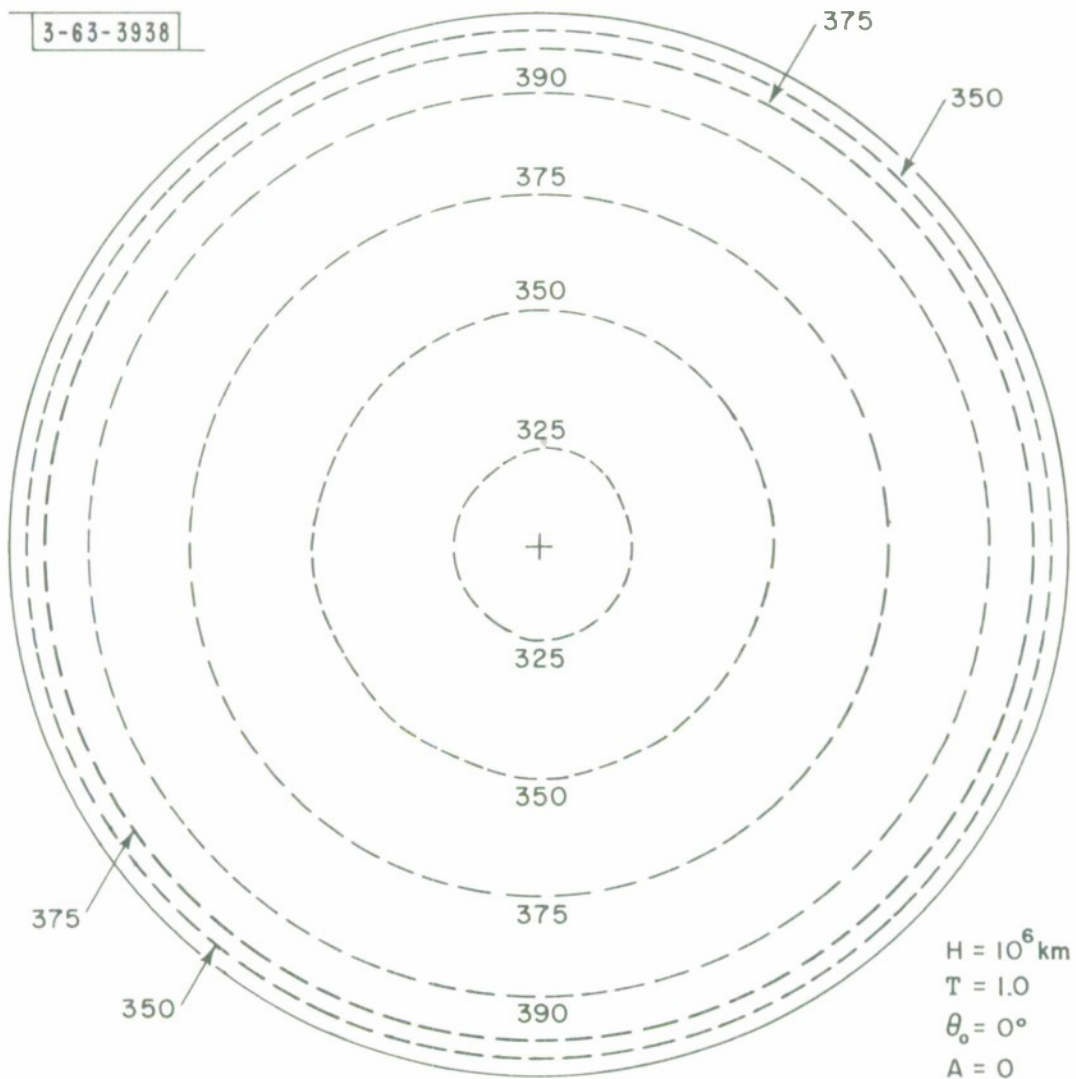
Fig. 24 Map of isophotes for $H = 10^6$ km, $\theta_o = 0$

150
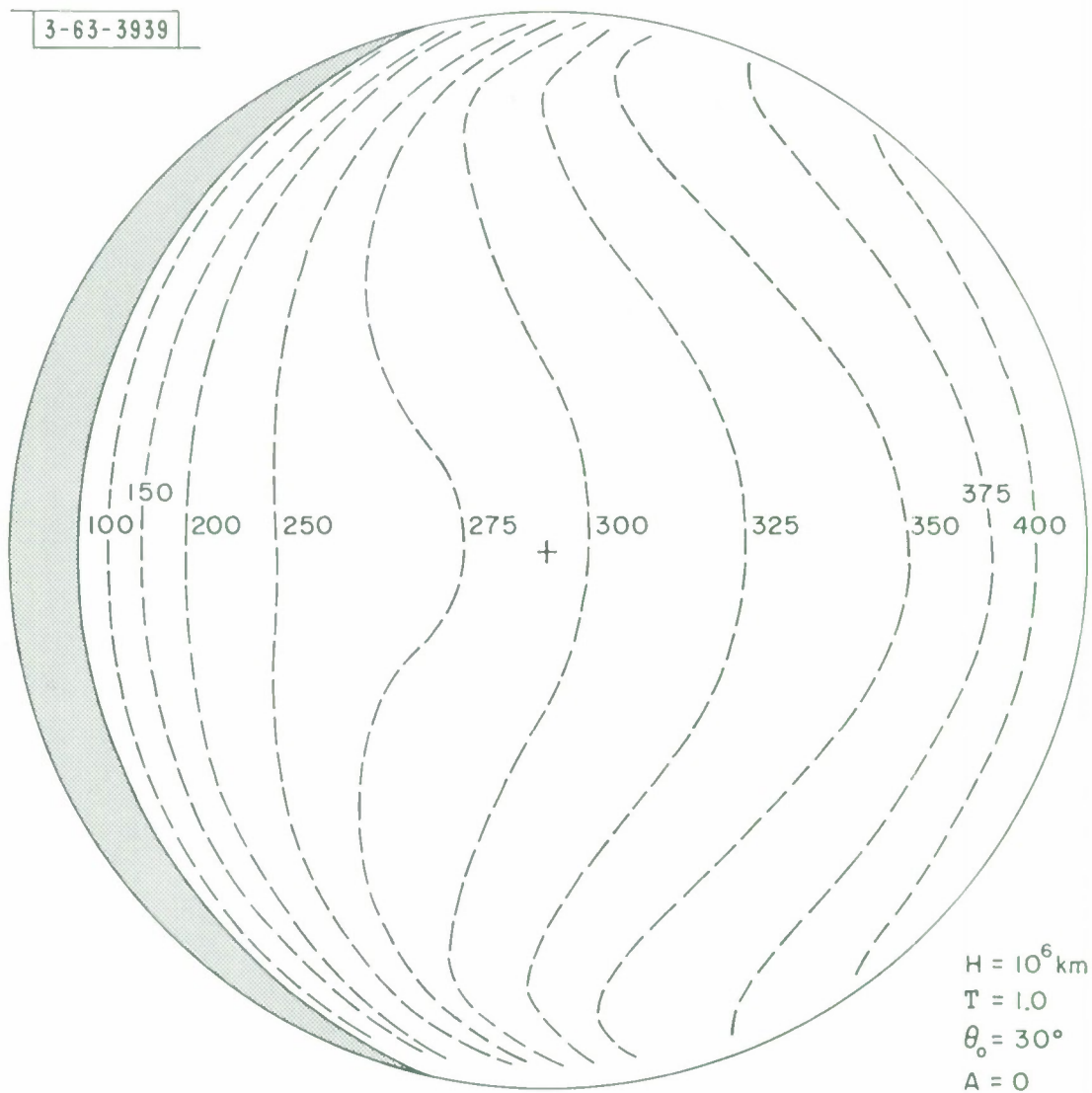100   200   250   275   300   325   350   375   400

+

$H = 10^6$ km
$T = 1.0$
$\theta_o = 30°$
$A = 0$

Fig. 25 Map of isophotes for $H = 10^6$ km, $\theta_o = 30°$

800

200
100 250   350 400   450   500 550   600 650 700   900
150   300   +   750   850
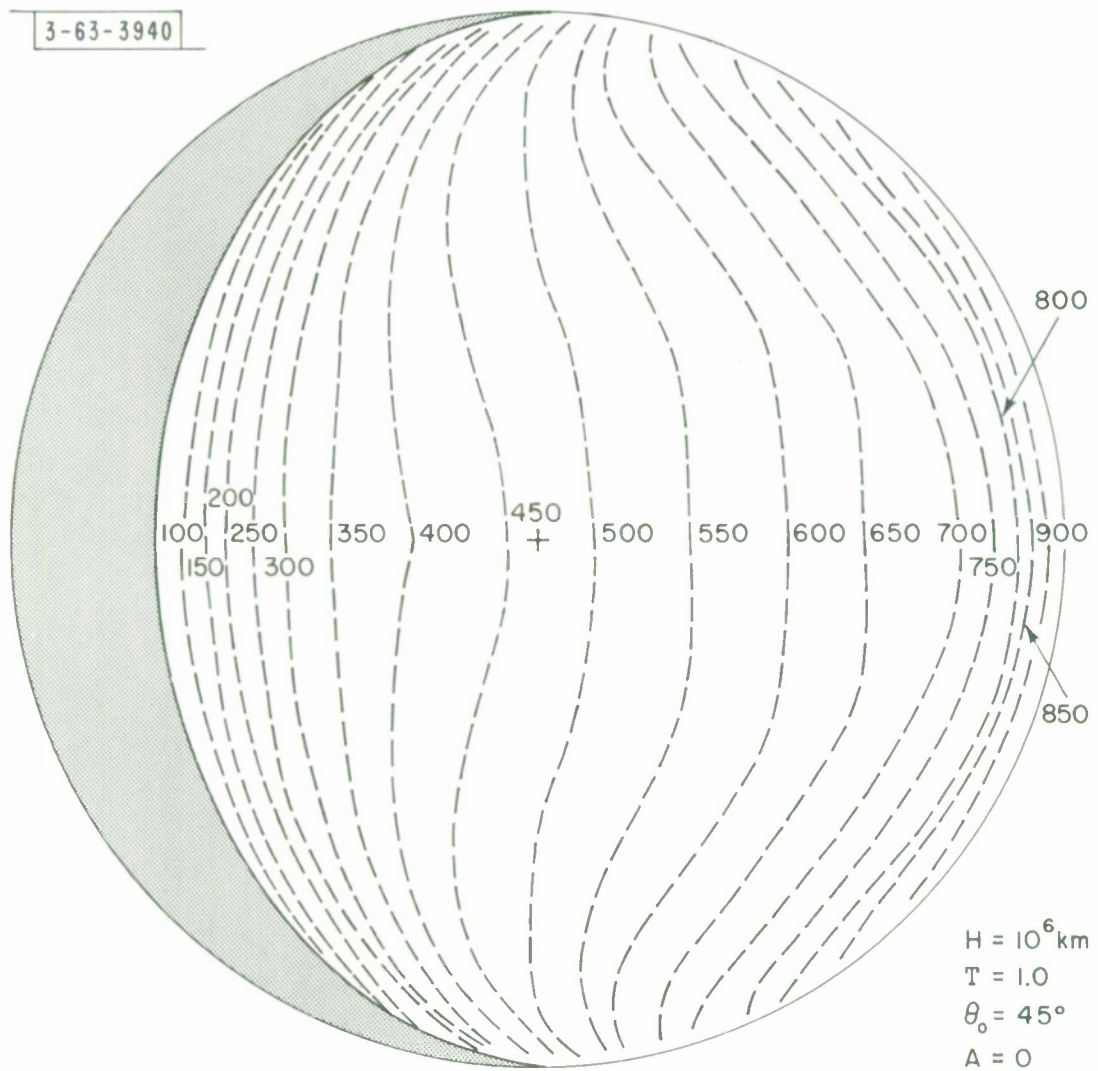
H = 10^6 km
T = 1.0
θ_0 = 45°
A = 0

Fig. 26 Map of isophotes for H = 10^6 km, θ_0 = $45°$

38

Fig. 27 Map of isophotes for H = 10^6 km, θ_o = 60°

50 100 150 200 250 300 350

H = 10^6 km
T = 1.0
θ_o = 90°
A = 0

Fig. 28 Map of isophotes for H = 10^6 km, θ_o = 90°

200 |400
100| |300|
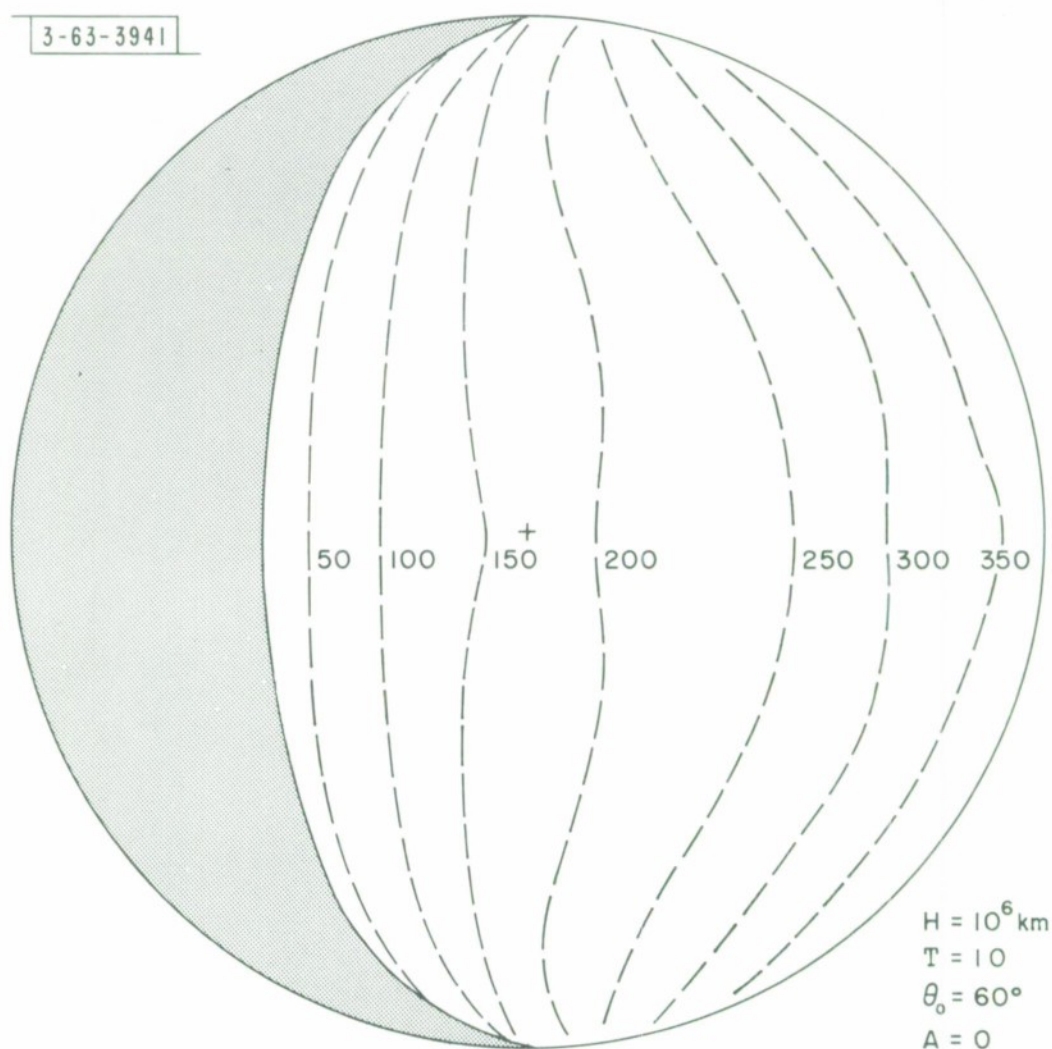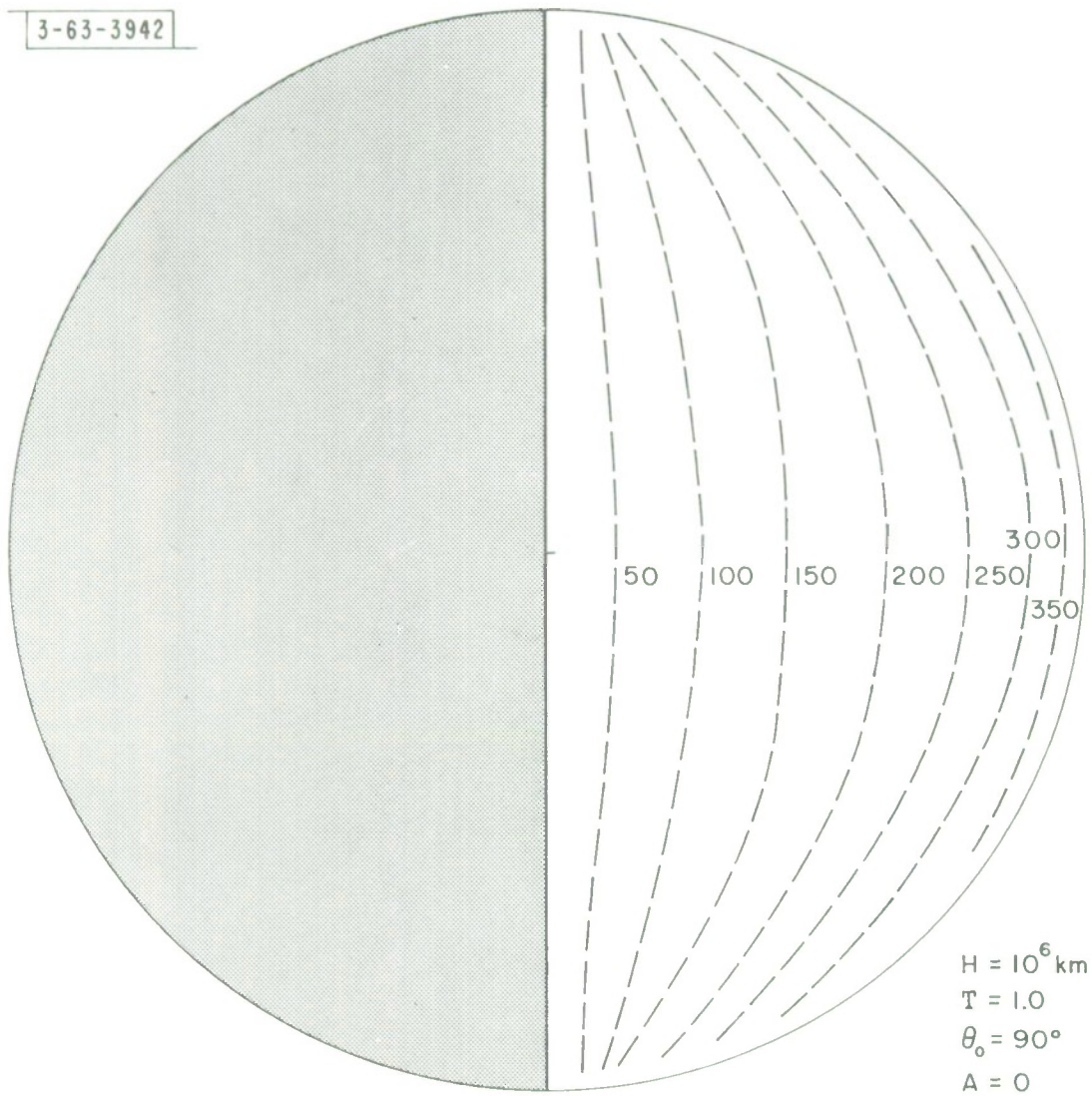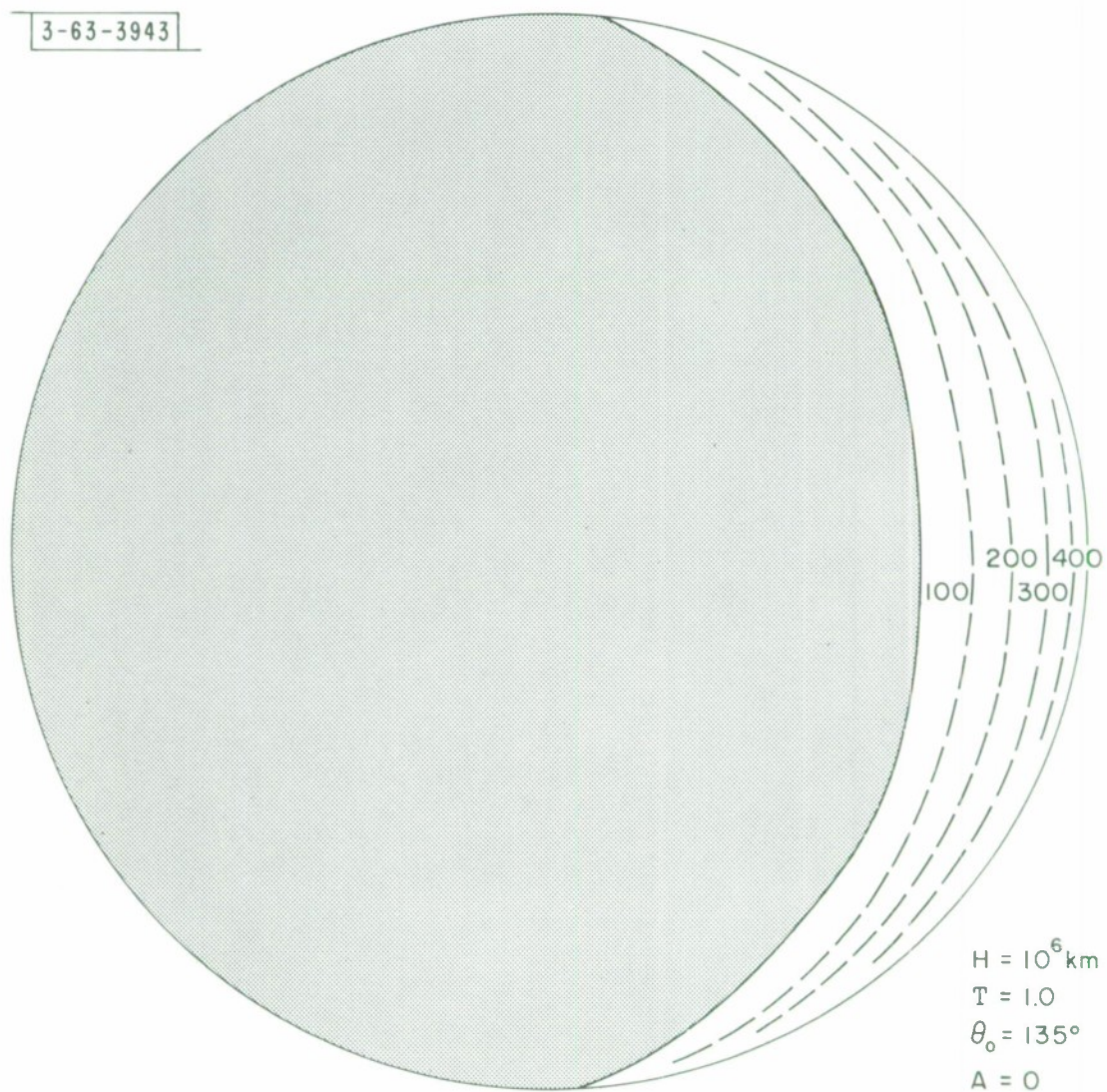
$H = 10^6 km$
$T = 1.0$
$\theta_0 = 135°$
$A = 0$

Fig. 29 Map of isophotes for $H = 10^6$ km, $\theta_0 = 135°$
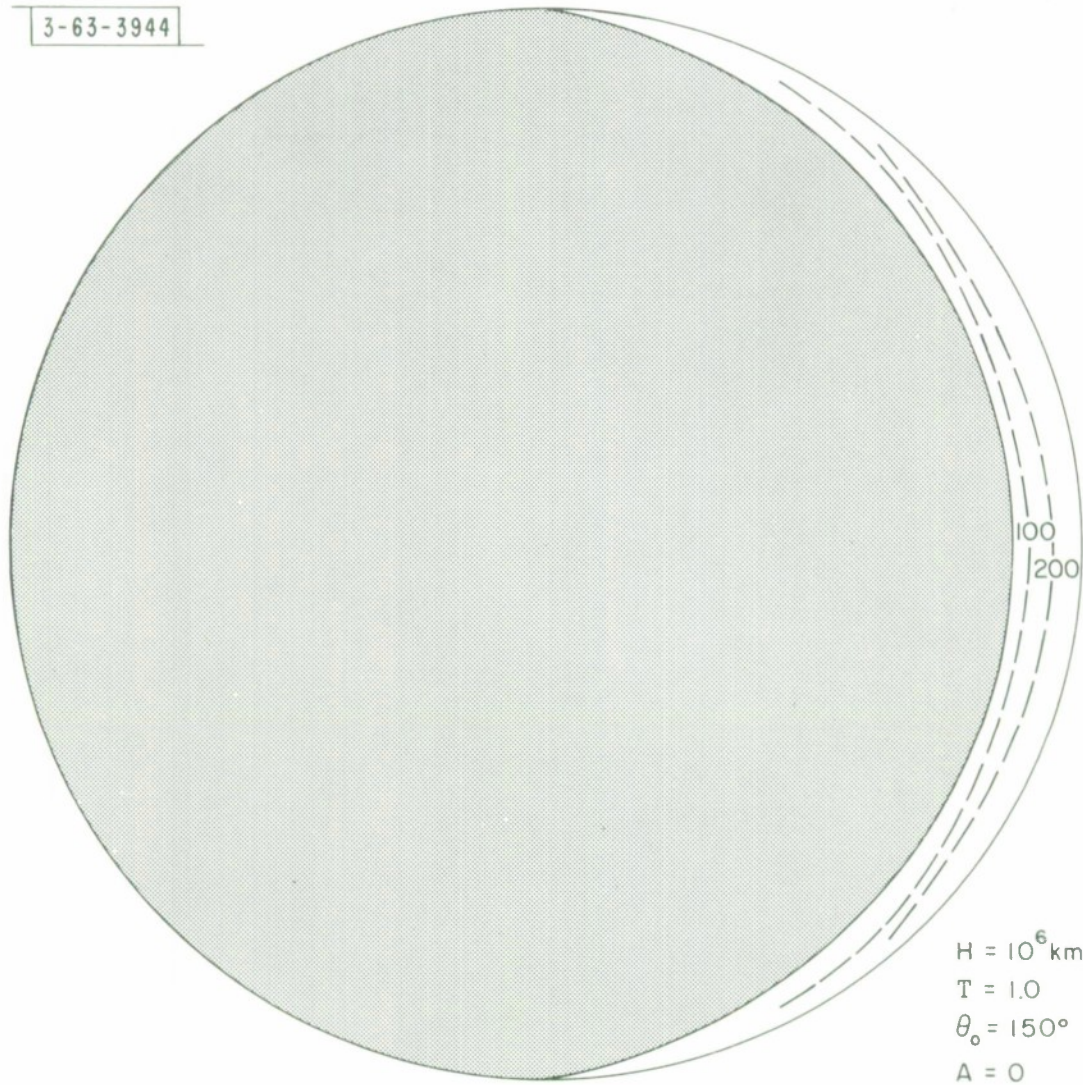
41

100
|200

$H = 10^6$ km
$T = 1.0$
$\theta_o = 150°$
$A = 0$

Fig. 30 Map of isophotes for $H = 10^6$ km, $\theta_o = 150°$

42

400 375 350 340 335   335 340 350 375 400

$H = 10^3$ km
$T = 1.0$
$\theta_o = 0°$
$A = 0$

Fig. 31 Map of isophotes for $H = 10^3$ km, $\theta_o = 0°$

500 450 400 375 350 325 + 300 275 275 300 350 325
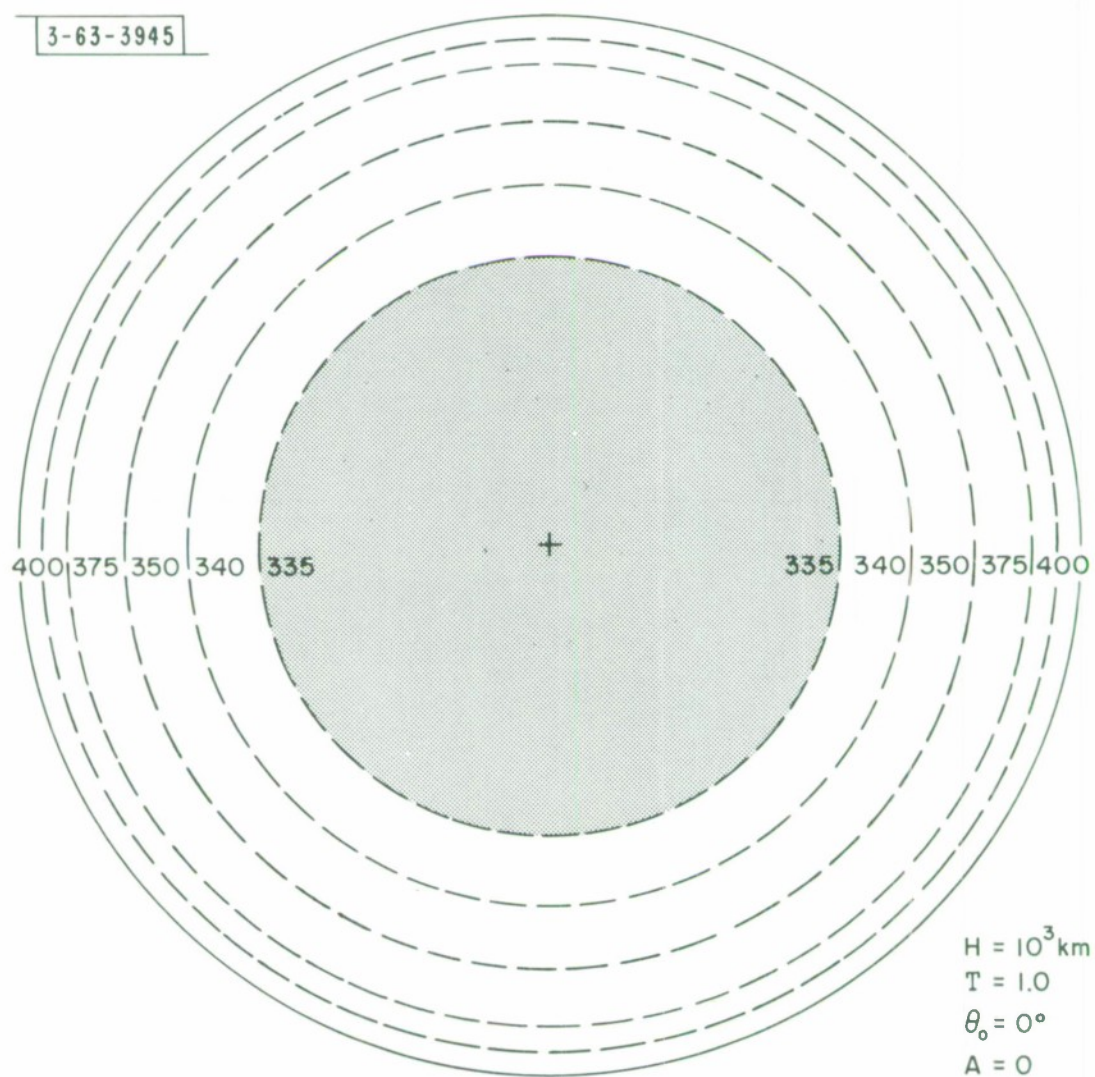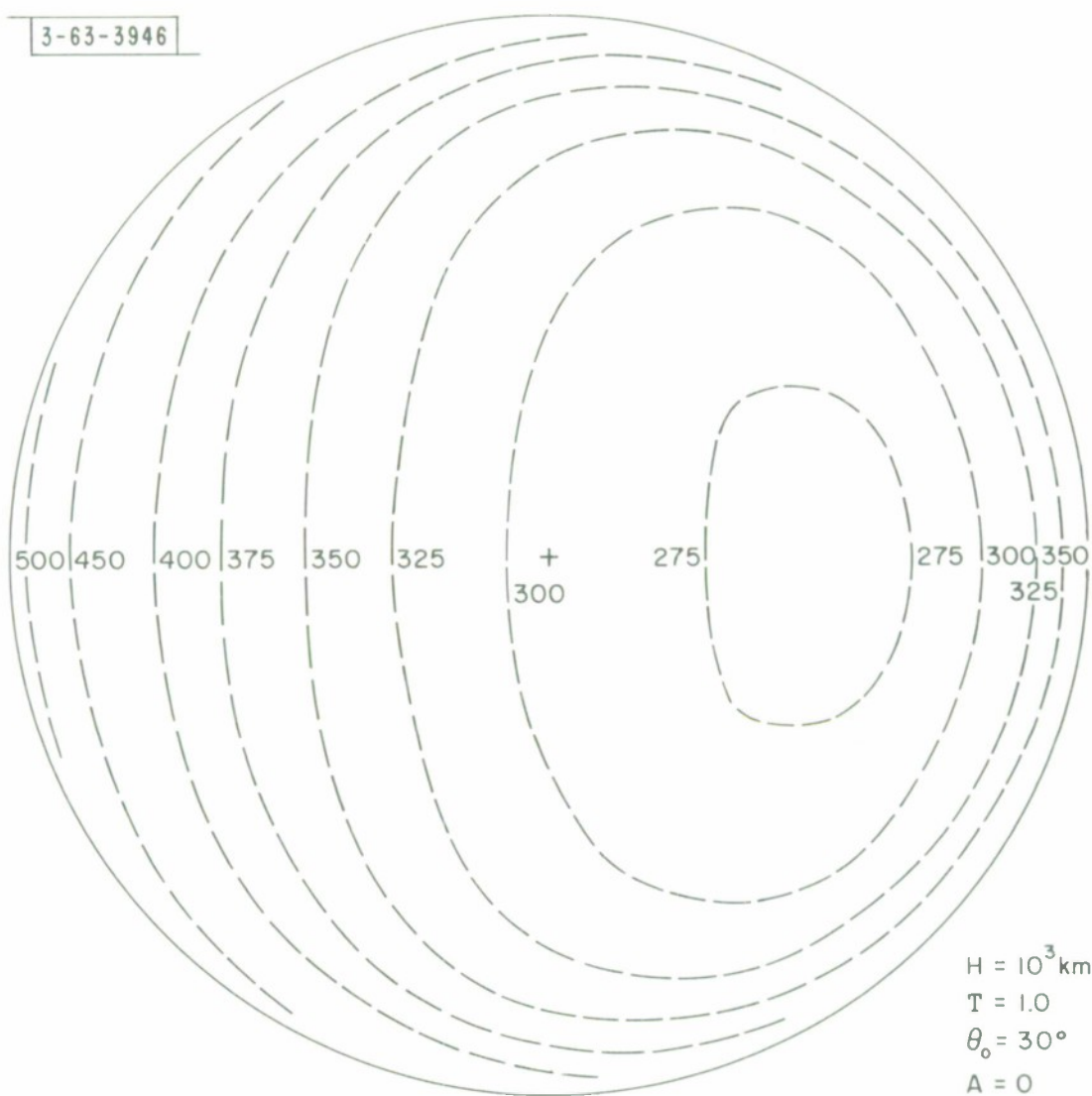
H = 10^3 km
T = 1.0
θ_o = 30°
A = 0

Fig. 32 Map of iosphotes for H = 10^3 km, θ_o = 30°

400
450 | 375 | 350   300 | 275 | 250   225   225 | 250 | 275 | 350
                                                                              | 300 |

+
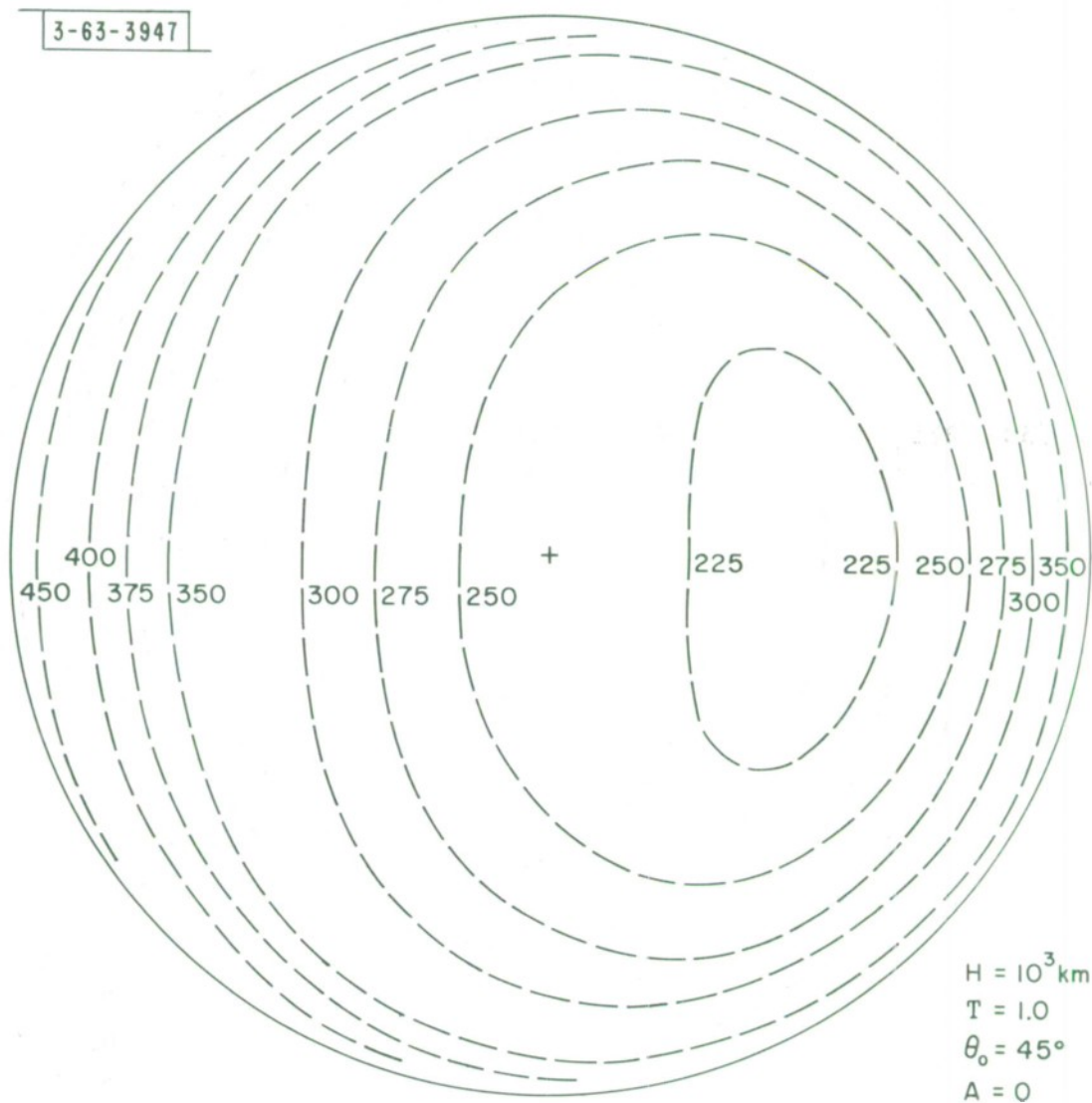
H = 10³ km
T = 1.0
θ_o = 45°
A = 0

Fig. 33 Map of isophotes for H = 10³ km, θ_o = 45°
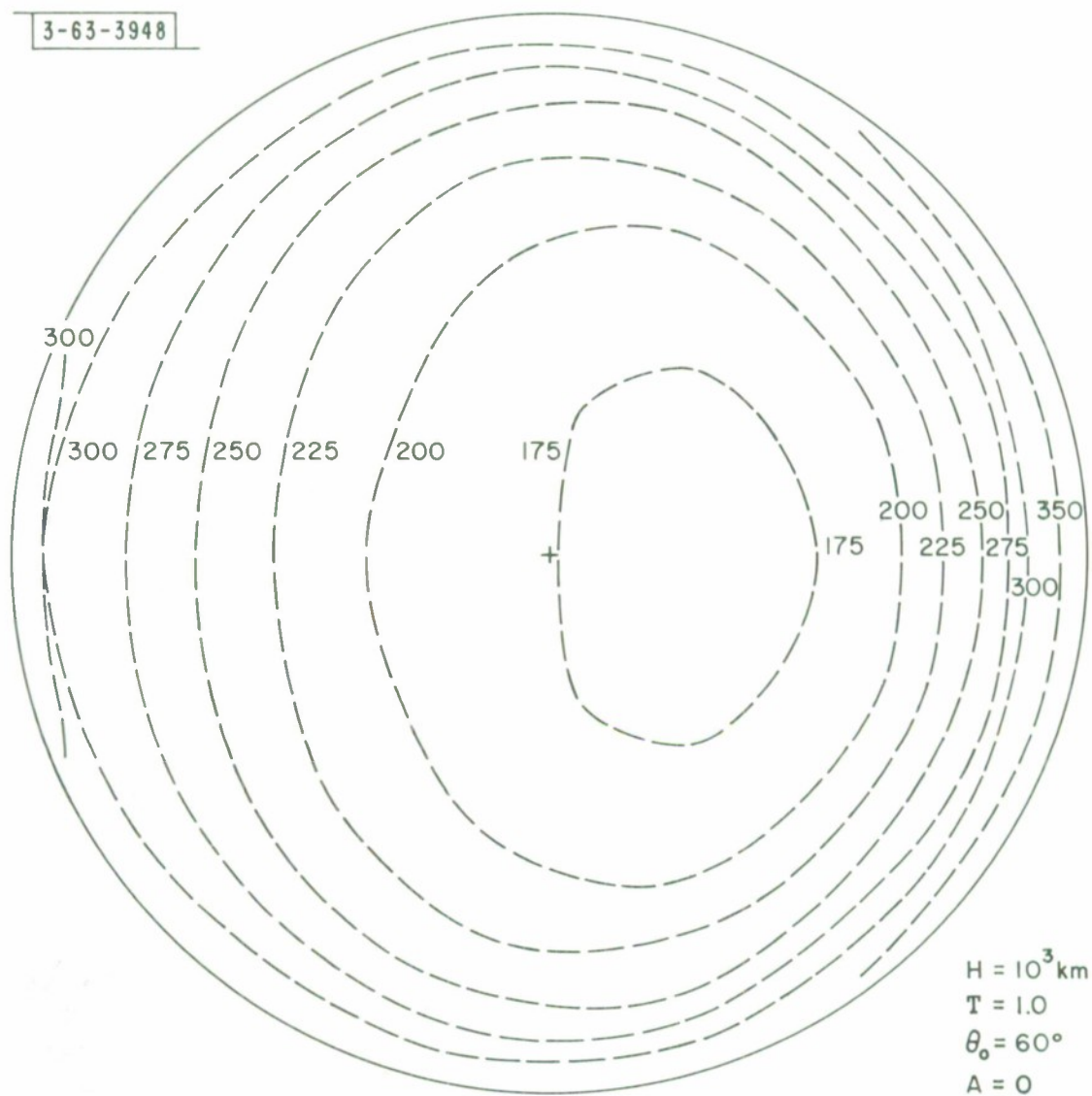
Fig. 34 Map of isophotes for $H = 10^3$ km, $\theta_o = 60^o$

Fig. 35 Map of isophotes for H = 10^3 km, θ_0 = 85°

25   50   75 100 150 200
                        300
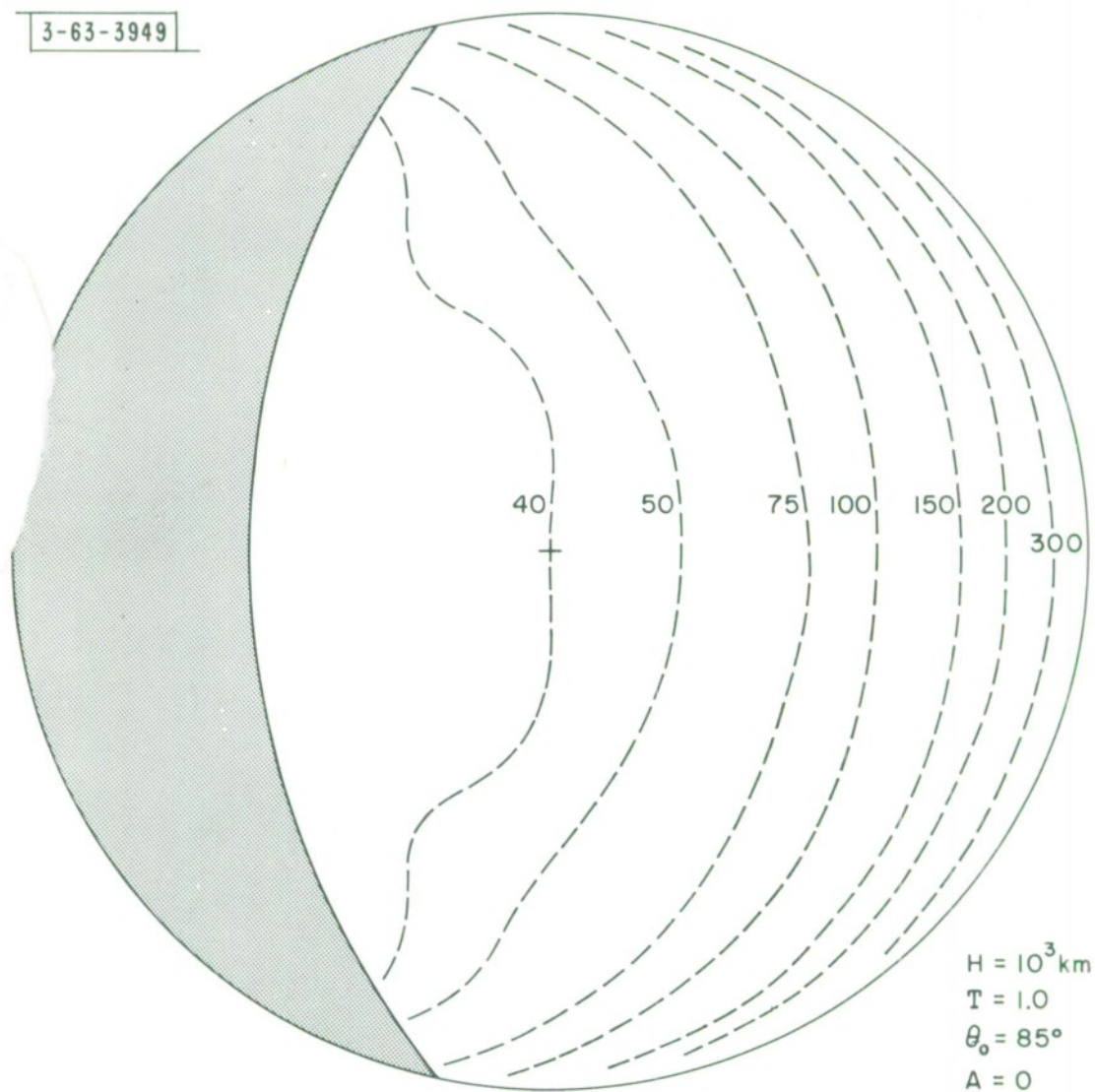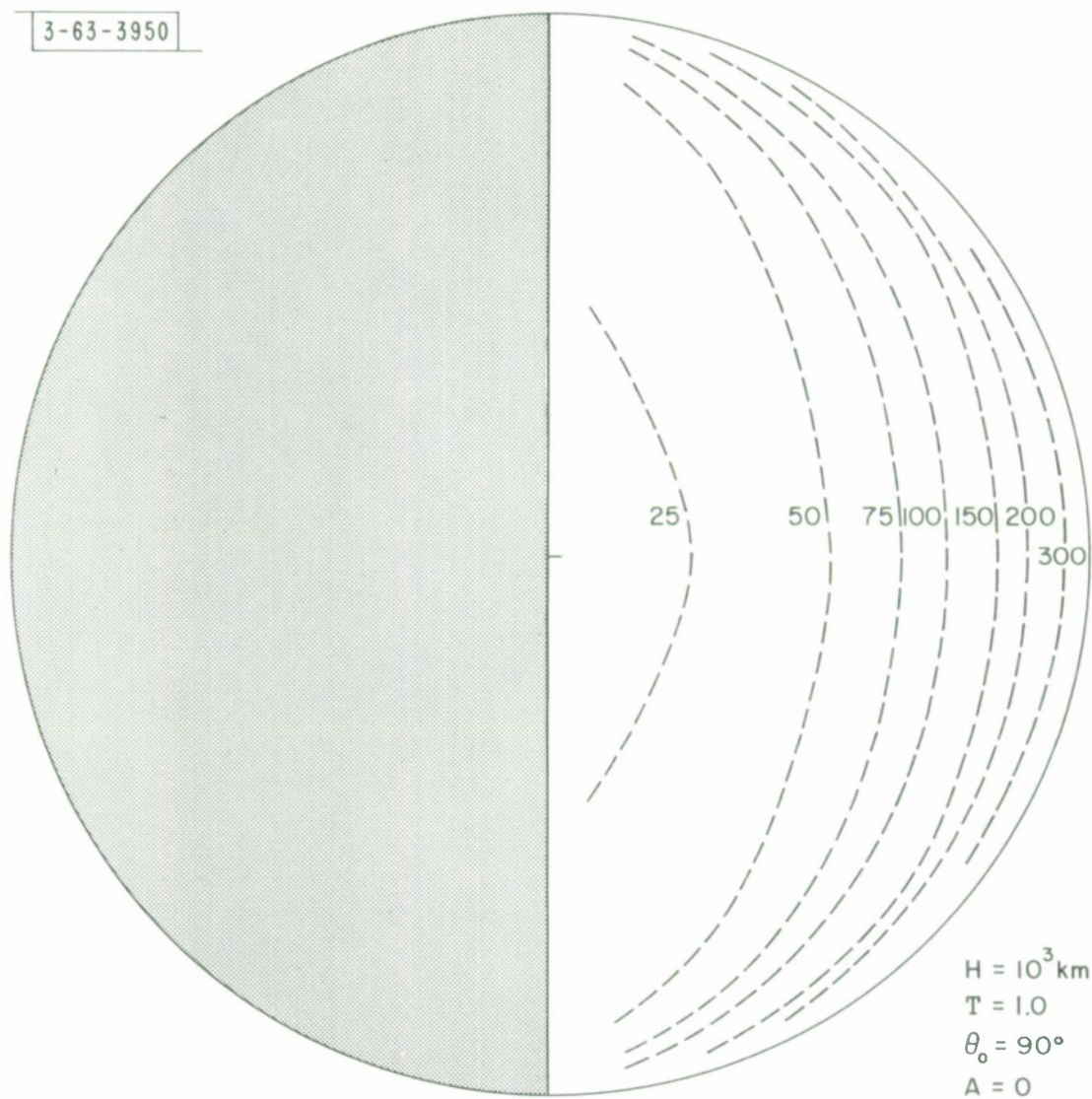
$H = 10^3 km$
$T = 1.0$
$\theta_o = 90°$
$A = 0$

Fig. 36 Map of isophotes for $H = 10^3$ km, $\theta_o = 90°$

48

200

50 |100|

H = 10^3km

T = 1.0

θ_o = 95°

A = 0

Fig. 37 Map of Isophotes for H = 10^3 km, θ_o = 95°

49

450 |400|350 |300 |250 |200 + 200 | 300| |450
250 |350 |

400
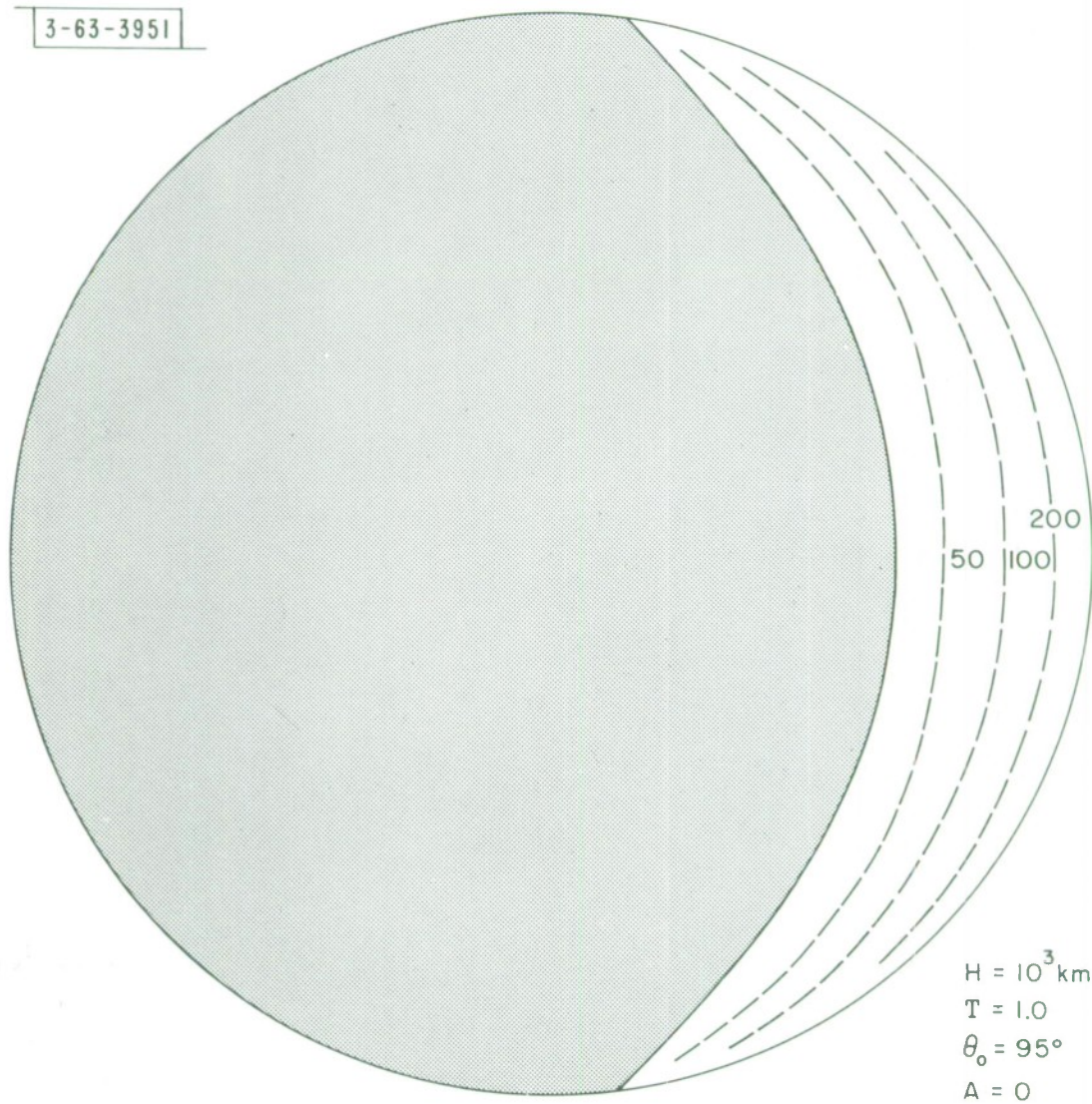
$H = 10^2$ km
$T = 1.0$
$\theta_0 = 60°$
$A = 0$
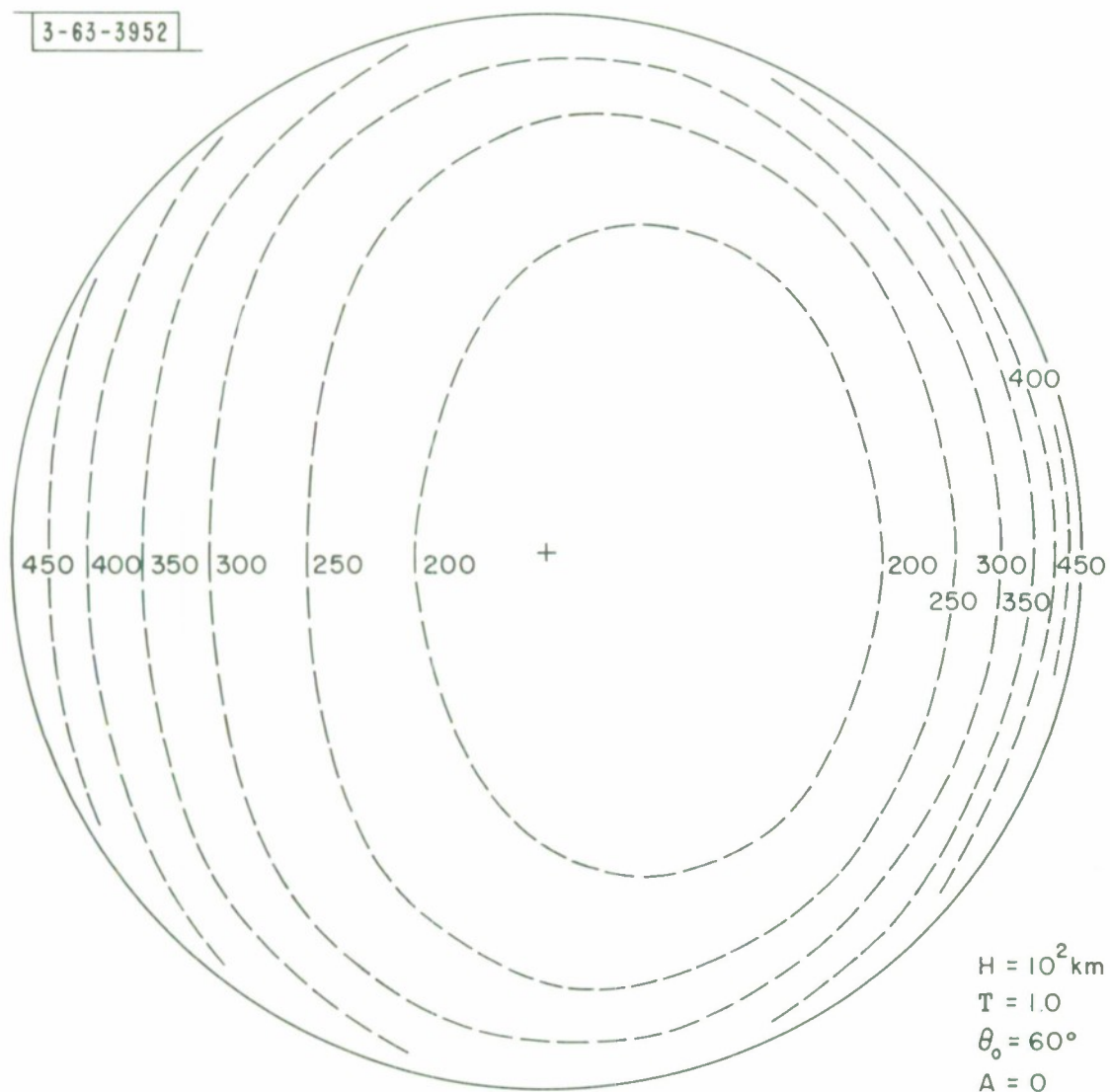
Fig. 38 Map of isophotes for $H = 10^2$ km

50
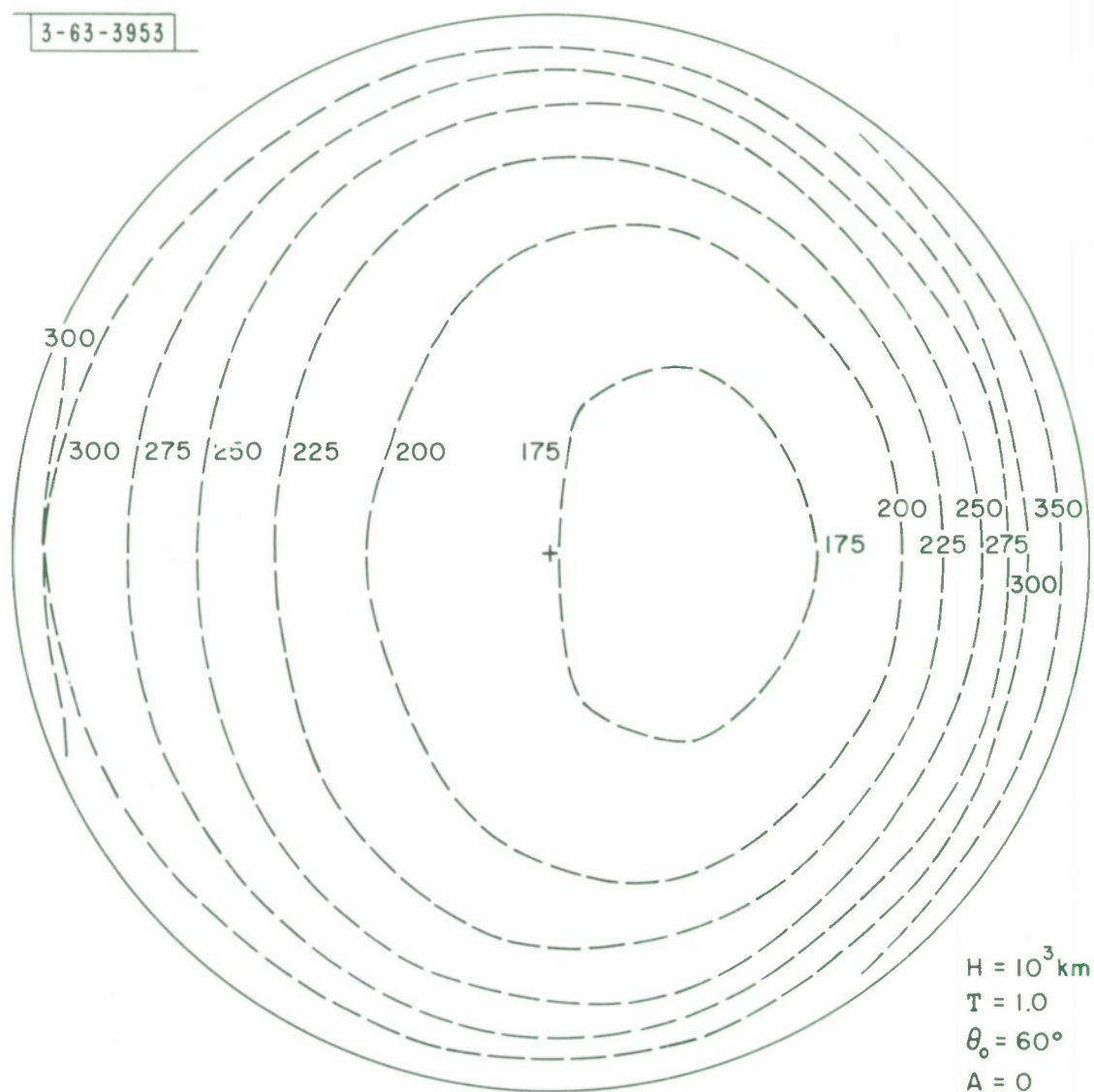
Fig. 39 Map of isophotes for $H = 10^3$ km
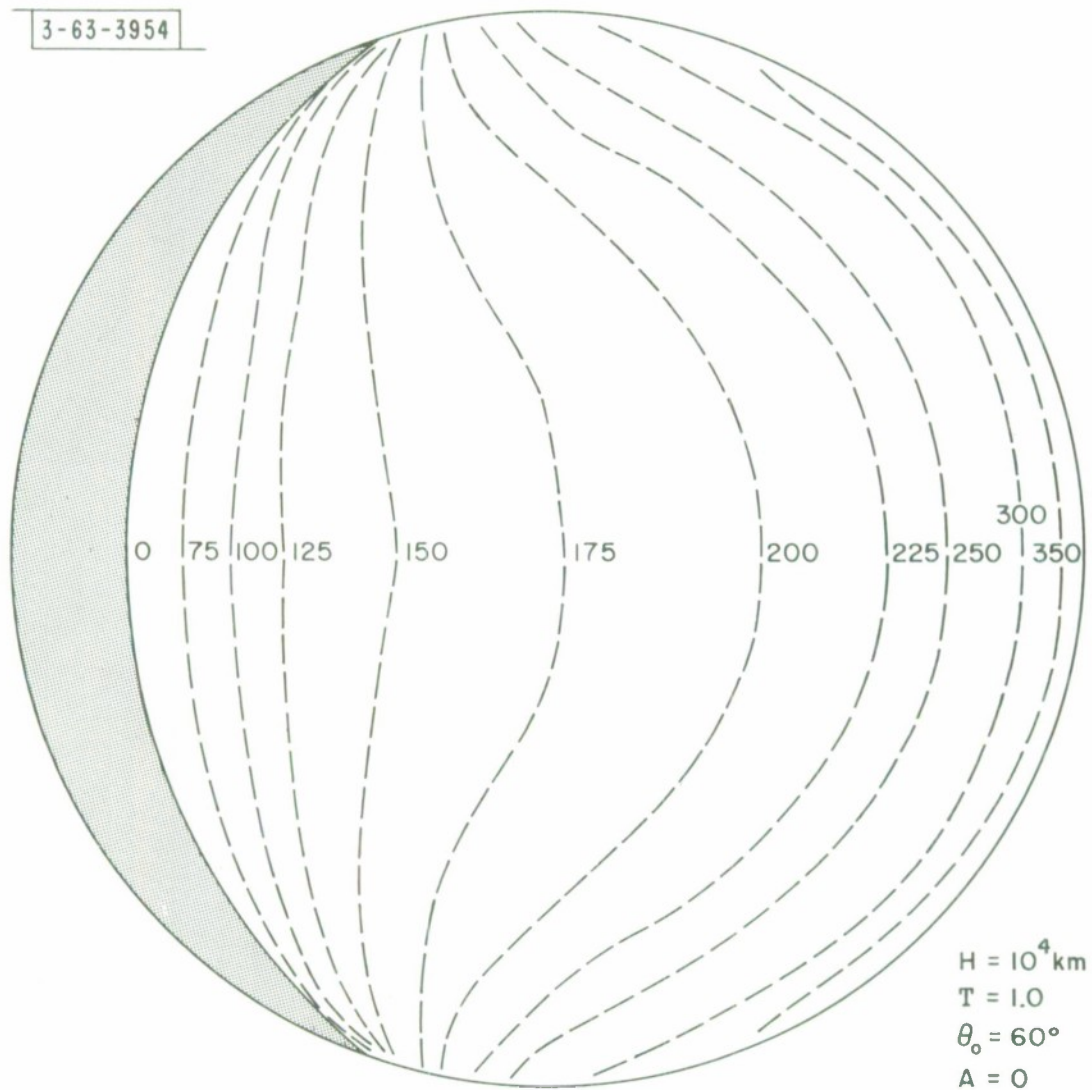
Fig. 40 Map of isophotes for H = 10^4 km

50 |100 |150 |200 250 |300 350

+

$H = 10^5 \, km$

$T = 1.0$

$\theta_o = 60°$

$A = 0$
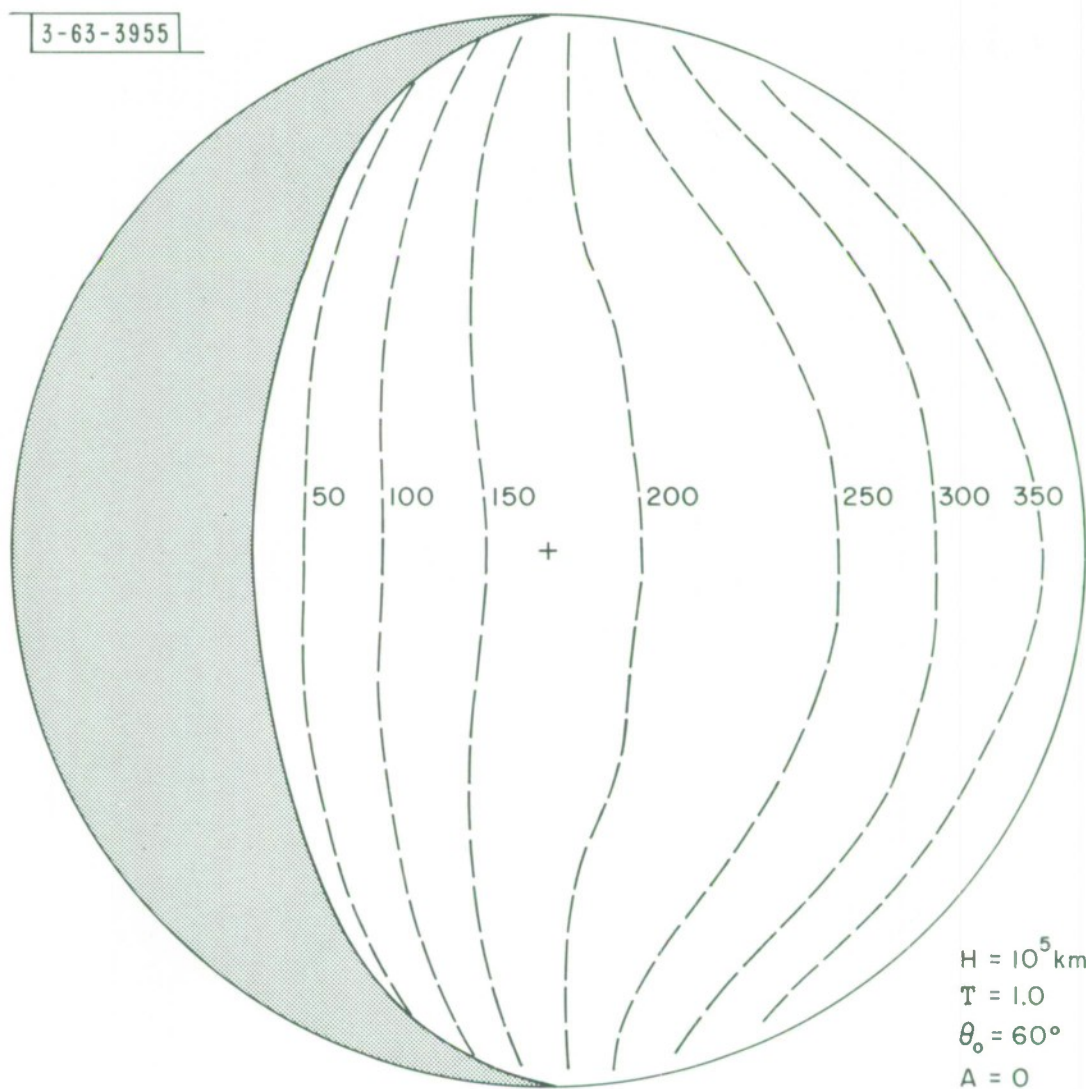
Fig. 41 Map of isophotes for $H = 10^5$ km

53

50 |100 |150 |200 250 |300 350
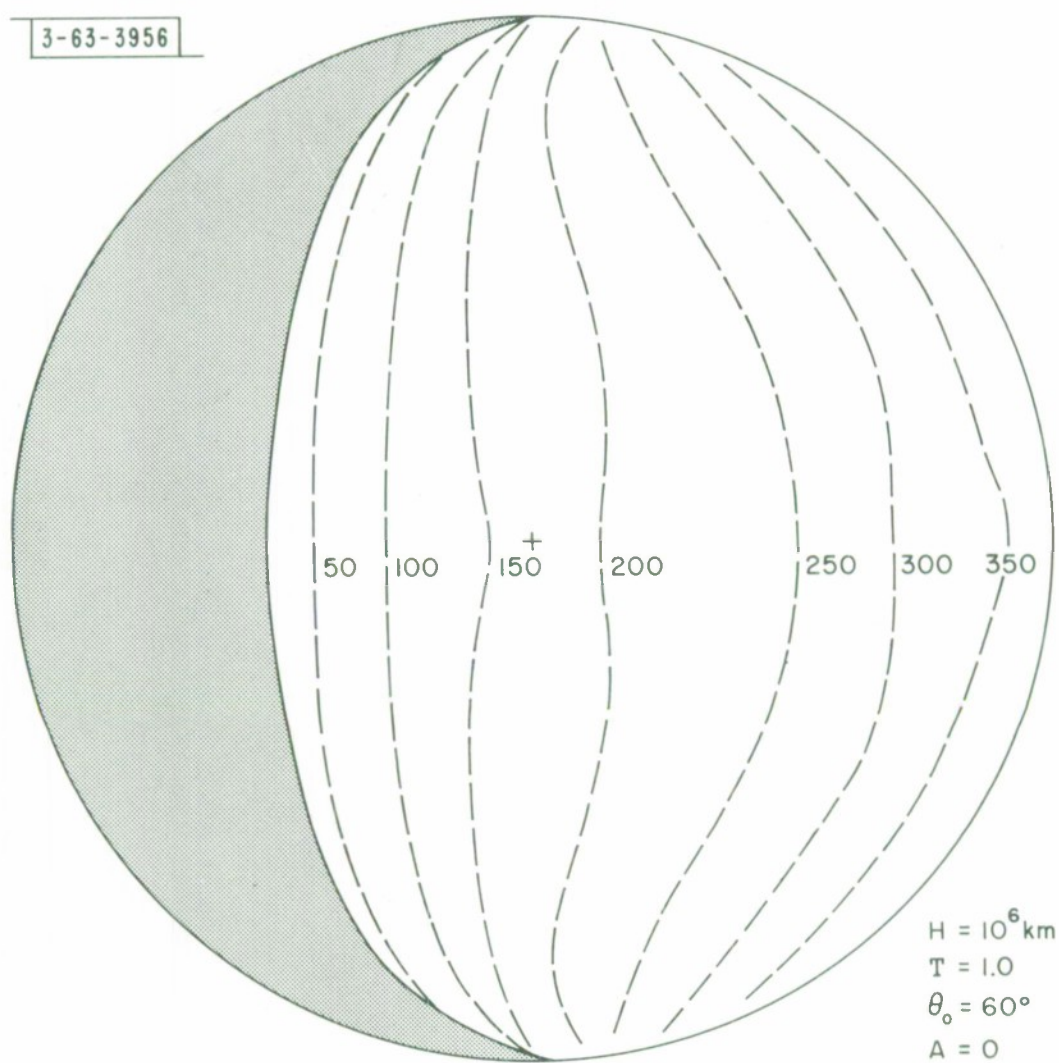
$H = 10^6 km$
$T = 1.0$
$\theta_0 = 60°$
$A = 0$

Fig. 42 Map of isophotes for $H = 10^6$ km

Fig. 43 Map of isophotes for $H = 10^6$ km, $A = 0$

55

100 150 200 250 300   350   400   450   500

+
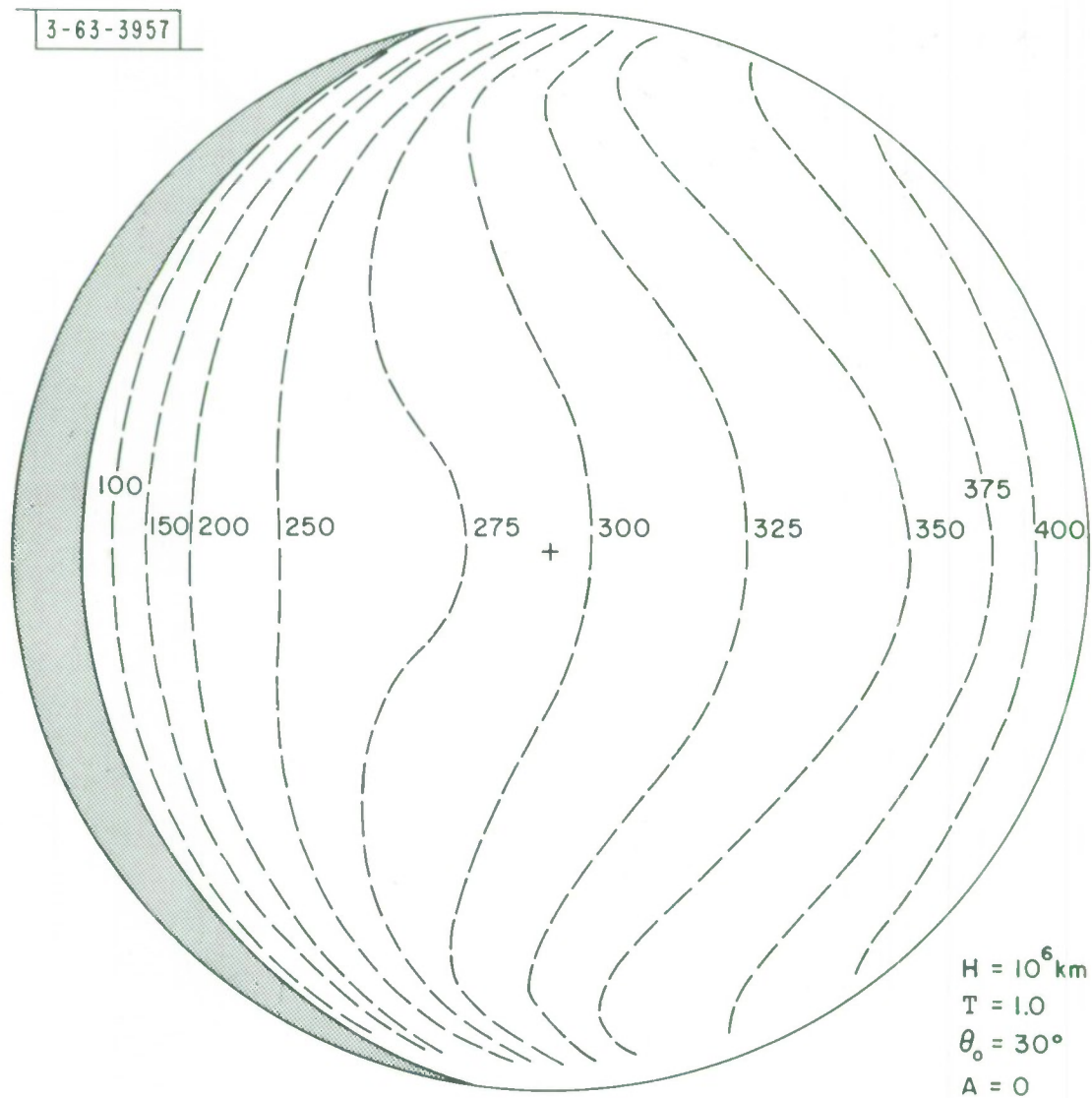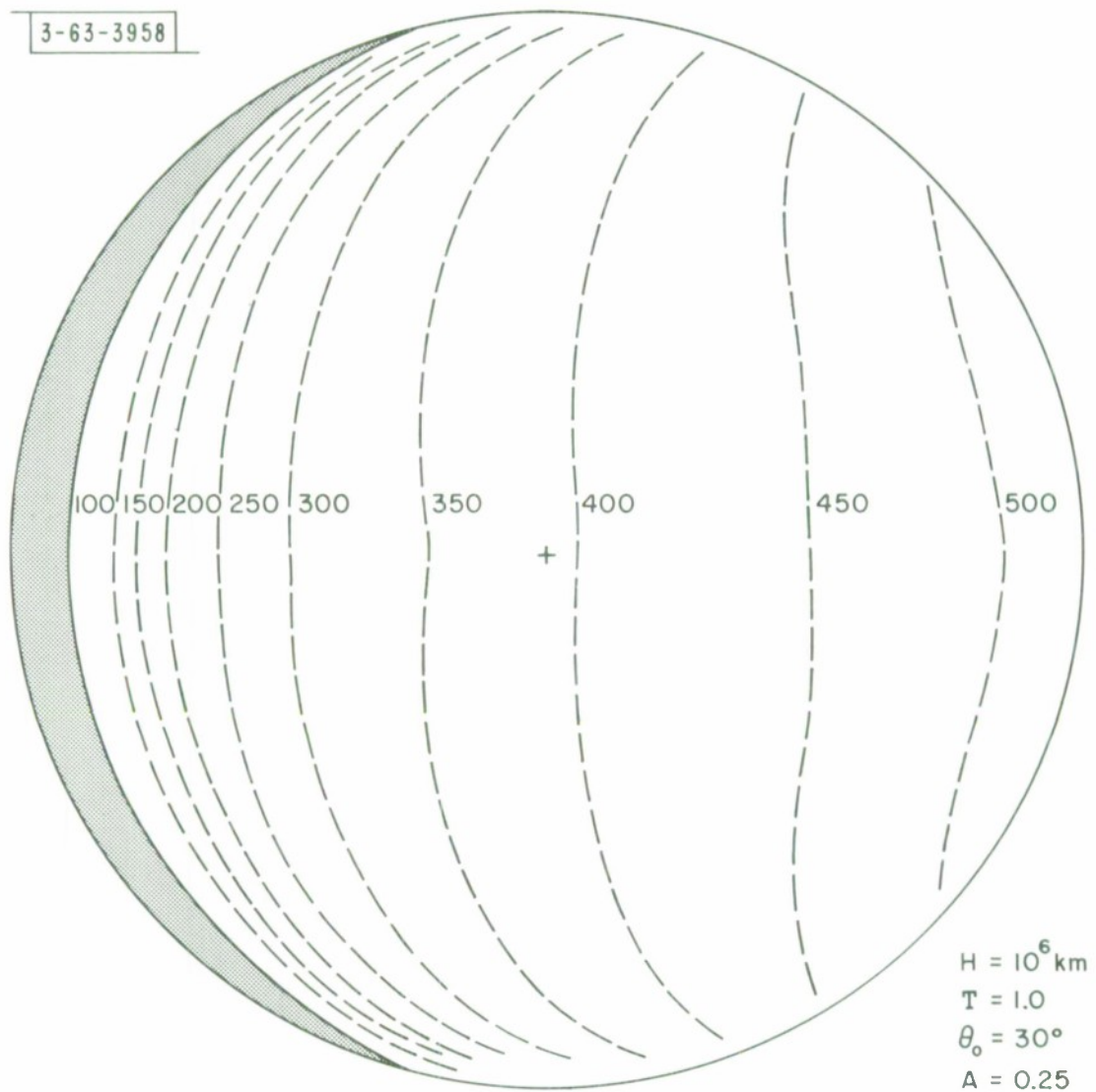
$H = 10^6 \, km$
$T = 1.0$
$\theta_o = 30°$
$A = 0.25$

Fig. 44 Map of isophotes for $H = 10^6$ km, $A = 0.25$

200

100   300 400 500 600   700   800

+

H = 10^6 km
T = 1.0
θ_o = 30°
A = 0.80
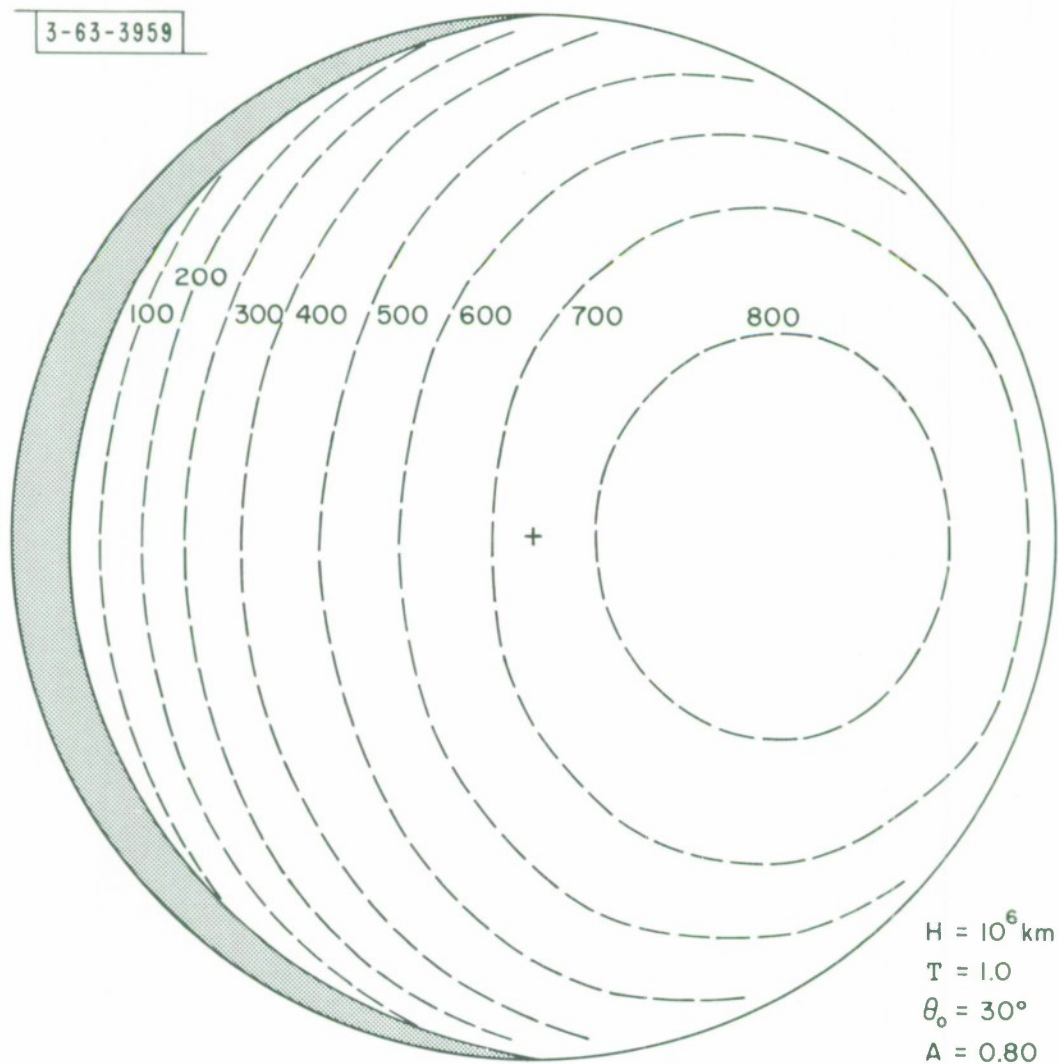
Fig. 45 Map of isophotes for H = 10^6 km, A = 0.80

Fig. 46 Map of isophotes for H = 10^3 km, A = 0

525 500 475   450   425   400   375   400 425

+
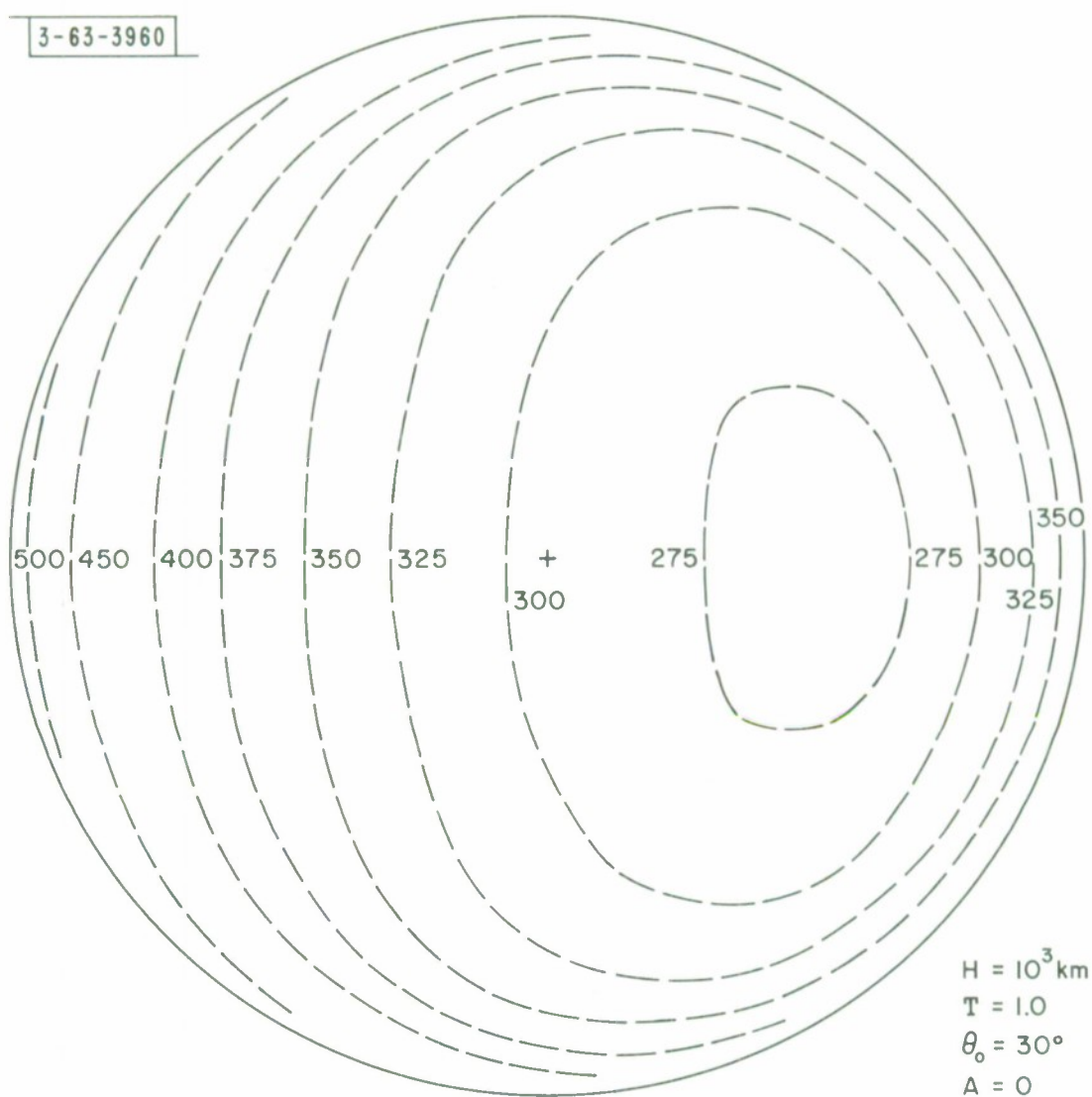
H = 10³ km
T = 1.0
θ_0 = 30°
A = 0.25
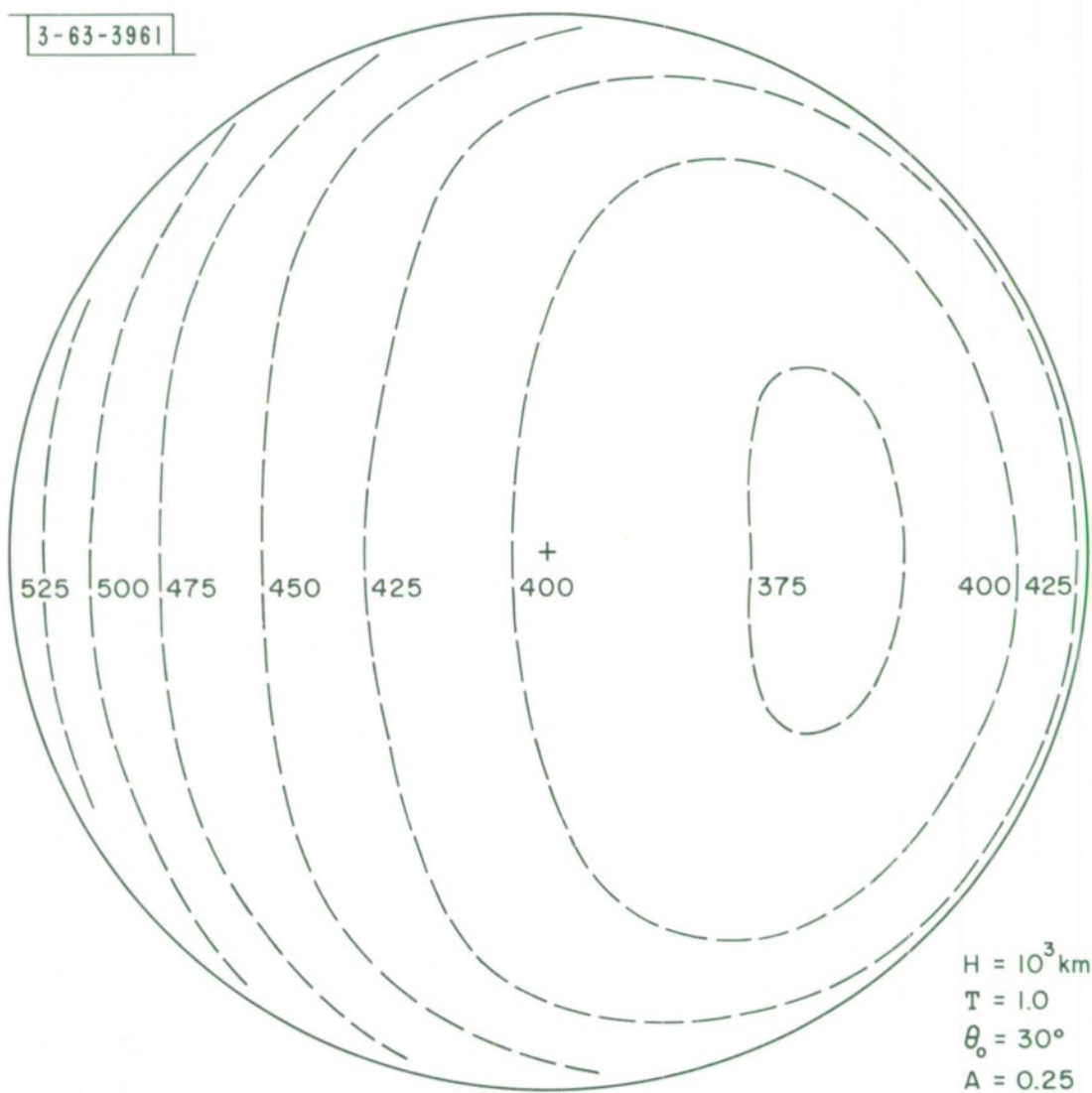
Fig. 47 Map of isophotes for H = 10³ km, A = 0.25
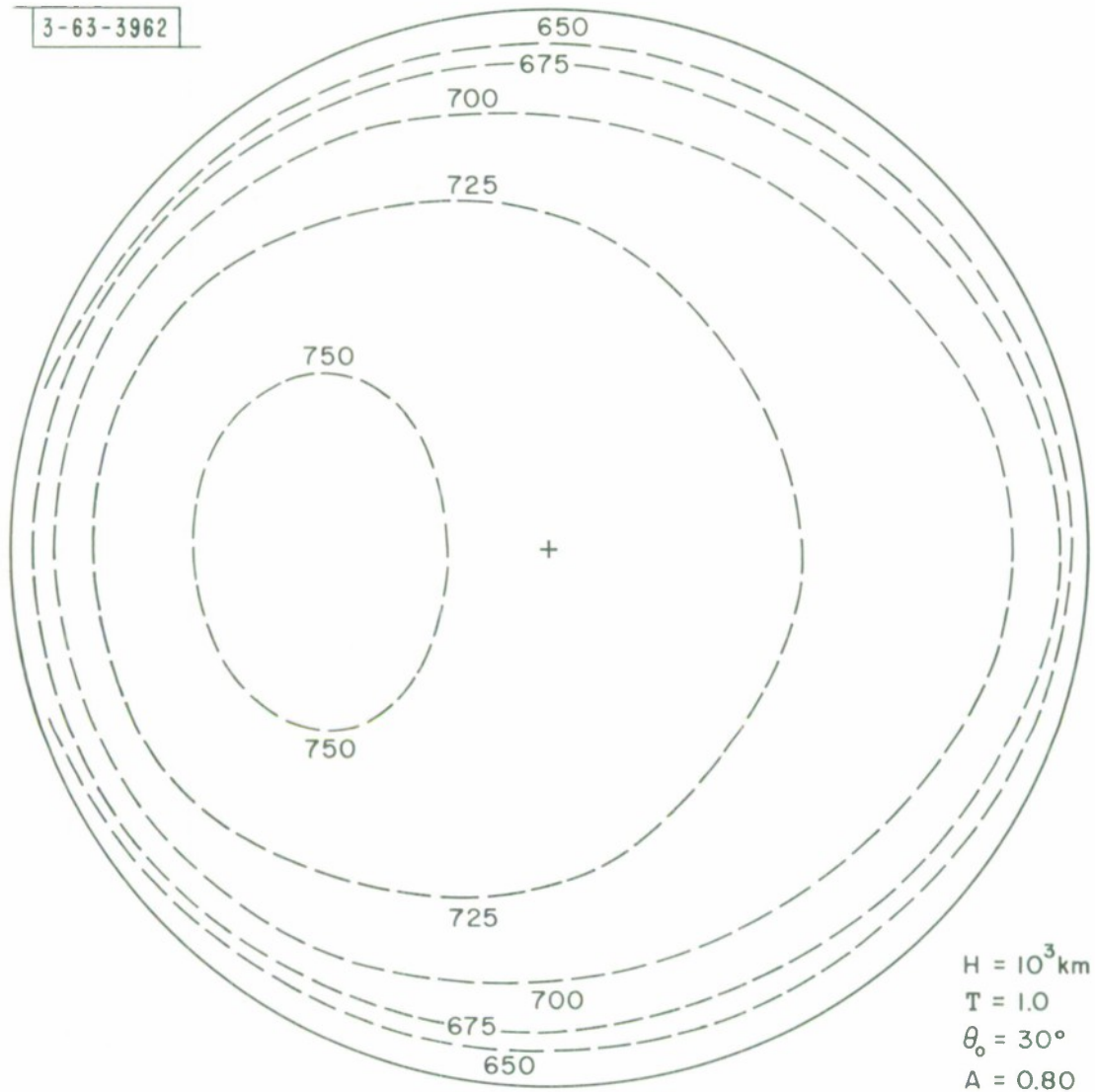
Fig. 48 Map of isophotes for H = 10^3 km, A = 0.80
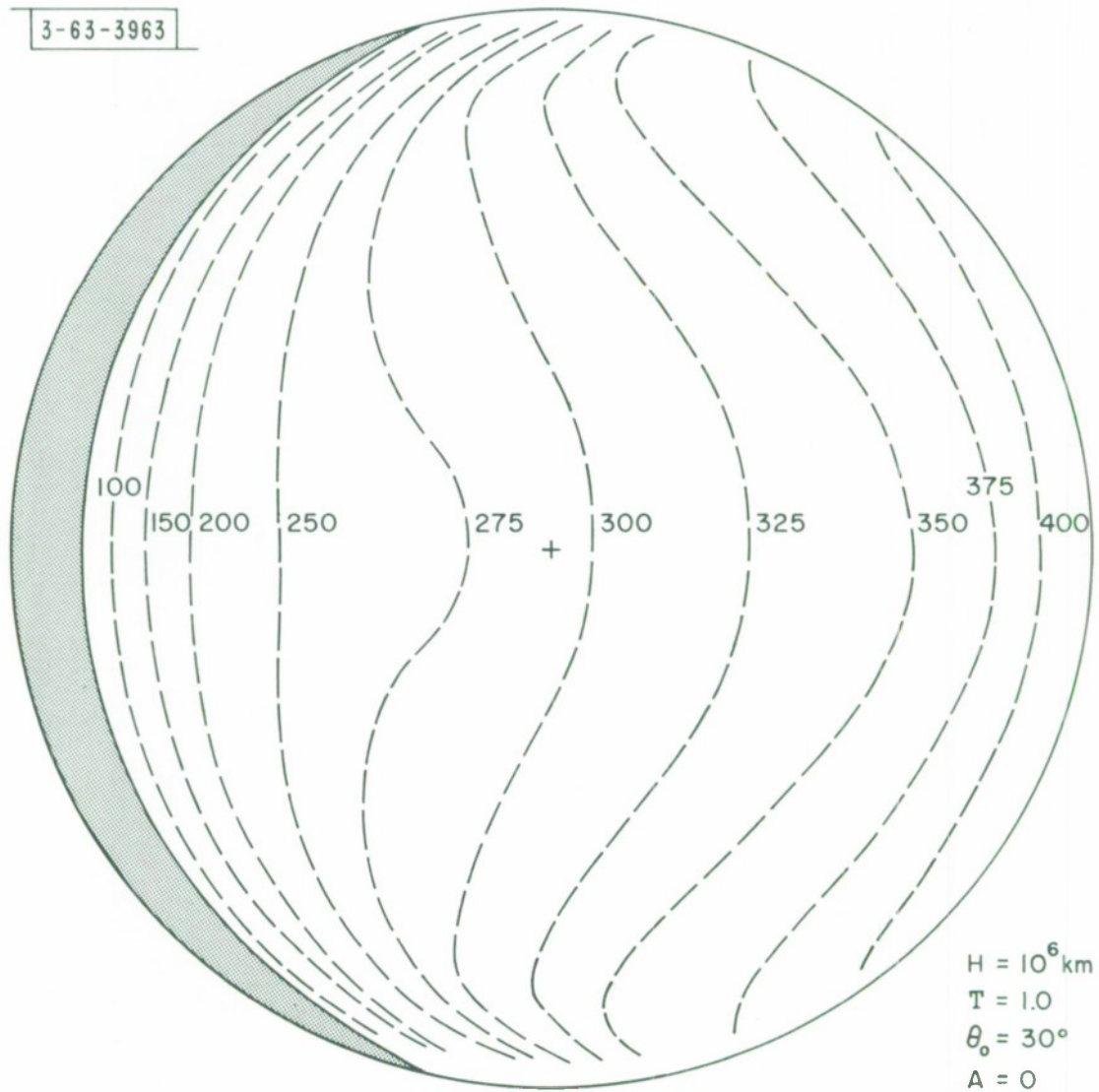
Fig. 49 Map of isophotes for H = 10^6 km, τ = 1.00

Labels on figure: 100, 150, 200, 250, 275, 300, 325, 350, 375, 400

H = 10^6km
T = 1.0
θ_0 = 30°
A = 0

Fig. 50 Map of isophotes for H = 10^6 km, τ = 0.50

The figure labels within the map:

100
50 125   150   160   175   200 250 350
                                                                225   300

H = 10^6 km
T = 0.5
θ_0 = 30°
A = 0

62
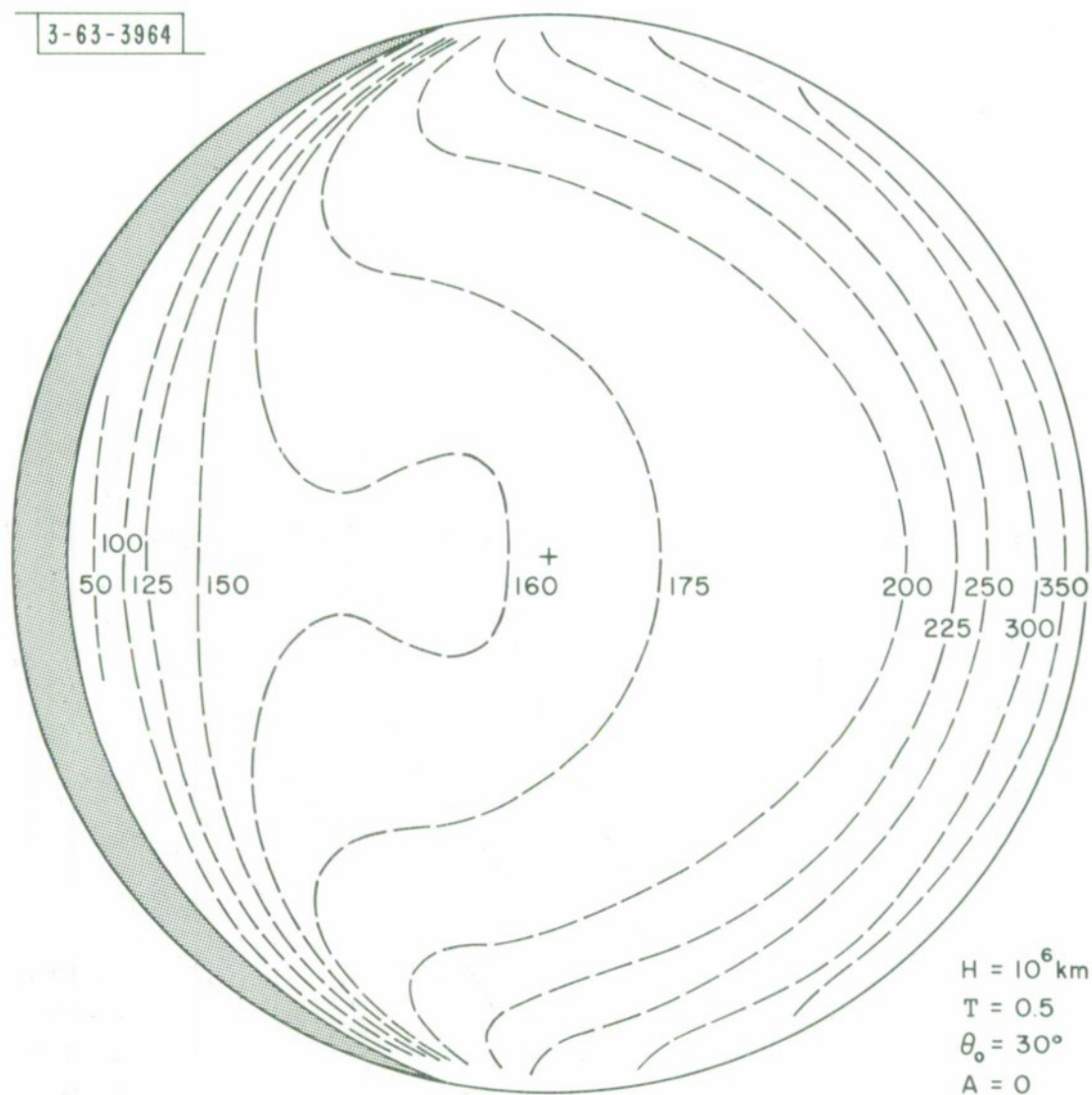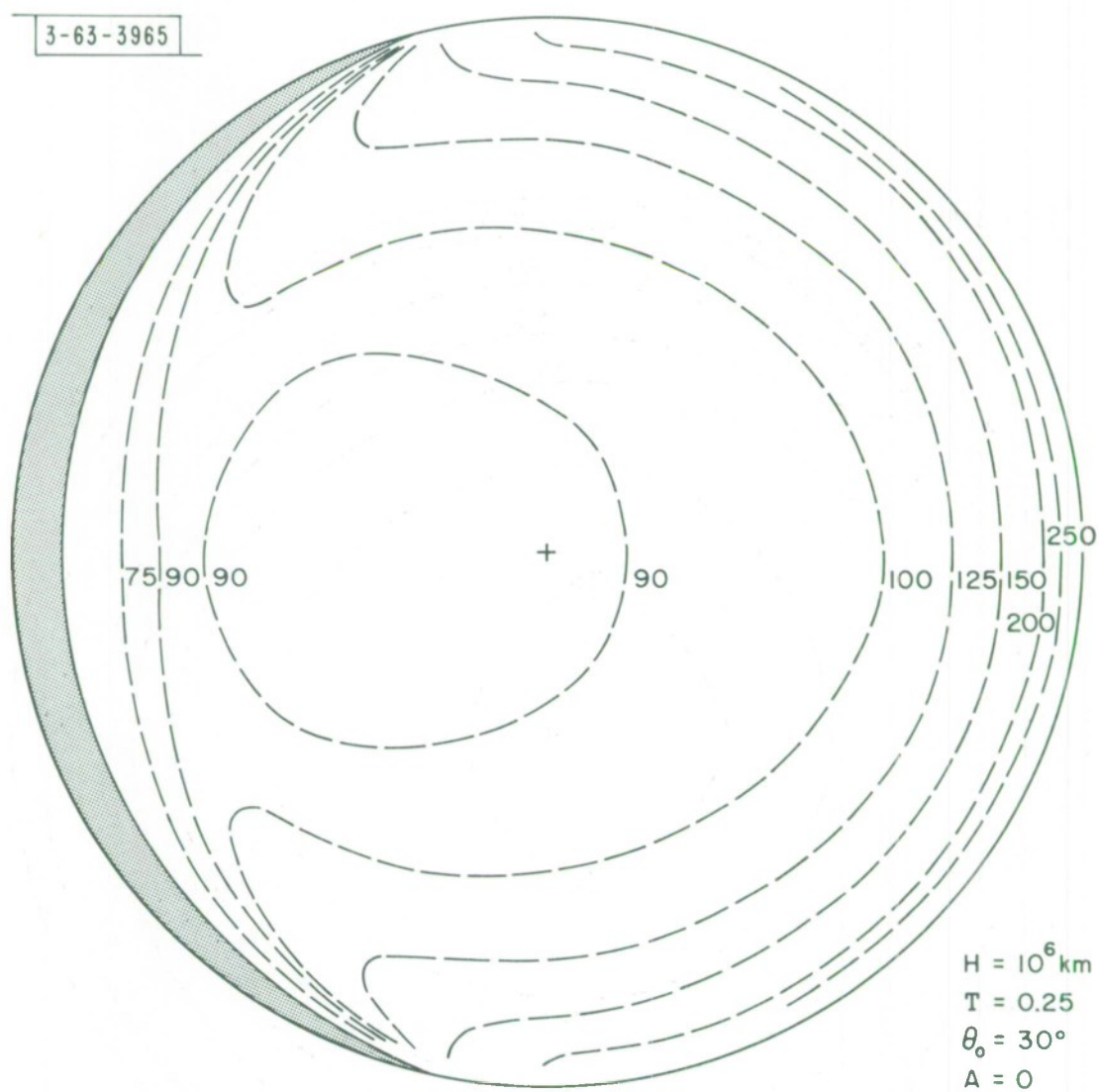
Fig. 51 Map of isophotes for $H = 10^6$ km, $\tau = 0.25$

Fig. 52 Map of isophotes for $H = 10^6$ km, $\tau = 0.10$

$H = 10^6$ km
$T = 0.10$
$\theta_o = 30°$
$A = 0$

64

500 450 400 375 350 325 + 275 275 300 350

300 325
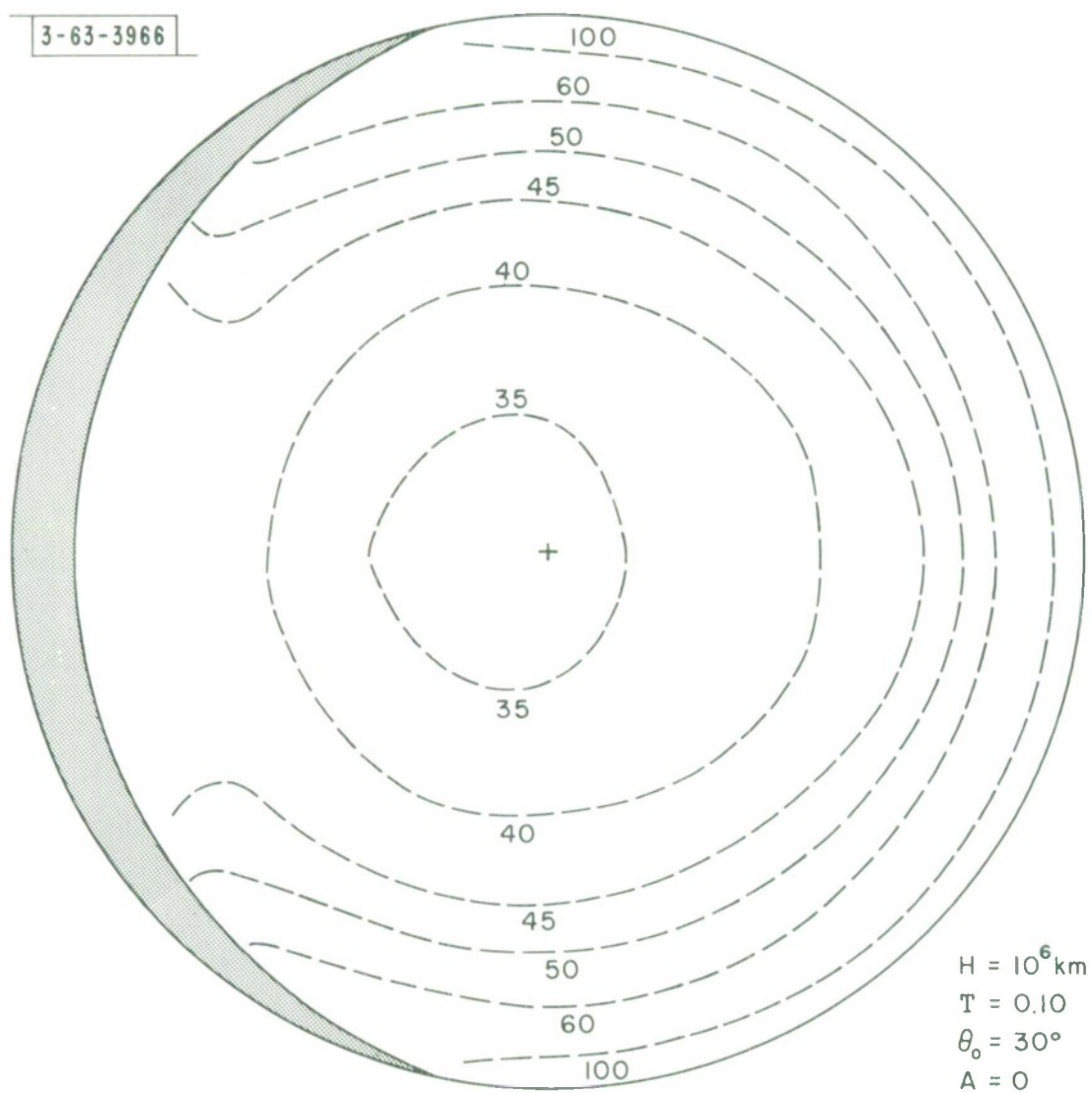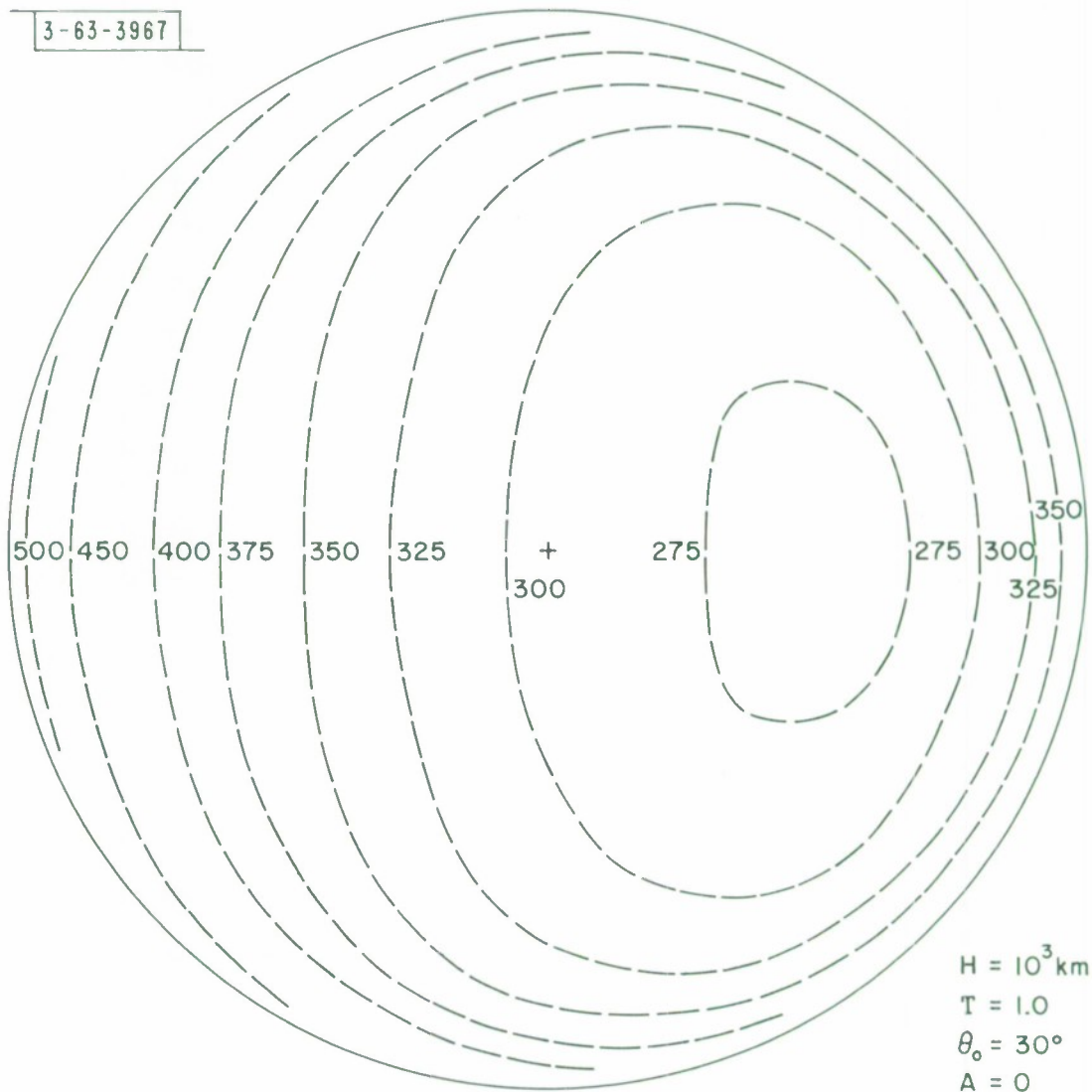
$H = 10^3$ km
$T = 1.0$
$\theta_0 = 30°$
$A = 0$

Fig. 53 Map of isophotes for $H = 10^3$ km, $\tau = 1.00$

350

400 300 275 250 225   200   175   +   150   150   175 225   250

200
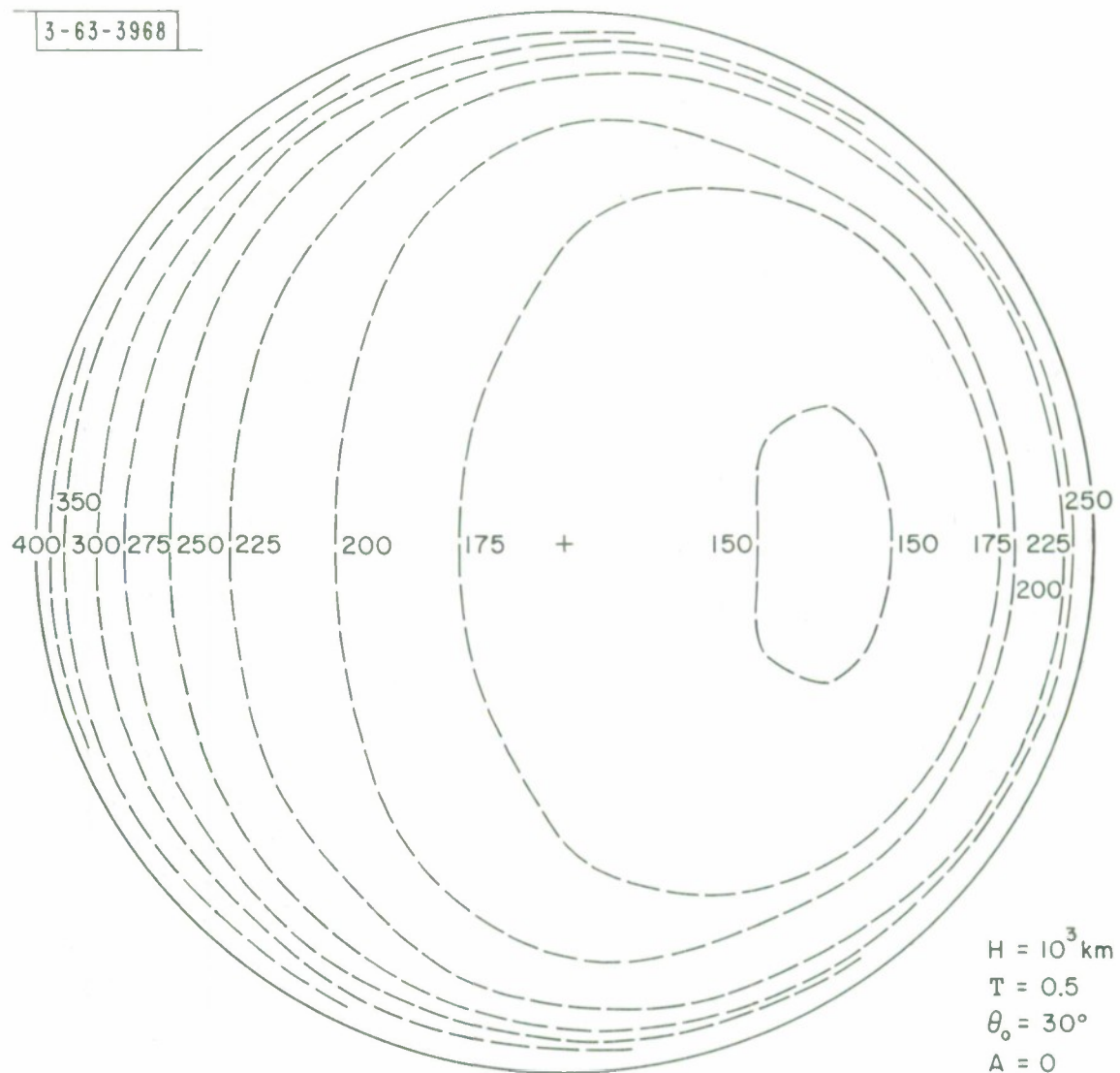
$H = 10^3$ km
$T = 0.5$
$\theta_o = 30°$
$A = 0$

Fig. 54 Map of isophotes for $H = 10^3$ km, $\tau = 0.50$
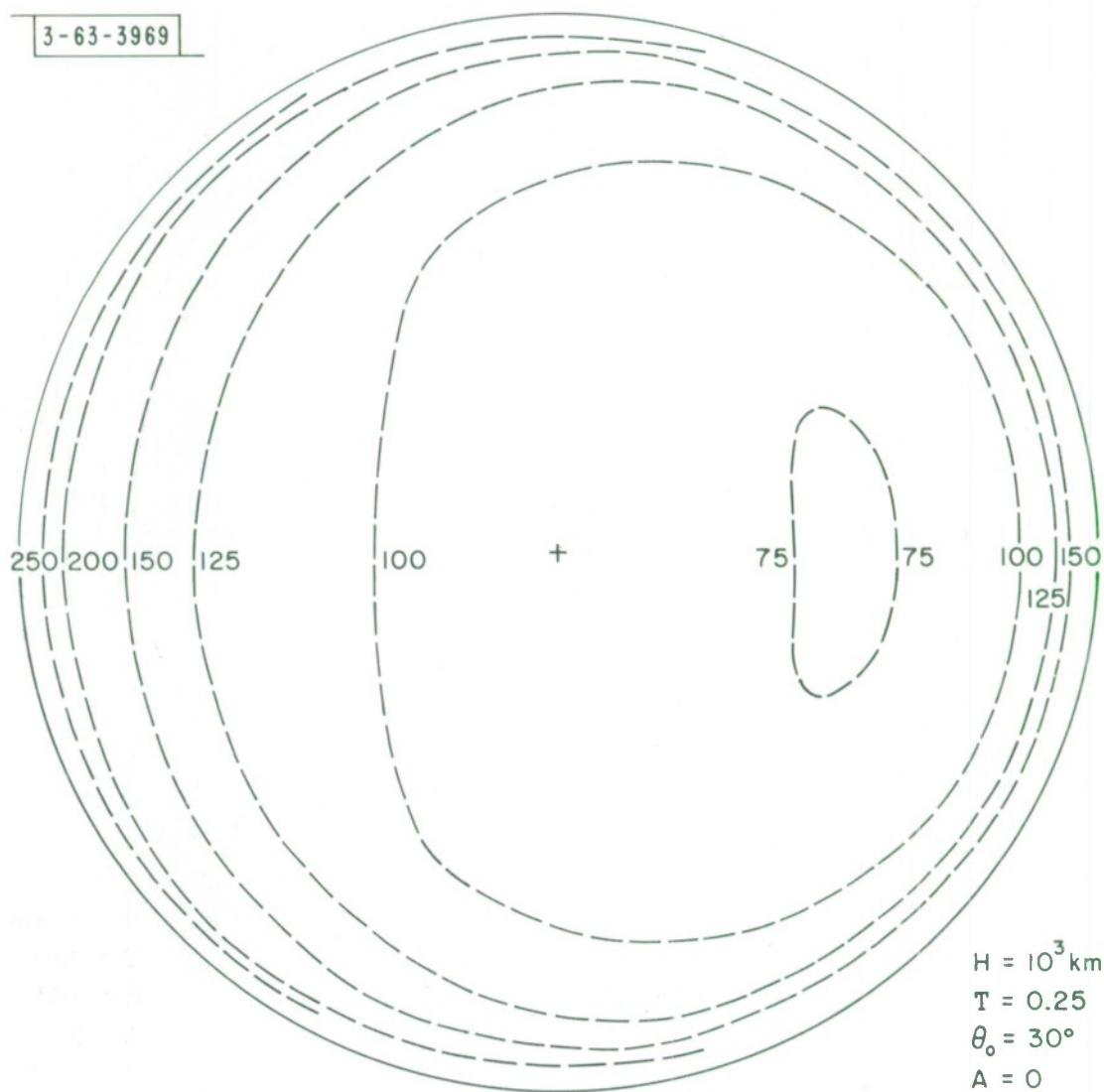
Fig. 55 Map of isophotes for H = 10^3 km, τ = 0.25

67
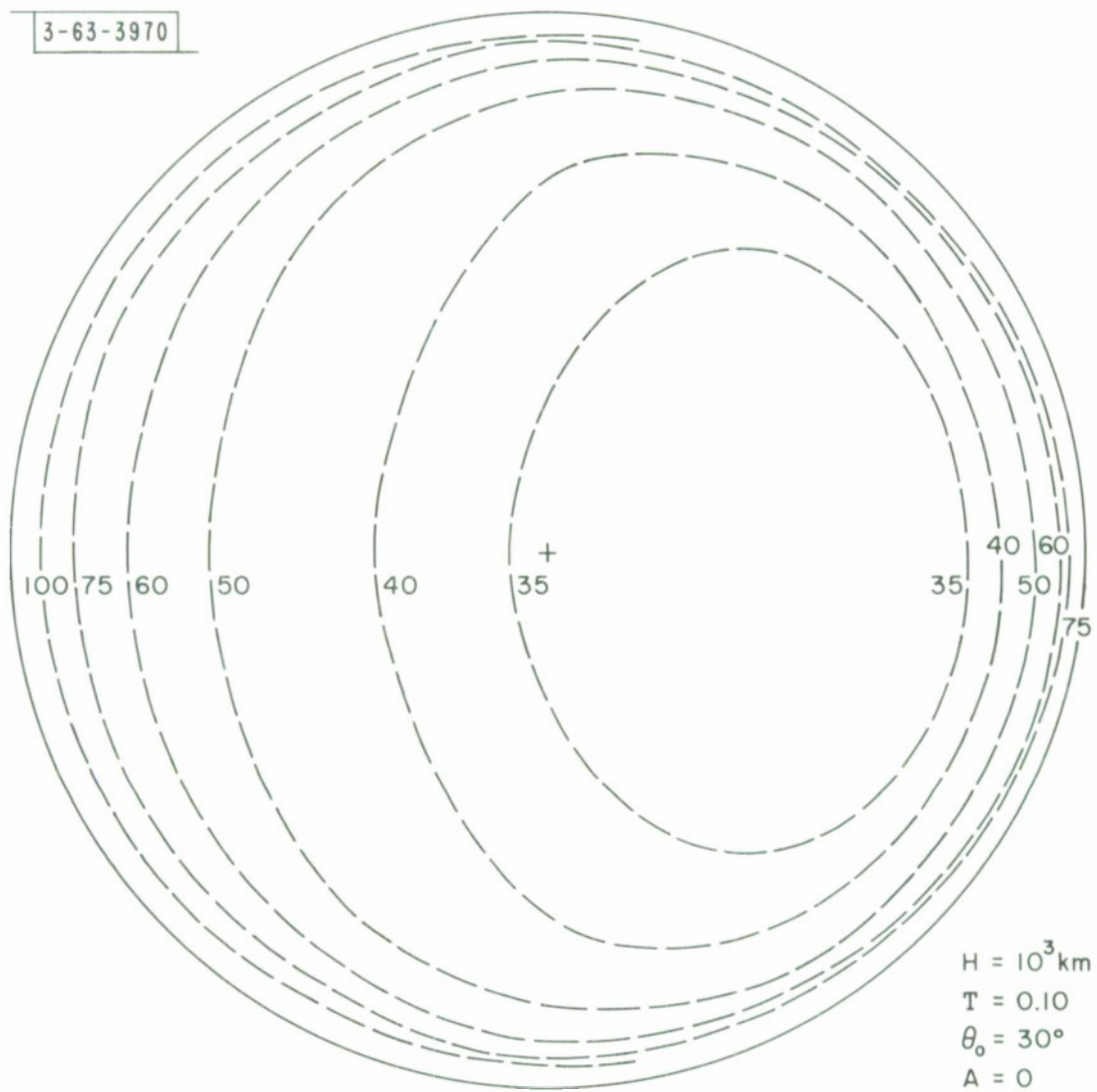
Fig. 56 Map of isophotes for H = 10^3 km, τ = 0.10
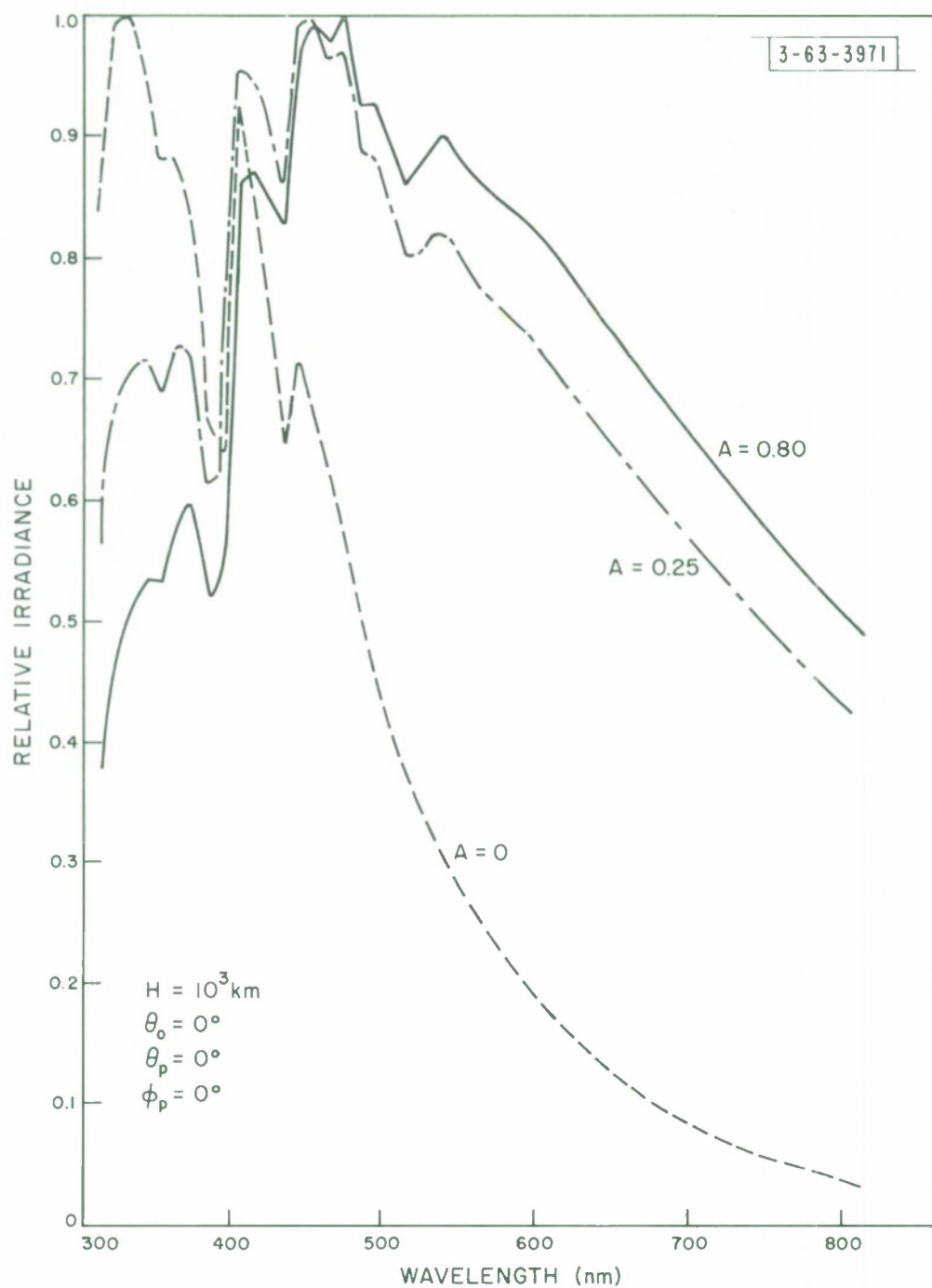
Fig. 57 Relative irradiance for A = 0, 0.25, and 0.80
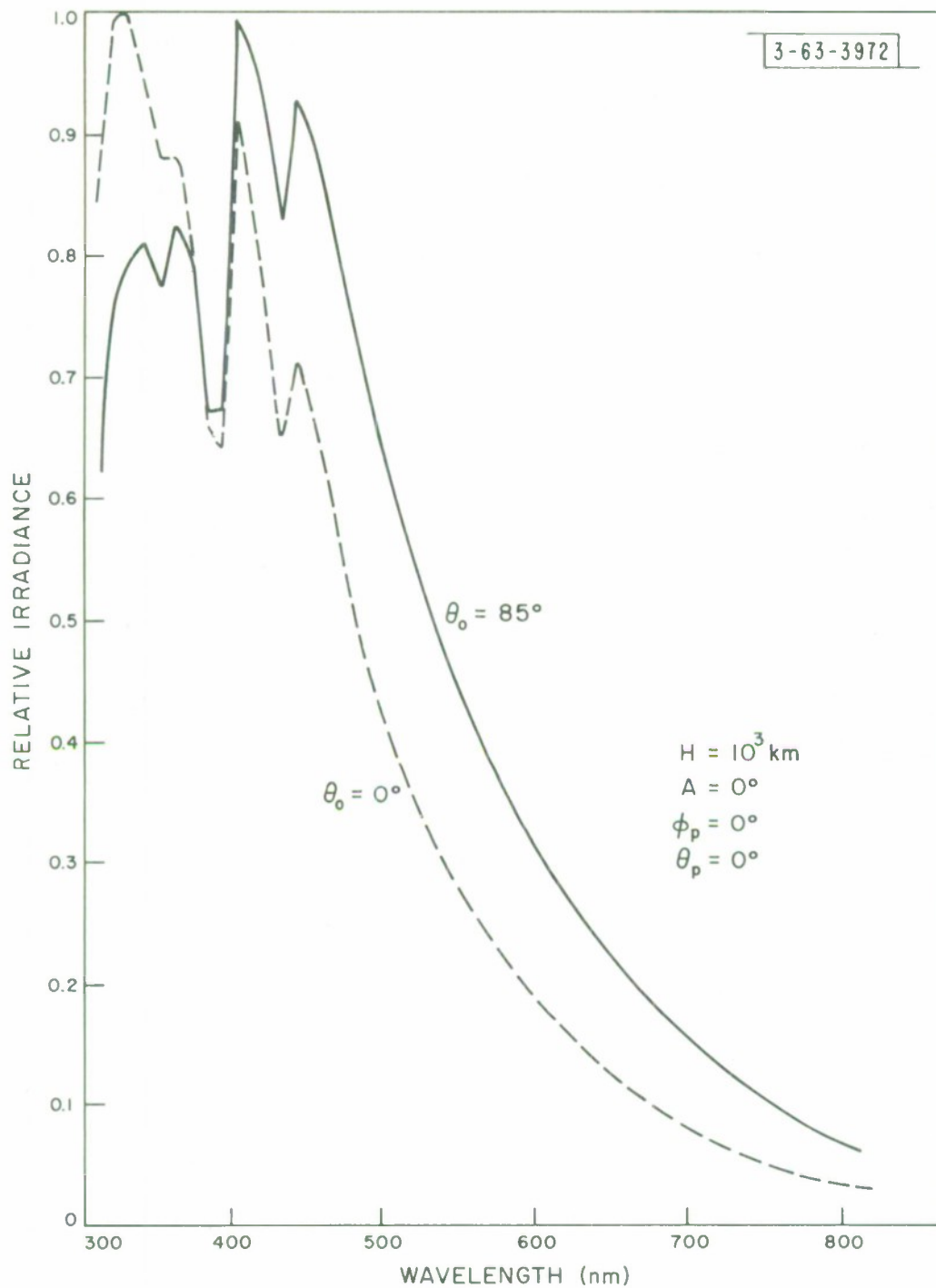
Fig. 58 Relative irradiance for $\theta_o = 0$ and $85°$
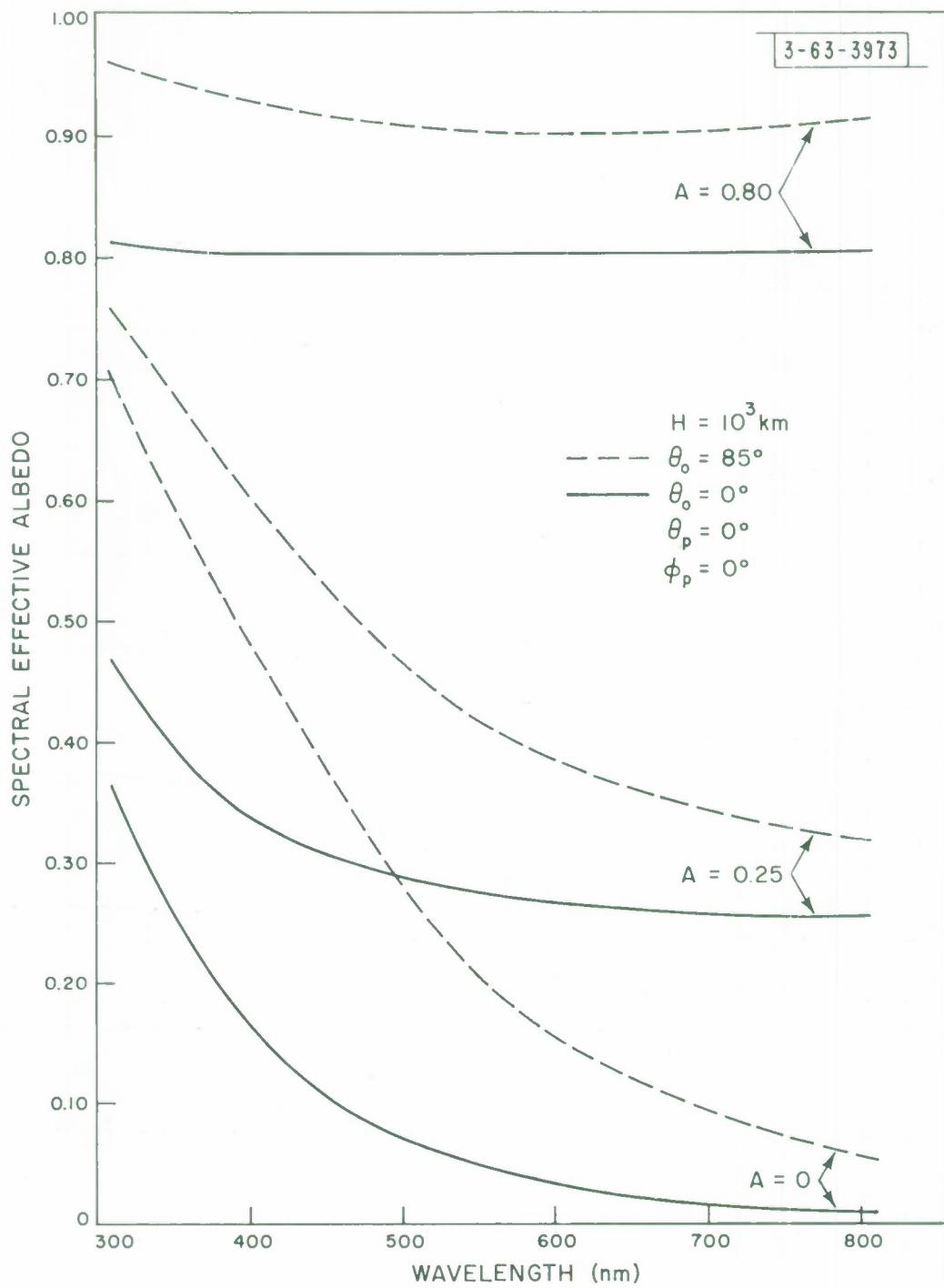
Fig. 59 Spectral effective albedo for A = 0, 0.25 and 0.80; θ_o = 0° and 85°.

71
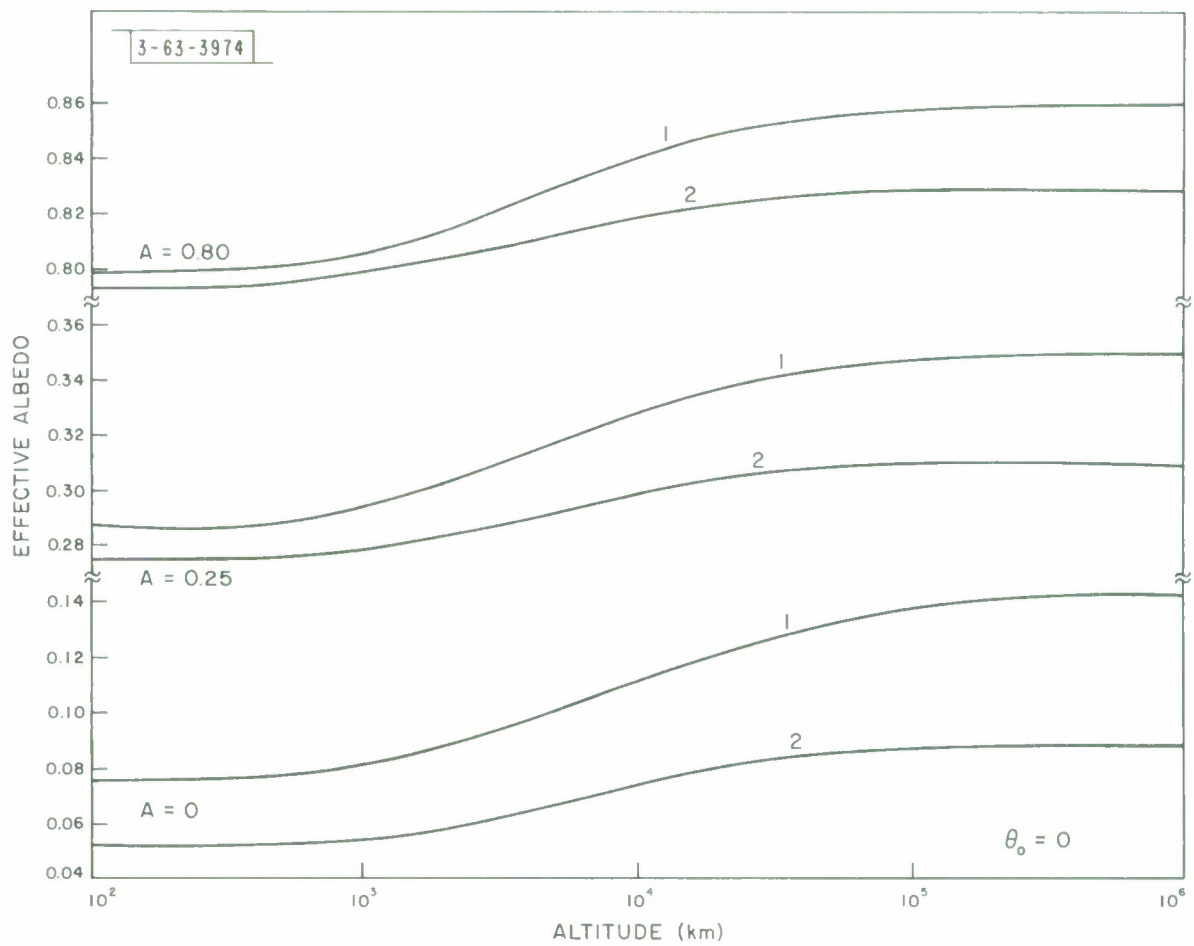
Fig. 60 Effective albedo as a function of altitude for $\theta_o = 0^o$
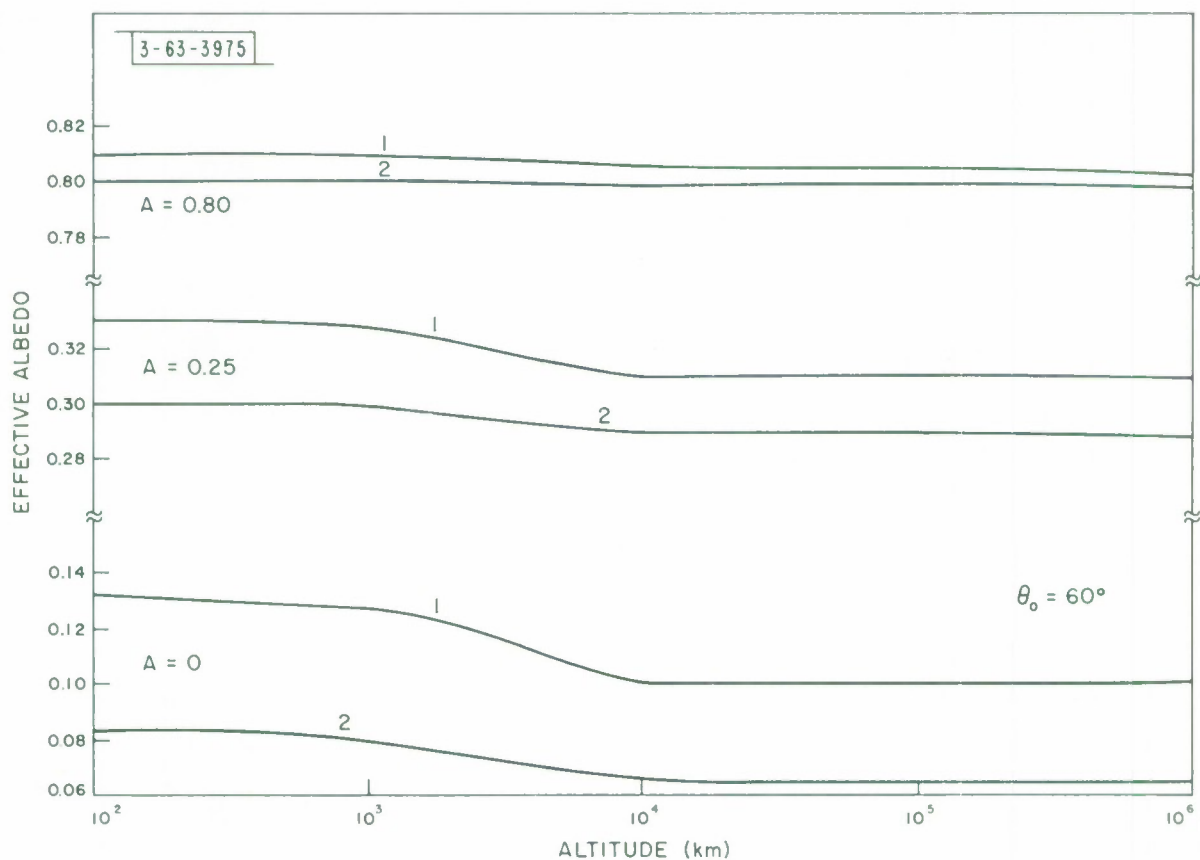
Fig. 61   Effective albedo as a function of altitude for $\theta_o = 60^o$

Continuing the type of calculations, the results of which were presented above, the intensity distribution seen by a sensor at synchronous altitude is presented below for specific cases. The numbers have been arrived at by using an extremely useful reference. "Tables Related to Radiation Emerging from a Planetary Atmosphere with Rayleigh Scattering" by Coulson, Dave and Sekera. [9]

In what follows it has been assumed that the sun, the satellite earth sensor, and the center of the earth all lie on a straight line. The symbols used are defined by Figs. 21 - 22. The sensor sweeps from a spot directly below to the edge of the earth. Corrections have not been made for the curvature of the earth's atmosphere because corrections are only necessary for very oblique angles of incidence (sun zenith angles over 82°) and in such cases the scattered intensity is large (for this geometry).

Figure 62 illustrates the intensity (relative to an incident intensity of 1.0) of scattered light as a function of angle δ with wavelength as a parameter. The same information is presented in Fig. 63, but here the intensity is a function of the sensor nadir angle. This makes the sharp increase in intensity near the limb of the earth much more apparent. The increased backscatter near the limb is the reason why a sharp halo of violet rings the earth in the color Gemini IV photographs.

Although the relative intensity of scattered light increases as wavelength decreases, the intensity of sunlight decreases as λ approaches UV wavelengths. The graphs of Fig. 64 have been multiplied by the spectral flux of the sun to obtain the relative intensity of scattered sunlight at various wavelengths.

The data contained in these graphs has been multiplied by the sensor response at two values of δ and displayed as a function of λ in Fig. 65. Note that the graph on the right for $\delta = 78.45^O$ is two times larger than the graph for $\delta = 0$. The graphs have been put in proper perspective in Fig. 66 where graph (2) is for $\delta = 78.45^O$ graph (3) is for $\delta = 0^O$ and graph (1) is for the intensity distribution over wavelength for a diffusely reflecting atmosphere-less earth for $\delta = 0$.

Fig. 62 Relative intensity of scattered light at synchronous altitudes, as a function of the central angle of a great circle ($\Phi = 180^{\circ}$, $\alpha = 180^{\circ}$, $\theta_o = 0^{\circ}$).

Fig. 63 Relative intensity of scattered light at synchronous altitudes as a function of sensor nadir angle ($\Phi = 180^O$, $\alpha = 180^O$, $\theta_o = 0^O$).
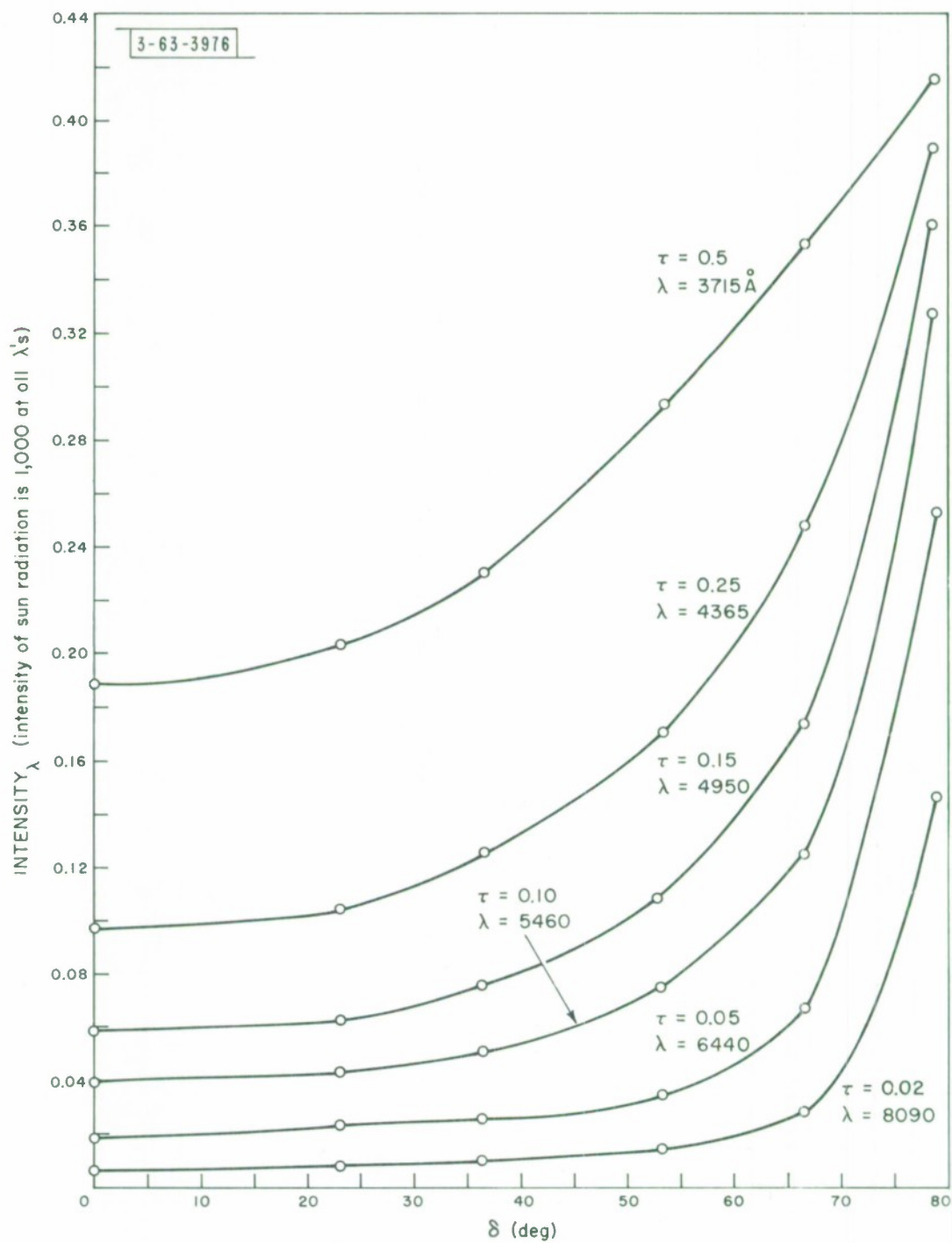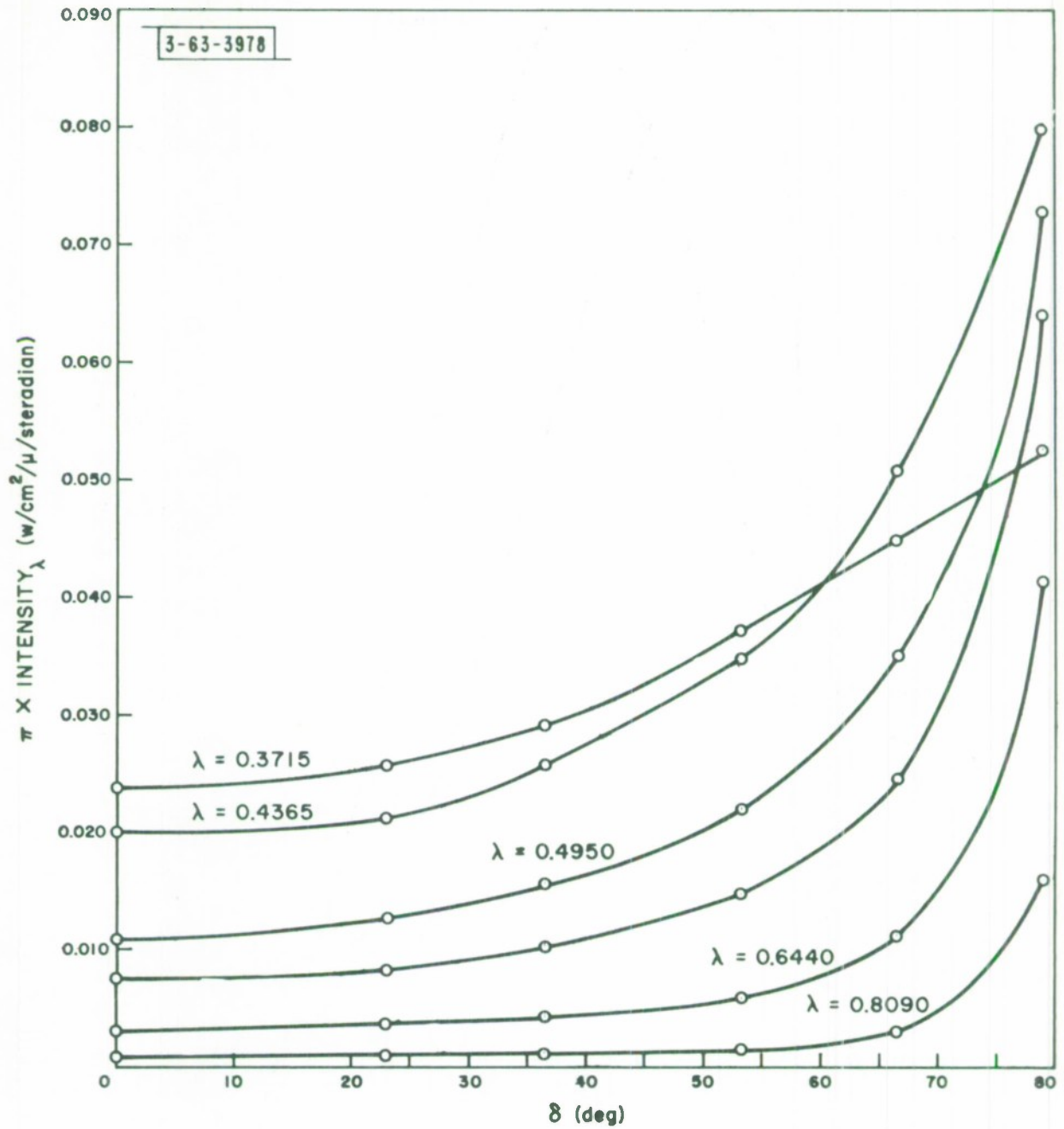
Fig. 64 Relative intensity of scattered sunlight at various wavelengths as a function of the central angle of a great circle ($\Phi = 180^{\circ}$, $\alpha = 180^{\circ}$, $\theta_{o} = 0^{\circ}$).
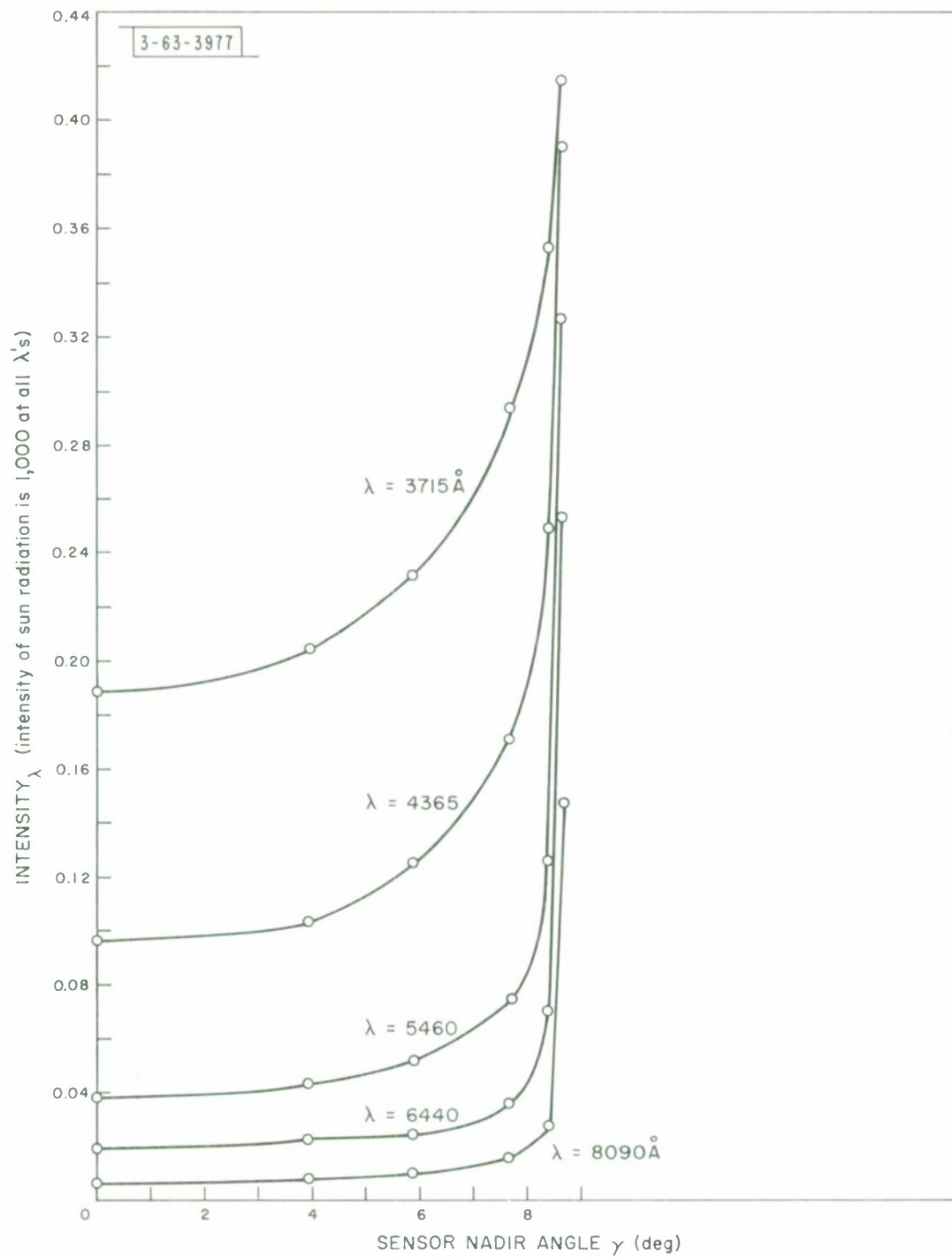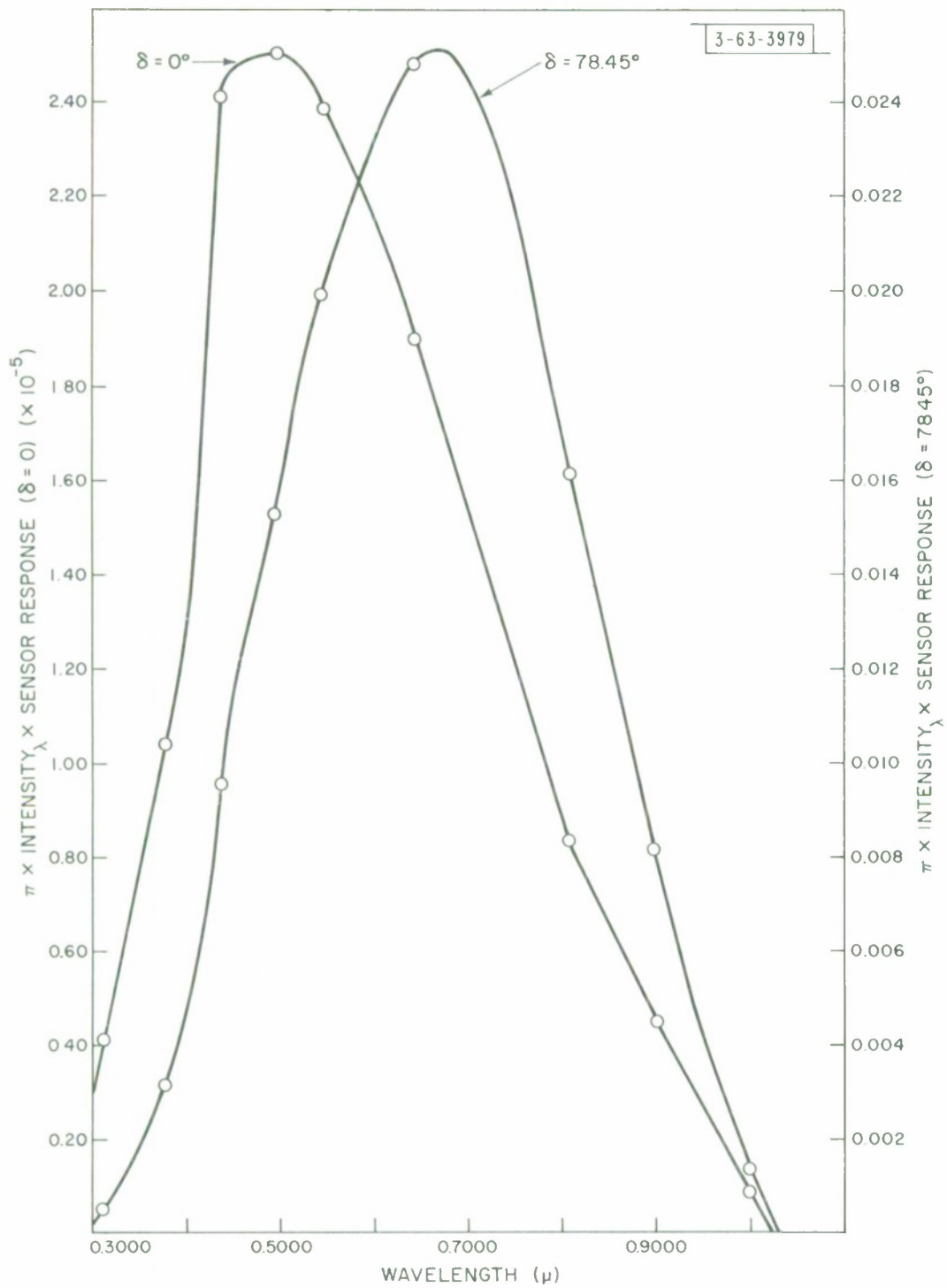
Fig. 65 Light intensity seen by sensor after adjustment for sensor response.

78
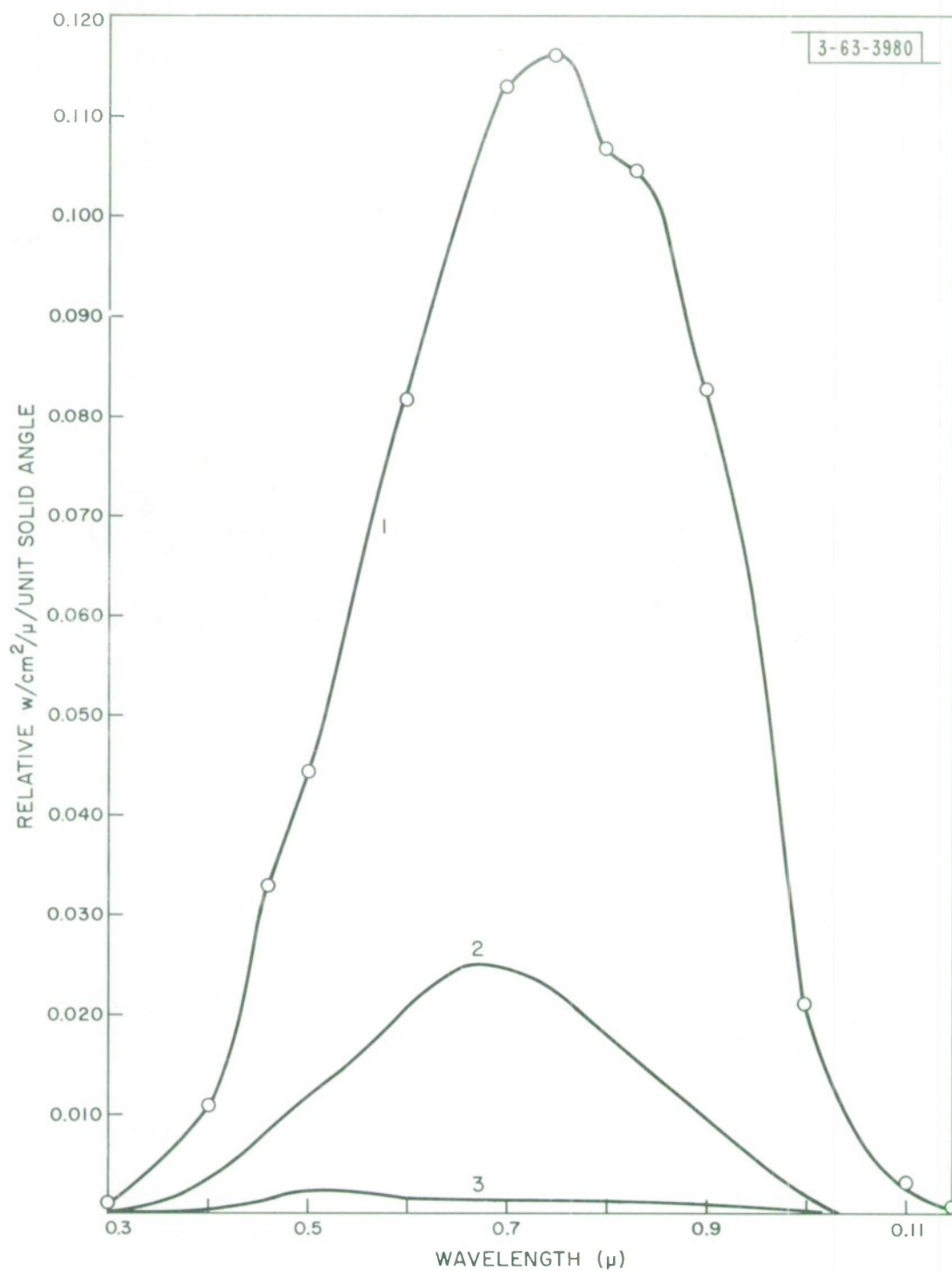
Fig. 66
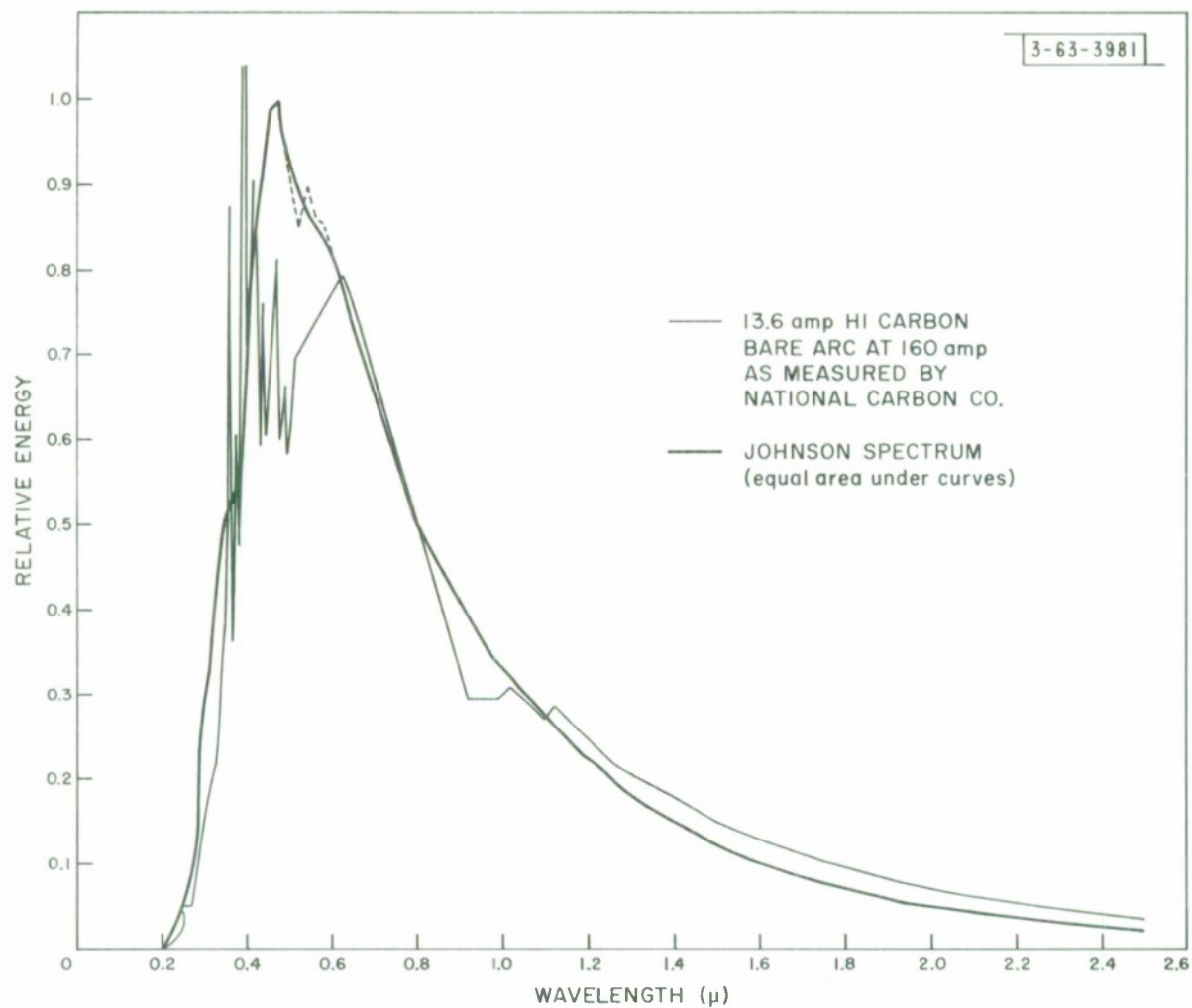
Fig. 67 Relative spectral distribution of the sun

The area under the curves is proportional to the flux seen by the sensor and the current produced. The earth has been assumed flat and the intensity constant in the region viewed. The ratio of the area of graph (2) or (3) to the area of graph (1) is the sensor backscatter coefficient "b_2".

To predict the current produced by the sensor a very simple experiment can be performed. Measure the current produced by the sensor looking straight down at the light reflected from a diffusely reflecting flat source, illuminated by one solar constant with the same wavelength distribution of intensity as the sun. If this current is I_o and if the response of the sensor is linear, the current output, I, in outer space for a particular configuration is:

$$I = b_2 I_o$$

b_2 for $\delta = 0.0$ is .0201

b_2 for $\delta = 78.45$ is .204

The calculation was done as follows: The geometry of the sun, the earth, and the satellites, is drawn. A value of γ is chosen and the corresponding value of δ is gotten from Appendix II. Then $\gamma + \delta = \cos^{-1}\mu$. The angles $\cos^{-1}\mu_o$ and φ are gotten from the geometry. The relative intensity can then be found in Table VI of Coulson's tables for all τ and hence λ. The value of intensity at a particular λ is multiplied by the flux from the sun at the same wavelength in watts/cm^2/micron. (The relative spectral distribution of the sun is given in Fig. 67. The sun's output has been smoothed out so that undue weight is not placed on dips in the curve. This curve must be multiplied by .220 to make the curve absolute.) This value is then multiplied by the relative sensor response. The data points are then plotted versus wavelength in microns and the area under the curve is computed. The ratio of this area to the area under curve (1) in Fig. 66 is the sensor backscatter coefficient "b_2". This

area is 189.70 boxes or 474.25×10^{-4} sq. units (i. e. each box is $.05 \times .005 = 25 \times 10^{-4}$ sq. units). Alternately, if the curve (1) is multiplied by the relative sensor response and the area is found the answer is the same but the work is reduced.

Time did not permit additional calculations of b_2 for different satellite orientations. It is felt that the minimum possible value of b_2 for any geometry is not much lower than .02. The calculation, however, does not take into account the effects of water vapor and molecular absorption of radiation at large values of wavelength. Ozone absorption plays a minor role since it becomes important only below 3000 $\overset{o}{A}$. Scattering by dust, haze and aerosols would serve to increase the intensity of scattered light beyond that of a Rayleigh atmosphere.

APPENDIX I

The Monochromatic Reflectance R_ν of the Atmosphere-Surface System for Various Values of the Optical Thickness τ and Surface Reflectivity, A.

APPENDIX I

The Monochromatic Reflectance R_ν of the Atmosphere-Surface System for Various Values of the Optical Thickness τ and Surface Reflectivity, A.

τ	$\lambda(\overset{o}{A})$	μ_o	Surface Reflectivity, A						
			0	0.05	0.10	0.15	0.25	0.50	0.80
1.0	3120	0.02	0.751	0.758	0.765	0.773	0.790	0.840	0.922
		0.10	0.704	0.712	0.721	0.730	0.750	0.809	0.908
		0.20	0.650	0.660	0.670	0.681	0.705	0.775	0.891
		0.40	0.546	0.558	0.572	0.586	0.616	0.707	0.859
		0.60	0.458	0.474	0.490	0.507	0.543	0.651	0.831
		0.80	0.392	0.409	0.427	0.446	0.486	0.608	0.811
		0.92	0.359	0.377	0.396	0.416	0.469	0.587	0.801
		1.00	0.340	0.359	0.378	0.399	0.443	0.575	0.795
0.50	3660	0.02	0.675	0.687	0.698	0.711	0.737	0.809	0.915
		0.10	0.610	0.624	0.638	0.653	0.684	0.771	0.898
		0.20	0.523	0.540	0.558	0.576	0.614	0.720	0.875
		0.40	0.383	0.405	0.428	0.451	0.500	0.638	0.838
		0.60	0.297	0.322	0.348	0.374	0.430	0.587	0.816
		0.80	0.241	0.268	0.296	0.325	0.385	0.554	0.801
		0.92	0.216	0.244	0.273	0.303	0.365	0.540	0.795
		1.00	0.202	0.231	0.260	0.291	0.354	0.532	0.791
0.25	4365	0.02	0.609	0.625	0.641	0.658	0.693	0.785	0.909
		0.10	0.503	0.524	0.545	0.566	0.610	0.727	0.884
		0.20	0.375	0.401	0.427	0.454	0.509	0.657	0.854
		0.40	0.238	0.270	0.302	0.335	0.402	0.582	0.822
		0.60	0.173	0.207	0.242	0.278	0.351	0.546	0.807
		0.80	0.136	0.172	0.208	0.245	0.321	0.525	0.798
		0.92	0.120	0.157	0.194	0.231	0.309	0.517	0.794
		1.00	0.112	0.148	0.186	0.224	0.302	0.512	0.792
0.15	4950	0.02	0.569	0.588	0.607	0.627	0.667	0.771	0.905
		0.10	0.406	0.432	0.459	0.486	0.541	0.684	0.869
		0.20	0.270	0.302	0.335	0.368	0.436	0.612	0.839
		0.40	0.158	0.195	0.233	0.271	0.349	0.552	0.814
		0.60	0.111	0.151	0.191	0.231	0.313	0.528	0.803
		0.80	0.086	0.126	0.167	0.209	0.293	0.514	0.798
		0.92	0.076	0.116	0.158	0.200	0.285	0.508	0.796
		1.00	0.070	0.111	0.153	0.195	0.281	0.505	0.794

Note: The solar zenith angle θ_o is given in terms $\mu_o = \cos \theta_o$.

84

τ	$\lambda(\overset{o}{A})$	μ_o	Surface Reflectivity, A						
			0	0.05	0.10	0.15	0.25	0.50	0.80
0.10	5410	0.20	0.541	0.562	0.583	0.605	0.648	0.760	0.902
		0.10	0.323	0.355	0.386	0.418	0.482	0.647	0.855
		0.20	0.199	0.236	0.273	0.310	0.386	0.582	0.828
		0.40	0.111	0.152	0.193	0.235	0.319	0.536	0.809
		0.60	0.077	0.119	0.162	0.205	0.293	0.518	0.802
		0.80	0.059	0.102	0.146	0.190	0.279	0.509	0.798
		0:92	0.052	0.095	0.139	0.183	0.273	0.505	0.797
		1.00	0.048	0.091	0.136	0.180	0.270	0.503	0.796
0.05	6440	0.02	0.475	0.352	0.385	0.419	0.486	0.656	0.862
		0.10	0.198	0.136	0.180	0.225	0.315	0.541	0.815
		0.20	0.111	0.094	0.141	0.188	0.282	0.519	0.807
		0.40	0.059	0.072	0.120	0.168	0.265	0.508	0.802
		0.60	0.040	0.065	0.113	0.162	0.259	0.504	0.800
		0.80	0.030	0.061	0.110	0.158	0.256	0.501	0.799
		0.92	0.026	0.059	0.108	0.157	0.255	0.501	0.799
		1.00	0.024	0.059	0.107	0.156	0.254	0.500	0.799
0.02	8090	0.02	0.319	0.352	0.385	0.419	0.486	0.656	0.862
		0.10	0.091	0.136	0.180	0.225	0.315	0.541	0.815
		0.20	0.048	0.094	0.141	0.188	0.282	0.519	0.807
		0.40	0.024	0.072	0.120	0.168	0.265	0.508	0.802
		0.60	0.016	0.065	0.113	0.162	0.259	0.504	0.800
		0.80	0.012	0.061	0.110	0.158	0.256	0.501	0.799
		0.92	0.011	0.059	0.108	0.157	0.255	0.501	0.799
		1.00	0.011	0.059	0.107	0.156	0.254	0.500	0.799
0.01	9600	0.02	0.197	0.237	0.277	0.317	0.396	0.597	0.838
		0.10	0.048	0.095	0.142	0.189	0.284	0.521	0.808
		0.20	0.024	0.073	0.121	0.170	0.267	0.510	0.803
		0.40	0.012	0.061	0.110	0.159	0.257	0.504	0.801
		0.60	0.008	0.057	0.107	0.156	0.254	0.502	0.800
		0.80	0.006	0.055	0.105	0.154	0.253	0.501	0.800
		0.92	0.005	0.055	0.104	0.153	0.252	0.500	0.800
		1.00	0.005	0.054	0.104	0.153	0.252	0.500	0.799
0.003	12960	0.02	0.068	0.115	0.161	0.208	0.301	0.534	0.813
		0.10	0.013	0.063	0.112	0.161	0.260	0.506	0.802
		0.20	0.006	0.056	0.105	0.155	0.254	0.502	0.801
		0.40	0.002	0.052	0.102	0.152	0.251	0.500	0.800
		0.60	0.001	0.051	0.101	0.151	0.250	0.500	0.800
		0.80	0.001	0.050	0.100	0.150	0.250	0.500	0.800
		0.92	0.000	0.050	0.100	0.150	0.250	0.500	0.800
		1.00	0.000	0.050	0.100	0.150	0.250	0.500	0.800

τ	$\lambda(\overset{o}{A})$	μ_o	Surface Reflectivity, A						
			0	0.05	0.10	0.15	0.25	0.50	0.80
0.001	17000	0.02	0.023	0.072	0.121	0.170	0.267	0.512	0.805
		0.10	0.004	0.054	0.104	0.153	0.253	0.502	0.801
		0.20	0.002	0.051	0.101	0.151	0.251	0.501	0.800
		0.40	0.000	0.050	0.100	0.150	0.250	0.500	0.800
		0.60	0.000	0.050	0.100	0.150	0.250	0.500	0.800
		0.80	0.000	0.050	0.100	0.150	0.250	0.500	0.800
		0.92	0.000	0.050	0.100	0.150	0.250	0.500	0.800
		1.00	0.000	0.050	0.100	0.150	0.250	0.500	0.800

APPENDIX II

Angles γ and δ Defined by Fig. 21 for the Radius of the Earth = 6371 km
and the Radius of the Satellite Orbit = 42,160 km. Angles are Given in
Degrees.

δ	γ	δ	γ
0.8130846E 02	0.8691536E 01	0.6780846E 02	0.8440575E 01
0.8105846E 02	0.8691453E 01	0.6755846E 02	0.8431064E 01
0.8080846E 02	0.8691202E 01	0.6730846E 02	0.8421372E 01
0.8055846E 02	0.8690784E 01	0.6705846E 02	0.8411502E 01
0.8030846E 02	0.8690198E 01	0.6680846E 02	0.8401446E 01
0.8005846E 02	0.8689445E 01	0.6655846E 02	0.8391211E 01
0.7980846E 02	0.8688523E 01	0.6630846E 02	0.8380794E 01
0.7955846E 02	0.8687432E 01	0.6605846E 02	0.8370197E 01
0.7930846E 02	0.8686172E 01	0.6580846E 02	0.8359417E 01
0.7905846E 02	0.8684743E 01	0.6555846E 02	0.8348456E 01
0.7880846E 02	0.8683144E 01	0.6530846E 02	0.8337313E 01
0.7855846E 02	0.8681375E 01	0.6505846E 02	0.8325987E 01
0.7830846E 02	0.8679436E 01	0.6480846E 02	0.8314482E 01
0.7805846E 02	0.8677326E 01	0.6455846E 02	0.8302792E 01
0.7780846E 02	0.8675045E 01	0.6430846E 02	0.8290918E 01
0.7755846E 02	0.8672593E 01	0.6405846E 02	0.8278863E 01
0.7730846E 02	0.8669972E 01	0.6380846E 02	0.8266626E 01
0.7705846E 02	0.8667175E 01	0.6355846E 02	0.8254206E 01
0.7680846E 02	0.8664208E 01	0.6330846E 02	0.8241603E 01
0.7655846E 02	0.8661068E 01	0.6305846E 02	0.8228817E 01
0.7630846E 02	0.8657756E 01	0.6280846E 02	0.8215849E 01
0.7605846E 02	0.8654271E 01	0.6255846E 02	0.8202697E 01
0.7580846E 02	0.8650613E 01	0.6230846E 02	0.8189362E 01
0.7555846E 02	0.8646781E 01	0.6205846E 02	0.8175844E 01
0.7530846E 02	0.8642775E 01	0.6180846E 02	0.8162143E 01
0.7505846E 02	0.8638595E 01	0.6155846E 02	0.8148258E 01
0.7480846E 02	0.8634242E 01	0.6130846E 02	0.8134190E 01
0.7455846E 02	0.8629713E 01	0.6105846E 02	0.8119935E 01
0.7430846E 02	0.8625012E 01	0.6080846E 02	0.8105504E 01
0.7405846E 02	0.8620132E 01	0.6055846E 02	0.8090886E 01
0.7380846E 02	0.8615077E 01	0.6030846E 02	0.8076084E 01
0.7355846E 02	0.8609848E 01	0.6005846E 02	0.8061095E 01
0.7330846E 02	0.8604443E 01	0.5980846E 02	0.8045932E 01
0.7305846E 02	0.8598862E 01	0.5955846E 02	0.8030578E 01
0.7280846E 02	0.8593104E 01	0.5930846E 02	0.8015042E 01
0.7255846E 02	0.8587170E 01	0.5905846E 02	0.7999322E 01
0.7230846E 02	0.8581059E 01	0.5880846E 02	0.7983419E 01
0.7205846E 02	0.8574770E 01	0.5855846E 02	0.7967332E 01
0.7180846E 02	0.8568305E 01	0.5830846E 02	0.7951061E 01
0.7155846E 02	0.8561662E 01	0.5805846E 02	0.7934607E 01
0.7130846E 02	0.8554842E 01	0.5780846E 02	0.7917970E 01
0.7105846E 02	0.8547843E 01	0.5755846E 02	0.7901149E 01
0.7080846E 02	0.8540666E 01	0.5730846E 02	0.7884144E 01
0.7055846E 02	0.8533311E 01	0.5705846E 02	0.7866956E 01
0.7030846E 02	0.8525777E 01	0.5680846E 02	0.7849585E 01
0.7005846E 02	0.8518065E 01	0.5655846E 02	0.7832030E 01
0.6980846E 02	0.8510173E 01	0.5630846E 02	0.7814292E 01
0.6955846E 02	0.8502102E 01	0.5605846E 02	0.7796370E 01
0.6930846E 02	0.8493853E 01	0.5580846E 02	0.7778266E 01
0.6905846E 02	0.8485423E 01	0.5555846E 02	0.7759978E 01
0.6880846E 02	0.8476814E 01	0.5530846E 02	0.7741507E 01
0.6855846E 02	0.8468024E 01	0.5505846E 02	0.7722853E 01
0.6830846E 02	0.8459054E 01	0.5480846E 02	0.7704017E 01
0.6805846E 02	0.8449905E 01	0.5455846E 02	0.7684997E 01

δ	γ	δ	γ
0.5430846E 02	0.7665795E 01	0.4080846E 02	0.6362944E 01
0.5405846E 02	0.7646411E 01	0.4055846E 02	0.6334040E 01
0.5380846E 02	0.7626843E 01	0.4030846E 02	0.6304972E 01
0.5355846E 02	0.7607094E 01	0.4005846E 02	0.6275733E 01
0.5330846E 02	0.7587163E 01	0.3980846E 02	0.6246332E 01
0.5305846E 02	0.7567049E 01	0.3955846E 02	0.6216765E 01
0.5280846E 02	0.7546753E 01	0.3930846E 02	0.6187034E 01
0.5255846E 02	0.7526276E 01	0.3905846E 02	0.6157138E 01
0.5230846E 02	0.7505617E 01	0.3880846E 02	0.6127082E 01
0.5205846E 02	0.7484777E 01	0.3855846E 02	0.6096859E 01
0.5180846E 02	0.7463754E 01	0.3830846E 02	0.6066475E 01
0.5155846E 02	0.7442552E 01	0.3805846E 02	0.6035932E 01
0.5130846E 02	0.7421168E 01	0.3780846E 02	0.6005223E 01
0.5105846E 02	0.7399603E 01	0.3755846E 02	0.5974356E 01
0.5080846E 02	0.7377857E 01	0.3730846E 02	0.5943329E 01
0.5055846E 02	0.7355932E 01	0.3705846E 02	0.5912142E 01
0.5030846E 02	0.7333826E 01	0.3680846E 02	0.5880796E 01
0.5005846E 02	0.7311540E 01	0.3655846E 02	0.5849293E 01
0.4980846E 02	0.7289074E 01	0.3630846E 02	0.5817631E 01
0.4955846E 02	0.7266429E 01	0.3605846E 02	0.5785813E 01
0.4930846E 02	0.7243604E 01	0.3580846E 02	0.5753837E 01
0.4905846E 02	0.7220600E 01	0.3555846E 02	0.5721707E 01
0.4880846E 02	0.7197418E 01	0.3530846E 02	0.5689421E 01
0.4855846E 02	0.7174056E 01	0.3505846E 02	0.5656980E 01
0.4830846E 02	0.7150517E 01	0.3480846E 02	0.5624386E 01
0.4805846E 02	0.7126799E 01	0.3455846E 02	0.5591638E 01
0.4780846E 02	0.7102904E 01	0.3430846E 02	0.5558738E 01
0.4755846E 02	0.7078832E 01	0.3405846E 02	0.5525686E 01
0.4730846E 02	0.7054580E 01	0.3380846E 02	0.5492483E 01
0.4705846E 02	0.7030153E 01	0.3355846E 02	0.5459129E 01
0.4680846E 02	0.7005549E 01	0.3330846E 02	0.5425625E 01
0.4655846E 02	0.6980769E 01	0.3305846E 02	0.5391973E 01
0.4630846E 02	0.6955812E 01	0.3280846E 02	0.5358172E 01
0.4605846E 02	0.6930680E 01	0.3255846E 02	0.5324223E 01
0.4580846E 02	0.6905372E 01	0.3230846E 02	0.5290128E 01
0.4555846E 02	0.6879890E 01	0.3205846E 02	0.5255886E 01
0.4530846E 02	0.6854232E 01	0.3180846E 02	0.5221499E 01
0.4505846E 02	0.6828400E 01	0.3155846E 02	0.5186967E 01
0.4480846E 02	0.6802394E 01	0.3130846E 02	0.5152291E 01
0.4455846E 02	0.6776215E 01	0.3105846E 02	0.5117472E 01
0.4430846E 02	0.6749862E 01	0.3080846E 02	0.5082511E 01
0.4405846E 02	0.6723336E 01	0.3055846E 02	0.5047408E 01
0.4380846E 02	0.6696637E 01	0.3030846E 02	0.5012164E 01
0.4355846E 02	0.6669767E 01	0.3005846E 02	0.4976780E 01
0.4330846E 02	0.6642724E 01	0.2980846E 02	0.4941257E 01
0.4305846E 02	0.6615511E 01	0.2955846E 02	0.4905595E 01
0.4280846E 02	0.6588126E 01	0.2930846E 02	0.4869796E 01
0.4255846E 02	0.6560572E 01	0.2905846E 02	0.4833861E 01
0.4230846E 02	0.6532845E 01	0.2880846E 02	0.4797789E 01
0.4205846E 02	0.6504950E 01	0.2855846E 02	0.4761582E 01
0.4180846E 02	0.6476885E 01	0.2830846E 02	0.4725241E 01
0.4155846E 02	0.6448652E 01	0.2805846E 02	0.4688766E 01
0.4130846E 02	0.6420258E 01	0.2780846E 02	0.4652159E 01
0.4105846E 02	0.6391681E 01	0.2755846E 02	0.4615421E 01

δ	γ	δ	γ
0.2730846E 02	0.4578551E 01	0.1380846E 02	0.2420494E 01
0.2705846E 02	0.4541552E 01	0.1355846E 02	0.2377984E 01
0.2680846E 02	0.4504424E 01	0.1330846E 02	0.2335403E 01
0.2655846E 02	0.4467167E 01	0.1305846E 02	0.2292752E 01
0.2630846E 02	0.4429784E 01	0.1280846E 02	0.2250033E 01
0.2605846E 02	0.4392274E 01	0.1255846E 02	0.2207246E 01
0.2580846E 02	0.4354639E 01	0.1230846E 02	0.2164394E 01
0.2555846E 02	0.4316879E 01	0.1205846E 02	0.2121476E 01
0.2530846E 02	0.4278996E 01	0.1180846E 02	0.2078495E 01
0.2505846E 02	0.4240992E 01	0.1155846E 02	0.2035451E 01
0.2480846E 02	0.4202863E 01	0.1130846E 02	0.1992346E 01
0.2455846E 02	0.4164615E 01	0.1105846E 02	0.1949182E 01
0.2430846E 02	0.4126248E 01	0.1080846E 02	0.1905959E 01
0.2405846E 02	0.4087761E 01	0.1055846E 02	0.1862678E 01
0.2380846E 02	0.4049157E 01	0.1030846E 02	0.1819342E 01
0.2355846E 02	0.4010437E 01	0.1005846E 02	0.1775951E 01
0.2330846E 02	0.3971600E 01	0.9808463E 01	0.1732506E 01
0.2305846E 02	0.3932649E 01	0.9558464E 01	0.1689009E 01
0.2280846E 02	0.3893584E 01	0.9308463E 01	0.1645461E 01
0.2255846E 02	0.3854407E 01	0.9058464E 01	0.1601864E 01
0.2230846E 02	0.3815117E 01	0.8808464E 01	0.1558218E 01
0.2205846E 02	0.3775717E 01	0.8558463E 01	0.1514525E 01
0.2180846E 02	0.3736207E 01	0.8308464E 01	0.1470786E 01
0.2155846E 02	0.3696589E 01	0.8058464E 01	0.1427003E 01
0.2130846E 02	0.3656863E 01	0.7808463E 01	0.1383177E 01
0.2105846E 02	0.3617031E 01	0.7558464E 01	0.1339309E 01
0.2080846E 02	0.3577093E 01	0.7308464E 01	0.1295401E 01
0.2055846E 02	0.3537050E 01	0.7058463E 01	0.1251453E 01
0.2030846E 02	0.3496905E 01	0.6808464E 01	0.1207467E 01
0.2005846E 02	0.3456657E 01	0.6558464E 01	0.1163445E 01
0.1980846E 02	0.3416308E 01	0.6308463E 01	0.1119388E 01
0.1955846E 02	0.3375859E 01	0.6058464E 01	0.1075297E 01
0.1930846E 02	0.3335311E 01	0.5808464E 01	0.1031173E 01
0.1905846E 02	0.3294665E 01	0.5558464E 01	0.9870182E 00
0.1880846E 02	0.3253922E 01	0.5308464E 01	0.9428329E 00
0.1855846E 02	0.3213083E 01	0.5058464E 01	0.8986192E 00
0.1830846E 02	0.3172150E 01	0.4808464E 01	0.8543785E 00
0.1805846E 02	0.3131124E 01	0.4558464E 01	0.8101116E 00
0.1780846E 02	0.3090005E 01	0.4308464E 01	0.7658202E 00
0.1755846E 02	0.3048795E 01	0.4058463E 01	0.7215055E 00
0.1730846E 02	0.3007495E 01	0.3808463E 01	0.6771689E 00
0.1705846E 02	0.2966106E 01	0.3558464E 01	0.6328119E 00
0.1680846E 02	0.2924629E 01	0.3308463E 01	0.5884355E 00
0.1655846E 02	0.2883066E 01	0.3058463E 01	0.5440413E 00
0.1630846E 02	0.2841417E 01	0.2808464E 01	0.4996306E-00
0.1605846E 02	0.2799684E 01	0.2558463E 01	0.4552047E-00
0.1580846E 02	0.2757869E 01	0.2308463E 01	0.4107649E-00
0.1555846E 02	0.2715971E 01	0.2058464E 01	0.3663127E-00
0.1530846E 02	0.2673992E 01	0.1808463E 01	0.3218493E-00
0.1505846E 02	0.2631934E 01	0.1558463E 01	0.2773761E-00
0.1480846E 02	0.2589798E 01	0.1308464E 01	0.2328946E-00
0.1455846E 02	0.2547585E 01	0.1058463E 01	0.1884058E-00
0.1430846E 02	0.2505295E 01	0.8084639E 00	0.1439115E-00
0.1405846E 02	0.2462931E 01	0.5584636E 00	0.9941271E-01
		0.3084633E-00	0.5491085E-01
		0.5846386E-01	0.1040748E-01

REFERENCES

(The References with asterisks are those actually referred to in the paper.)

*1. Fritz, Sigmund, "Solar Radiant Energy and its Modification by the Earth and its Atmosphere," Compendium of Meteorology, 1951 pp 13-33.

*2. Nordberg, W. and collaborators, "Preliminary Results of Radiation Measurements from the Tiros III Meteorlogical Satellite," NASA Technical Note D-1338, May 1962.

*3. Viezee, W. and collaborators, "Variations of Satellite Daytime Radiation Data with Viewing Geometry," Contract AF 19(628)-2777, Scientific Report 3, Air Force Cambridge Research Laboratories, Bedford, Mass., June 1964.

*4. Viezee, W. and Davis, P. A., "Analysis of Daytime Radiation Data from Tiros IV," Contract AF 19(628)-2777, Scientific Report 4, Air Force Cambridge Research Laboratories, Bedford, Massachusetts, December 1964.

*5. Chandrasekhar, S., Radiative Transfer (Clarendon Press, Oxford 1960)

*6. Coulson, K. L., 1959 "Characteristics of the Radiation Emerging from the Top of a Rayleigh Atmosphere, Parts I and II. J. of Planetary and Space Sciences, vol. 1, pp 265-276 and pp 277-284.

*7. Coulson, K. L., and Furukawa, P. M., "Distributions of Atmospheric Radiative Heating and Cooling," Contract AF 19(604)-5967, Scientific Report 2, SRI Project 2994, Stanford Research Institute, Menlo Park, California, (Nov. 1960)

*8. Snoddy, William C., "Irradiation above the Atmosphere Due to Rayleigh Scattering and Diffuse Terrestrial Reflections," Masters Thesis, University of Alabama, 1964.

*9. Coulson, K. L., Dave, J. V., and Sekera, Z. "Table Related to Radiation Emerging from a Planetary Atmosphere with Rayleigh Scattering" 1960, University of California Press.

10. Bandeen, W. R., "Tiros II Radiation Data User's Manual," Goddard Space Flight Center, NASA, Greenbelt, Maryland (1962)

11. Bandeen, W. R., et al., "Infrared and Reflected Solar Radiation Measurements from the Tiros II Meteorological Satellite," J. of Geophysical Research, vol. 66, No. 10, Oct. 1961, pp 3169-3185.

12. Fritz, Sigmund, "The Albedo of the Planet Earth and of Clouds," J. Meterol., vol. 6, No. 4, pp 277-282, August 1949.

13. Hanel, R. A., and Stroud W. G., The Tiros II Radiation Experiment," NASA Technical Note D-1152, October 1961.

14. Johnson, F. S., "The Solar Constant," J. Meterol., vol. 11, pp 431-439, 1954.

15. Nicolet, M. 1951, "Sur la Determination du Flux Energitique du Rayonnement Extraterrestre du Soleil, "Archiv. Meteor., Geophys. u Bioklim, Serie B, vol. 3., p. 209.

16. Sherr, P. E. and Wexler, R., Operational Use of Tiros Radiation Measurements," Contract AF 19(628)-4074, Final Report, Air Force Cambridge Research Laboratories, Bedford, Massachusetts, April 1965.

17. Viezee, W. and Davis, P. A., Preliminary Examination of Daytime Radiation Data from Tiros III over Cloudy Regions," Contract AF 19(628)-2777, Scientific Report 1, Air Force Cambridge Research Laboratories, Bedford, Massachusetts, August 1963.

18. Viezee, W. and Davis, P. A., "Studies of Daytime Radiation from Tiros," Contract AF 19(628)-2777, Final Report, Air Force Cambridge Research Laboratories, Bedford, Massachusetts, February 1965.

19. Wexler, R. and Sherr, R., "Synoptic Analysis of Tiros III Radiation Measurements," Contract AF 19(628)-429, Final Report, Air Force Cambridge Research Laboratories, Bedford, Massachusetts, Jan. 1964.

DISTRIBUTION

Division 6

W. E. Morrow
P. Rosen

Group 63

H. Sherman
D. C. MacLellan
P. Waldron
M. Ash
G. H. Ashley
R. S. Berg
J. H. Binsack
D. R. Bold
A. Braga-Illa
C. Burrowes
R. W. Chick
N. B. Childs
J. B. Connolly
M. C. Crocker
F. W. Floyd
A. I. Grayzel
L. J. Hoffman
B. Howland
E. Landsman
C. L. Mack
J. Max
J. D. McCarron
R. E. McMahon
L. D. Michelove

D. M. Nathanson
B. J. Moriarty
D. Parker
J. L. Ryan
F. W. Sarles
V. J. Sferrino
I. I. Shapiro
R. L. Sicotte
W. B. Smith
D. M. Snider
A. G. Stanley
D. D. Tang
L. J. Travis
N. R. Trudeau
E. A. Vrablik
W. W. Ward

Group 63 Files (10)

DOCUMENT CONTROL DATA – R&D

(Security classification of title, body of abstract and indexing annotation must be entered when the overall report is classified)

1. ORIGINATING ACTIVITY *(Corporate author)*	2a. REPORT SECURITY CLASSIFICATION
Lincoln Laboratory, M.I.T.	Unclassified
	2b. GROUP None

3. REPORT TITLE

Survey on Earth Albedo

4. DESCRIPTIVE NOTES *(Type of report and inclusive dates)*
Technical Note

5. AUTHOR(S) *(Last name, first name, initial)*

Whitehill, Laird P.

6. REPORT DATE	7a. TOTAL NO. OF PAGES	7b. NO. OF REFS
11 October 1966	98	19

8a. CONTRACT OR GRANT NO. AF 19(628)-5167	9a. ORIGINATOR'S REPORT NUMBER(S)
b. PROJECT NO. 649L	Technical Note 1966-53
c.	9b. OTHER REPORT NO(S) *(Any other numbers that may be assigned this report)*
d.	ESD-TR-66-455

10. AVAILABILITY/LIMITATION NOTICES

Distribution of this document is unlimited.

11. SUPPLEMENTARY NOTES	12. SPONSORING MILITARY ACTIVITY
None	Air Force Systems Command, USAF

13. ABSTRACT

This paper is a study of the conditions that can be expected for the intensity of light reflected and scattered from the earth. The albedo of the earth is defined and the albedo of various surfaces, and regions of the earth are discussed. An attempt is made to survey typical results of measurements of Tiros data. The albedo of the earth covered by a Rayleigh atmosphere is presented in graphical form and the intensity distribution over the earth is plotted for various orientations of observer viewed spot and sun. A calculation of expected minimum response is made for a specific photodiode for a certain geometry and a method is presented to enable interested persons to easily perform similar calculations for different geometries.

14. KEY WORDS

reflectivity
scattering

Tiros satellites
Rayleigh scattering